CATABOLIC EFFECTS OF CHEMOTHERAPY DRUGS-INFLAMMATORY CYTOKINES COMBINATION ON MYOTUBES AND ENDOTHELIAL CELLS

ARMITA HELFOROUSH

A THESIS SUBMITTED TO THE FACULTY OF GRADUATE STUDIES IN PARTIAL FULFILLMENT OF THE REQUIREMENTS FOR THE DEGREE OF MASTER OF SCIENCE

GRADUATE PROGRAM IN KINESIOLOGY AND HEALTH SCIENCES
YORK UNIVERSITY
TORONTO, ONTARIO

August 2025

Abstract

Chemotherapy-induced muscle atrophy significantly impairs quality of life in cancer patients. While tumor-related inflammation partly explains cachexia-associated wasting, the mechanisms affecting myotubes and endothelial cells remain poorly understood. This thesis examines the catabolic effects of chemotherapy drugs and inflammatory cytokines on C2C12 myotubes and primary skeletal muscle endothelial cells. Myotubes were treated with CPT-11 (20 μg/mL), 5-fluorouracil (50 μg/mL), leucovorin (10 μg/mL), IL-6 (20 ng/mL), and TNF-α (100 ng/mL). Treatment significantly reduced myofibrillar proteins, including MHC-1(−36%), tropomyosin (−65%), and troponin T (−76%), and suppressed anabolic signaling. SNAT1 and LAT1 expression increased by 78% and 127%, respectively. Endothelial cells exposed to the same agents at full and half doses (100% and 50%) for 24 and 48 hours showed heightened stress responses and upregulation of p53 and p21. Partial recovery was observed following treatment removal, though not fully restored. These findings reveal distinct chemotherapy-induced vulnerabilities in muscle and endothelial cells, offering insight into potential therapeutic strategies.

Acknowledgements

First, I want to express my deepest gratitude to Dr. Ola Adegoke for your incredible support, guidance, and mentorship throughout my Master's journey. Your patience and encouragement, especially during tough times, made all the difference. I'm so grateful to have learned under your supervision.

Thank you to Dr. Emilie Roudier for your helpful advice and constant support. I truly enjoyed our conversations and learning from your expertise. Your passion for your work is inspiring.

To my amazing lab mates—Lilia, Miriam, Gagan, Jason and specially Stephen—thank you for all the laughs, troubleshooting, and moments of celebration along the way. You made the lab feel like a second home.

To my sister, your strength and encouragement kept me grounded. Knowing you were always there meant everything to me.

To my best friend Ghazal, thank you for cheering me on through every setback and success, from late-night talks to hunting for the BCAT-2 antibody, and reminding me to stay calm when my cells were dying, you never let me give up.

To my father, Gary, thank you for always answering my "car broke down" calls and showing up no matter what so I could keep going. Your help made this possible.

To my dear best friend Niloofar, thank you for standing by me every step of the way with endless support and understanding.

And finally, to my boyfriend Arshia, thank you for your love and encouragement, even spending weekends at York just to check on my cells. Your support has meant the world to me.

Table of content

ABSTRACT ii

ACKNOWLEDGEMENTS iii

TABLE OF CONTENT iv

LIST OF ABBREVIATIONS vi

CHAPTER 1 GENERAL INTRODUCTION 1

CHAPTER 2 LITERATURE REVIEW 5

2.1 Skeletal Muscle and Health 5
2.1.1 Factors Regulating Skeletal Muscle Anabolism 6
2.1.2 Mechanisms Regulating Skeletal Muscle Growth and Anabolic Pathways 7
2.1.2.1 IGF-Akt Pathway and Its Role in Muscle Anabolism 7
2.1.2.2 mTORC1 Signaling and Its Role in Muscle Anabolism 8
2.1.2.3 Role of Capillaries and Endothelial Cells in Nutrient Transport and Muscle Anabolism 10
2.1.3 Factors Regulating Skeletal Muscle Catabolism 11
2.1.3.1 Aging and Sarcopenia 11
2.1.3.2 Muscle Disuse and Atrophy 12
2.1.3.3 Chemotherapy-Induced Muscle Atrophy 12
2.1.3.4 Overlap Between Catabolic Conditions 13
2.2 Endothelial Cells and Their Role in Vascular and Skeletal muscle 14
2.2.1 Skeletal Muscle Microvasculature 14
2.2.2 Endothelial Cells in Microvascular Regulation 15
2.2.3 Endothelial Response to Mechanical Stimuli and Muscle Health 16
2.2.4 Endothelial Mediated Signaling Pathways in Skeletal Muscle Health 17
2.3 Endothelial Dysfunction and Muscle Atrophy 18
2.3.1 Chemotherapy-Induced Endothelial Dysfunction 18
2.3.1.1 Endothelial Apoptosis and Vascular Complications 18
2.3.1.2 Increased Inflammation and Cytokine Release 19
2.3.2 Endothelial-Myotube Crosstalk and Chemotherapy-Induced Muscle Atrophy 20
2.3.2.1 Chemotherapy-Induced Disruption of Protein Synthesis 20
2.3.2.2 Endothelial-Mediated Catabolic Pathways 21

CHAPTER 3 RATIONALE, OBJECTIVE AND HYPOTHESES 23

3.1 Rational 23
3.2 Objectives 24
3.3 Hypothesis 24

CHAPTER 4 26

CATABOLIC EFFECTS OF CHEMOTHERAPY DRUGS-INFLAMMATORY CYTOKINES COMBINATION ON C2C12 MYOTUBES AND SKELETAL MUSCLE MICROVASCULAR ENDOTHELIAL CELLS 26
4.1 MATERIALS AND METHODS 27
4.1.1-Reagents 27
4.1.2-Cell Culture Procedure for C2C12 Myotubes and Endothelial Cells 28
4.1.2.1 Chemotherapy and Cytokine Treatments 29
4.2 Harvesting Cells and Western Blotting 33
4.3 Immunofluorescence Microscopy: Measuring Myotube Diameter 35
4.4 BCKD Activity Assay 36
4.5 Graphical Representation of Western Blots and Statistics 37
4.6 Additional information on protein measurements and isoforms: 37
Results 39
Discussion 54
Limitations and Future Directions 61
REFERENCES 62
CHAPTER 8 APPENDIX 76
Appendix A- In Vitro Drug and inflammatory cytokine Dosages 76
Appendix B – Immunofluorescence Microscopy (*In-vitro)* Materials: 78
Appendix C – In-vitro BCKD Activity Assay Materials and Protocol 81
Appendix D – In-vitro BCKD Activity Assay Calculations 83
Appendix E - Preparation of 1.5% Gelatin Solution 84
Appendix F – Gelatin Coating Procedure 85

List of Abbreviations

4E-BP1	eIF4e-binding protein-1
5-FU	5-Fluorouracil
AA	Amino Acids
ACE	Angiotensin-Converting Enzyme
AKT	Protein Kinase B
AMP	Adenosine Monophosphate
AMPK	AMP-Activated Protein Kinase
aPKC	Atypical Protein Kinase C
ATG13	Autophagy-Related Protein 13
ATP	Adenosine Triphosphate
BCAA	Branched-Chain Amino Acid
BCAT1	Branched-Chain Amino Transferase 1
BCAT2	Branched-Chain Amino Transferase 2
BCKA	Branched-Chain Keto Acid
BCKD	Branched-Chain α-Keto Acid Dehydrogenase Complex
BCKDH	Branched-Chain Alpha-Keto Acid Dehydrogenase Complex
BDK	Branched-Chain α-Keto Acid Dehydrogenase Kinase
BW	Body Weight
CO_2	Carbon Dioxide
CPT-11	Irinotecan Hydrochloride
DC	Drugs and Cytokines
D0	Day 0
DAPI	6-Diamidino-2-Phenylindole 4′
ddH_2O	Double Distilled Water
DM	Differentiation Medium
DMSO	Dimethyl Sulfoxide
E3	Protein E3 Ubiquitin Ligases
EC	Endothelial Cell
ECs	Endothelial Cells
eIF2β	Eukaryotic Translation Initiation Factor 2 Subunit β
eIF4E	Eukaryotic Translation Initiation Factor 4E
eIF4F	Eukaryotic Translation Initiation Factor 4F
eIF4G	Eukaryotic Translation Initiation Factor 4G
eNOS	Endothelial Nitric Oxide Synthase
FBS	Fetal Bovine Serum
FOLFIRI	Folinic Acid (Leucovorin), Fluorouracil, Irinotecan
FoxO	Forkhead Box O
FOXO1	Forkhead Box O1
GH	Growth Hormone
GLUT4	Glucose Transporter Type 4
GM	Growth Medium
HIF-1α	Hypoxia-Inducible Factor 1-Alpha
IGF-1	Insulin-Like Growth Factor 1
IGF-2	Insulin-Like Growth Factor 2

IL-1	Interleukin-1
IL-1β	Interleukin-1 Beta
IL-6	Interleukin-6
IRS-1	Insulin Receptor Substrate-1
KIC	2-Keto-Isocaproate/4-Methyl-2-Oxopentanoic Acid
KIV	2-Keto-Isovalerate/3-Methyl-2-Oxobutanoic Acid
KLF15	Krueppel-Like Factor 15
KMV	α-Keto-β-Methylvaleric Acid/3-Methyl-2-Oxopentanoate
LAT1	L-Type Amino Acid Transporter 1
LEU	Leucovorin
MAFbx	F-Box Only Protein 32
MAPK	Mitogen-Activated Protein Kinase
MHC-1	Myosin Heavy Chain 1
MPB	Muscle Protein Breakdown
MPS	Muscle Protein Synthesis
mTOR	Mechanistic Target of Rapamycin
mTORC1	Mechanistic Target of Rapamycin Complex 1
MuRF1	Muscle RING Finger-1
MuRF-1	Muscle RING Finger Protein-1
NAD	Nicotinamide Adenine Dinucleotide
NADH	Nicotinamide Adenine Dinucleotide Hydrogen
NF-KB	Nuclear Factor Kappa-Light-Chain-Enhancer of Activated B Cells
NO	Nitric Oxide
OPA	Phthalaldehyde
PBDK	Phosphorylated BCKD Kinase
PBS	Phosphate-Buffered Saline
PI3K	Phosphoinositide 3-Kinase
PP2CM	Protein Phosphatase 2Cm
ROS	Reactive Oxygen Species
S6	Ribosomal Protein S6
S6K1	p70 Ribosomal Protein S6 Kinase 1
Ser/S	Serine
SNAT1	Sodium-Coupled Neutral Amino Acid Transporter 1
SNAT2	Sodium-Coupled Neutral Amino Acid Transporter 2
T1DM	Type 1 Diabetes Mellitus
T2DM	Type 2 Diabetes Mellitus
TCA	Trichloroacetic Acid
TGF-β	Transforming Growth Factor Beta
thr	Threonine
THBS1	Thrombospondin-1
TNF-α	Tumor Necrosis Factor Alpha
UPP	Ubiquitin Proteasome Pathway
UPS	Ubiquitin-Proteasome System
VEGF	Vascular Endothelial Growth Factor
VEGF-A	Vascular Endothelial Growth Factor A

Chapter 1 General Introduction

Chemotherapy, a major treatment for cancer, has transformed the prognosis for numerous patients, leading to significant improvements of survival rates (1). However, the treatment has major side effects. One of the most notable adverse effects of chemotherapy is muscle atrophy (2). Muscle atrophy refers to loss of muscle mass due to certain conditions such as ageing, chronic diseases or muscle disuse (3). The onset of chemotherapy-induced skeletal muscle atrophy has profound implications for patients, exerting a substantial impact on their quality of life, treatment tolerance, overall prognosis, and, notably, the metabolic and functional aspects of their bodies (4).

Building upon this, cachexia increases these complications which is more than just severe muscle atrophy. Cachexia is a multifactorial syndrome marked by significant decrease in body weight due to lose in fat and muscle mass and is accompanied by fatigue. Although it's prevalent in various chronic illnesses, its connection with cancer is particularly concerning (5) This is not simply due to malnutrition but stems from a complex interplay of tumor progression, inflammation, and metabolic imbalances. With the onset of cachexia, patients find it even more intimidating to tolerate prolonged treatments, ultimately fading their survival chances (6).

Moreover, skeletal muscle is a highly vascularized tissue, and its interaction with the local microvascular environment is essential for nutrient and oxygen delivery, metabolic exchange, and muscle regeneration. Endothelial cells, which line the blood vessels in skeletal muscle, are vital for maintaining vascular health and supporting muscle function (7–9). As shown in Figure 1, chemotherapy drugs travel through the bloodstream and reach the capillaries, where they can affect both the endothelial cells and the surrounding muscle fibers (10–12). The

figure highlights this area of contact, known as the endothelial and muscle fiber interface, where damage to small blood vessels may contribute to muscle loss (10,13–15). However, the response of endothelial cells to chemotherapy and inflammation has been studied much less than that of muscle cells. Understanding how chemotherapy independently affects endothelial cells is crucial, as endothelial dysfunction may exacerbate muscle damage or impair recovery.

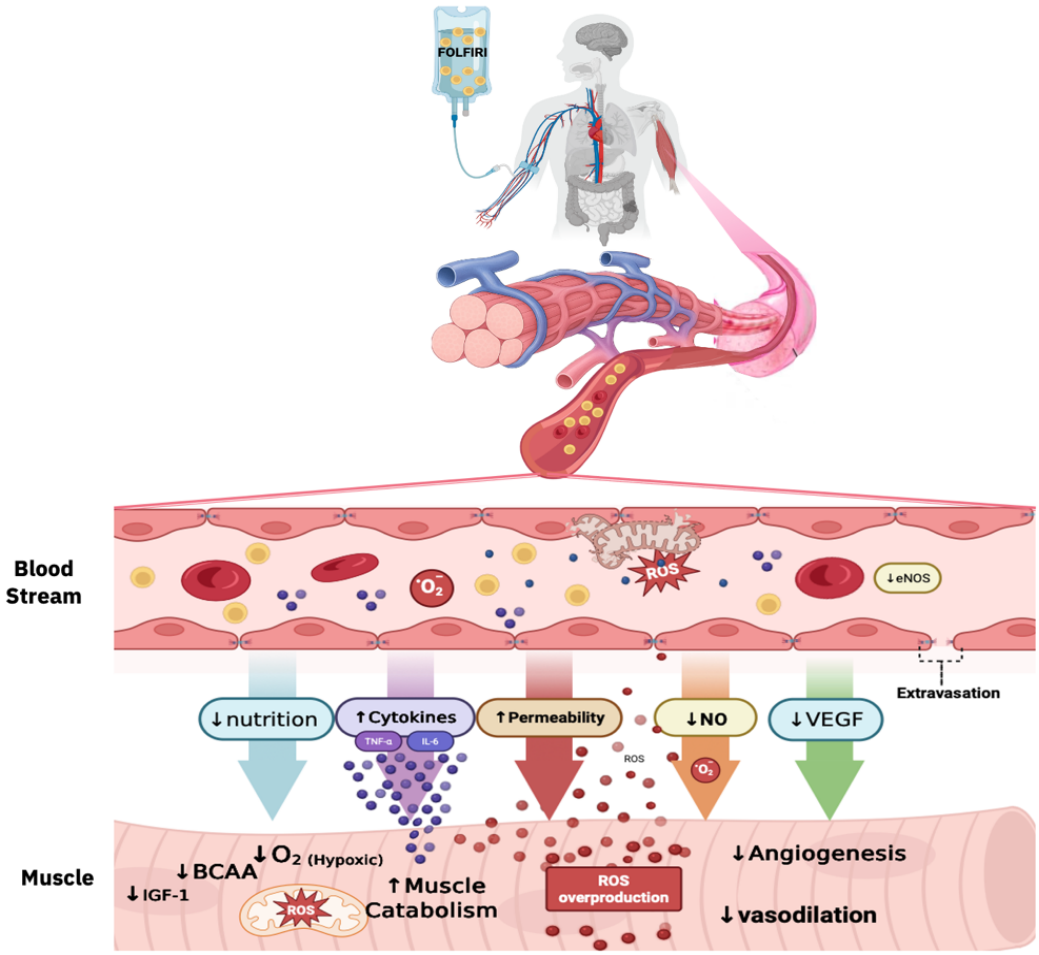

Figure 1. Skeletal muscle microvascular interface during chemotherapy exposure. Capillaries form an extensive network around muscle fibers. Chemotherapy circulating in the bloodstream reaches these capillaries, exposing both endothelial cells and adjacent myofibers to cytotoxic stress. Endothelial dysfunction may compromise perfusion, barrier function, and paracrine support, thereby contributing to chemotherapy-associated muscle wasting. Created with BioRender.

This thesis aims to investigate how a chemotherapy drug cocktail (CPT-11, 5-fluorouracil, and leucovorin) combined with pro-inflammatory cytokines (IL-6 and TNF-α) affects skeletal muscle myotubes and skeletal muscle-derived endothelial cells. These chemotherapeutic agents act through complementary mechanisms that collectively suppress cell proliferation. Irinotecan (CPT-11) inhibits DNA replication by targeting topoisomerase I, an enzyme responsible for relaxing supercoiled DNA during replication, resulting in single-strand DNA breaks and cell cycle arrest (16). 5-Fluorouracil (5-FU), a pyrimidine analog, interferes with RNA processing and DNA synthesis by inhibiting thymidylate synthase, leading to impaired nucleotide production and cytotoxic stress (17,18). Leucovorin (folinic acid) is non-toxic on its own but enhances the binding of 5-FU to thymidylate synthase, thereby amplifying its antitumor efficacy (19). This combination, commonly referred to as FOLFIRI, is widely used in colorectal cancer treatment protocols and provides a clinically relevant model of chemotherapy exposure for studying its effects on skeletal muscle and endothelial cells (20,21).

In addition to chemotherapy, cells were exposed to the pro-inflammatory cytokines tumor necrosis factor-α (TNF-α) and interleukin-6 (IL-6), which are elevated in cancer patients due to tumor secretion and systemic inflammation. TNF-α activates NF-κB signaling, promoting muscle protein degradation and endothelial inflammation, while IL-6 acts through the JAK/STAT3 pathway to further enhance proteolysis and vascular stress (22–30). These cytokines were included to reproduce the inflammatory environment accompanying cancer and chemotherapy, allowing evaluation of how combined cytotoxic and inflammatory stimuli affect skeletal muscle and endothelial cell function. The concentrations used for chemotherapy drugs and cytokines in this study were selected based on previous in vitro work modeling clinically relevant plasma levels observed in patients receiving FOLFIRI treatment, which have been

shown to induce metabolic and catabolic responses in skeletal muscle and endothelial cells (4,22,27,28,31–39).

Treatments were applied at two doses: a full dose equivalent to that used for C2C12 myotubes and half a dose representing 50% of this concentration, and two durations (24 and 48 hours) to capture early and progressive responses. Additionally, a recovery period following drug removal was included to assess whether cellular function could rebound. Importantly, this study examines these two cell types independently to establish a clearer understanding of their unique vulnerabilities and adaptations. By isolating their responses, this research lays the groundwork for future studies into endothelial-muscle crosstalk and potential therapeutic strategies to mitigate chemotherapy-induced muscle and vascular damage.

Chapter 2 Literature Review

2.1 Skeletal Muscle and Health

Skeletal muscle represents approximately 40% of total body mass and plays a critical role in both physical function and metabolic health (40) Beyond its primary function of facilitating locomotion through contraction and force generation, skeletal muscle is essential for the regulation of glucose homeostasis, fatty acid metabolism, and protein turnover (41). As the body's primary reservoir for amino acids, muscle supports numerous physiological functions and contributes significantly to overall energy balance (40,42).

The maintenance of muscle mass is not only important for physical strength and mobility but is also closely linked to long-term health outcomes. Loss of muscle mass, whether due to aging (sarcopenia), disease, or inactivity, can impair quality of life and increase the risk of morbidity and mortality (43). Loss of muscle mass is often seen in chronic illnesses such as cancer or cardiovascular disease, where it is associated with worsened prognosis and increased complications (44,45). Therefore, developing strategies to maintain and strengthen skeletal muscle is crucial for overall health (43,46,47)

Given the importance of skeletal muscle for health, understanding the factors that regulate its maintenance and growth is essential. Muscle mass is primarily regulated by protein turnover, which is the continuous process of muscle protein synthesis (MPS) and muscle protein breakdown (MPB) (48,49). The balance between these two processes determines whether muscle mass is gained, maintained, or lost. When MPS exceeds MPB, muscle mass increases, leading to an anabolic state. Conversely, when MPB outpaces MPS, muscle mass declines, resulting in a catabolic state (50).

2.1.1 Factors Regulating Skeletal Muscle Anabolism

Skeletal muscle anabolism refers to the process of building and synthesizing muscle tissue. This process is critical for muscle growth and maintenance and is influenced by a combination of factors including nutrition, resistance exercise, and hormonal signaling (48,51). These factors interact to repair damaged fibers, promote hypertrophy, and sustain muscle mass, particularly in response to mechanical stress and the body's metabolic demands (52,53).

Nutrition and Resistance Exercise play an integral role in muscle anabolism. Adequate dietary protein intake, especially essential amino acids (EAAs), is necessary for the synthesis of new muscle proteins. Among the EAAs, branched-chain amino acids (BCAAs) leucine, isoleucine, and valine are particularly vital, with leucine being the most effective in stimulating anabolic pathways like mTORC1 (48). Resistance exercise complements these nutritional effects by imposing mechanical stress on muscle fibers, activating key anabolic signaling cascades. Studies demonstrate that resistance exercise increases muscle sensitivity to amino acids, enhancing protein synthesis when combined with post-exercise protein intake (48,54).

Growth Factors and Hormonal Regulation further amplify anabolic responses. Insulin-like growth factor 1 (IGF-1), secreted in response to growth hormone (GH), plays a pivotal role in muscle growth (55,56). IGF-1 activates the Akt/mTOR pathway, a major regulator of protein synthesis and cell growth, and promotes satellite cell activation, essential for muscle repair and regeneration (53,57). Testosterone also contributes significantly by increasing protein synthesis and reducing muscle protein breakdown (58,59). Post-exercise testosterone elevation enhances anabolic responses, driving hypertrophy over time (60). Additionally, insulin facilitates the uptake of amino acids into muscle cells and inhibits proteolysis, helping maintain a positive protein balance crucial for muscle growth (54,61).

2.1.2 Mechanisms Regulating Skeletal Muscle Growth and Anabolic Pathways

To increase anabolic state in skeletal muscle, hormones such as insulin, growth hormone, and testosterone must activate specific signaling pathways to enhance muscle protein synthesis (62,63). It is crucial to understand these pathways, as they play a significant role in long term growth and maintenance of muscle tissue. Skeletal muscle anabolism is coordinated by signaling through IGF1-Akt, Mechanistic (mammalian) Target of Rapamycin Complex 1 (mTORC1) (57,62,64–66).

2.1.2.1 IGF-Akt Pathway and Its Role in Muscle Anabolism

The IGF-Akt pathway is a critical signaling mechanism that promotes skeletal muscle anabolism by facilitating protein synthesis and inhibiting protein degradation (64,66–68). This pathway is initiated when insulin-like growth factor 1 (IGF-1) binds to its receptor on the muscle cell membrane (69). Upon binding, the receptor activates insulin receptor substrate 1 (IRS1), which undergoes phosphorylation and subsequently activates phosphoinositide 3-kinase (PI3K). PI3K generates the lipid messenger phosphatidylinositol 3,4,5-triphosphate (PIP_3), which recruits both Akt and 3-phosphoinositide-dependent protein kinase-1 (PDK1) to the plasma membrane. PDK1 phosphorylates Akt at threonine-308 (Thr308), while mTOR complex-2 phosphorylates Akt at serine-473 (Ser473) (70,71).

Once phosphorylated, Akt becomes fully activated and plays a pivotal role in transmitting anabolic signals (71). Akt promotes muscle growth by activating downstream targets that regulate protein synthesis, most notably mTORC1, while also inhibiting processes that lead to protein degradation, such as the FoxO transcription factors (53,72). By coordinating these processes, the IGF-Akt pathway ensures a balance between protein synthesis and breakdown,

contributing to the maintenance and growth of skeletal muscle in response to anabolic signals, such as exercise and nutrient intake (51,57) .

2.1.2.2 mTORC1 Signaling and Its Role in Muscle Anabolism

The mTORC1 pathway is the primary effector of the IGF-Akt signaling cascade and plays a central role in regulating muscle anabolism (55,70,72–75). As it illustrated in figure 2, insulin signaling through the insulin receptor substrate-1 (IRS-1) activates the phosphoinositide 3-kinase (PI3K)/Akt signaling pathway, subsequently activating mTORC1. Activated Akt inhibits the TSC1/TSC2 complex, which normally suppresses mTORC1 via inhibition of Rheb, a crucial activator of mTORC1 (76). Additionally, amino acids, particularly branched-chain amino acids (BCAAs), facilitate mTORC1 activation through the sestrin2/GATOR and Ragulator complexes, enabling the localization of mTORC1 to the lysosomal surface where it becomes fully activated (73,74).

Once activated, mTORC1 phosphorylates key downstream targets that promote protein synthesis, notably S6 kinase 1(S6K1) (77). Phosphorylated S6K1 increases ribosome biogenesis and translation efficiency, enhancing protein synthesis capacity essential for muscle growth and repair (78). Furthermore, mTORC1 phosphorylates the ribosomal protein S6, directly augmenting translational efficiency of specific mRNAs crucial for muscle cell hypertrophy (78,79). Another downstream target, 4E-BP1, when phosphorylated by mTORC1, releases eukaryotic initiation factor 4E (eIF-4E), allowing efficient initiation of mRNA translation and further supporting anabolic processes (80,81).

Together, the coordinated actions of insulin/IRS-1/Akt signaling, amino acid sensing, and subsequent activation of mTORC1 and its downstream effectors, including S6K1, S6, and 4E-BP1, ensure efficient muscle protein synthesis, maintenance, and hypertrophy (figure 2) (76,82).

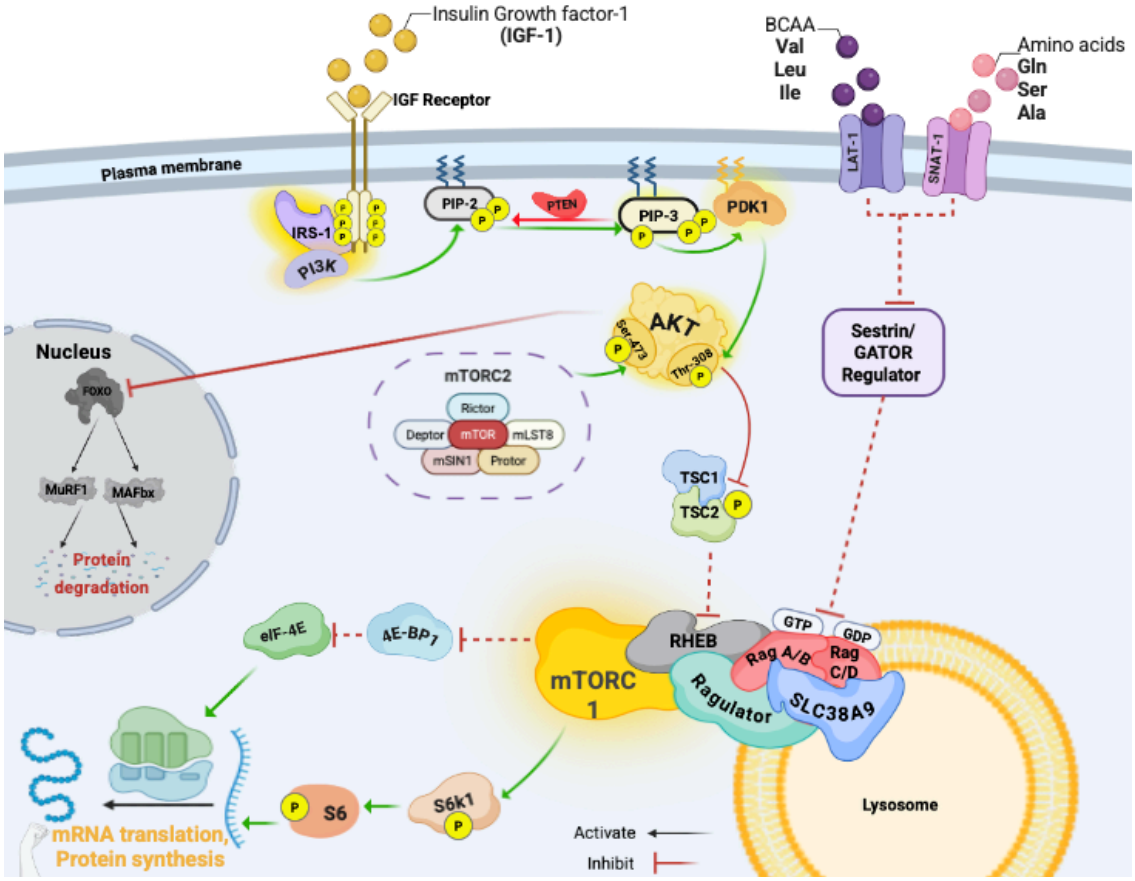

Figure 2. Integrated regulation of mTORC1 signaling in skeletal muscle anabolism. Insulin stimulation activates the IRS-1/PI3K/AKT signaling cascade, which inhibits the TSC1/TSC2 complex, relieving its suppression on Rheb, a direct activator of mTORC1. Simultaneously, amino acids, particularly BCAAs, promote mTORC1 translocation to the lysosomal membrane via the sestrin2/GATOR and Regulator complexes, enabling full activation. Activated mTORC1 phosphorylates downstream effectors such as S6K1, ribosomal protein S6, and 4E-BP1 to enhance ribosome biogenesis, mRNA translation, and protein synthesis, thereby supporting muscle growth and hypertrophy. Created with BioRender. Redrawn and inspired by Mann et al. (82).

2.1.2.3 Role of Capillaries and Endothelial Cells in Nutrient Transport and Muscle Anabolism

Capillaries, the smallest blood vessels, play a crucial role in the transport of nutrients and oxygen to muscle tissue and metabolic waste removal (83–86). They form an extensive network surrounding muscle fibers, ensuring efficient exchange of nutrients such as amino acids, glucose, and oxygen, which are essential for muscle anabolism (15,83,85–87). The muscle capillaries are formed a continuous endothelium. The endothelial cells cover the inner surface of these capillaries regulate the permeability of the capillary walls, controlling the passage of nutrients into the muscle (84). This process is vital for supporting protein synthesis, which fuels muscle growth and repair (88). In addition to nutrient delivery, capillaries are also responsible for removing metabolic waste products such as carbon dioxide, ammonia, and lactate, which accumulate during muscle activity. Efficient waste clearance is essential for maintaining cellular homeostasis and preventing metabolic stress. Therefore, proper nutrient delivery and metabolic waste removal are especially important during periods of increased metabolic demand, such as after resistance exercise or muscle injury (87,89,90).

In response to stimuli such as exercise, the capillary endothelium plays a key role in sensing changes in contractile activity and initiating vasodilation. Endothelial cells release nitric oxide (NO), a signaling molecule that induces vasodilation, defined as widening the blood flow, and thereby increases blood flow to active muscles, boosting oxygen and nutrient delivery to sustain muscle anabolism (91–93). Additionally, endothelial cells also drive angiogenesis, the formation of new capillaries, which becomes especially important during muscle hypertrophy when enlarging fibers require a richer nutrient supply (94–96). This vascular adaptation ensures that muscle tissue is well-supplied and capable of maintaining an anabolic state over time.

2.1.3 Factors Regulating Skeletal Muscle Catabolism

Muscle catabolism refers to the breakdown of muscle tissue, where protein degradation exceeds protein synthesis, leading to a loss of muscle mass and strength (97,98). This process is particularly prominent in conditions such as aging and muscle disuse, where anabolic signaling pathways become downregulated, while catabolic processes dominate (98–100). Key drivers of muscle catabolism include the activation of the ubiquitin-proteasome system (UPS) and the autophagy-lysosome pathway, which promote the breakdown of muscle proteins (98,100). The imbalance between muscle protein synthesis and degradation results in the gradual loss of muscle fibers, leading to muscle atrophy. Two of the most common contributors to this state of muscle breakdown are aging and physical inactivity, which can occur due to a lack of muscle use or immobilization (97–101).

2.1.3.1 Aging and Sarcopenia

As individuals age, the risk of muscle catabolism increases significantly, a condition referred to as sarcopenia (102,103). This age-related muscle wasting is driven by a decline in anabolic pathways such as the IGF-Akt-mTORC1 signaling cascade. With advancing age, the Akt signaling becomes less efficient, leading to the activation of FoxO transcription factors, which stimulate the expression of genes involved in protein degradation. These factors promote the ubiquitin-proteasome system (UPS), a primary mechanism of protein breakdown, and the autophagy-lysosome pathway, which contributes to the degradation of cellular components (104,105).

In addition to these molecular changes, aging is often associated with chronic low-grade inflammation, a condition known as inflammaging. Pro-inflammatory cytokines, such as TNF-α and IL-6, become elevated with age, further enhancing catabolic pathways (24,29,30,106,107).

This increase in inflammation suppresses anabolic signaling, exacerbating muscle degradation and reducing the body's ability to maintain muscle mass. The result is a steady decline in muscle size and strength, contributing to frailty, decreased mobility, and reduced quality of life in elderly populations (24,26,27,29–31,39,106,107).

2.1.3.2 Muscle Disuse and Atrophy

Muscle disuse is another significant contributor to muscle catabolism, occurring when muscles are not actively engaged over a prolonged period (108,109). This condition is commonly observed in individuals experiencing prolonged bed rest, immobilization due to injury, or leading sedentary lifestyles (108,109). When muscles are not used regularly, anabolic signaling, particularly through the mTORC1 pathway, is significantly reduced. This decline in protein synthesis creates an imbalance where muscle protein breakdown becomes more prominent, leading to muscle atrophy (101,108,110).

Disuse also results in increased expression of myostatin, a negative regulator of muscle growth, which further inhibits the mTORC1 pathway and prevents muscle recovery and growth (111–114). The reduction in muscle activity also decreases blood flow and nutrient delivery to muscle tissue, impairing the muscle's ability to sustain protein synthesis (115,116). Over time, this leads to a loss of muscle mass, strength, and endurance (115,117). In cases of long-term disuse, the effects can be severe, leading to significant muscle wasting and impaired physical function, which is difficult to recover from without targeted interventions (117–122).

2.1.3.3 Chemotherapy-Induced Muscle Atrophy

The FOLFIRI chemotherapy drug cocktail consisting of CPT-11 (irinotecan), 5-fluorouracil, and leucovorin contributes to skeletal muscle atrophy through its cytotoxic effects

(123). Chemotherapy drug cocktail provokes oxidative stress and systematic inflammation leading to the activation of catabolic pathways such as the ubiquitin proteasome and autophagy (123,124). Proinflammatory cytokines, including TNF-α and IL-6, rise during treatment, further accelerating muscle protein degradation while suppressing anabolic signaling and producing substantial muscle loss (24–27,29,30). This depletion of muscle mass contributes to cancer cachexia; a complex syndrome defined as muscle wasting and disrupted metabolic homeostasis. (5,24,26,29,125). Notably, it is critical to recognize that muscle degradation does not begin solely with chemotherapy treatment (126). Tumors themselves secrete pro-inflammatory cytokines such as TNF-α and IL-6, which contribute to systemic inflammation and activate catabolic signaling in skeletal muscle, the combination of chemotherapy driven and tumor related inflammatory mechanisms produce a synergistic effect that accelerates muscle loss and limits the capacity for repair (25,27,32,106,127).

2.1.3.4 Overlap Between Catabolic Conditions

Although sarcopenia, muscle disuse, and chemotherapy-induced muscle loss are caused by different factors, they share several key molecular pathways that leads to skeletal muscle wasting (99,118,128). In all three conditions, FoxO transcription factors become activated and stimulates the expression of Atrogin-1 and Murf1, two enzymes involved in breaking down muscle proteins (97,105). This results in increased activity of the ubiquitin-proteasome and autophagy-lysosome pathways which are responsible for protein degradation. Moreover, chronic inflammation characterized by elevated levels of pro-inflammatory cytokines, further amplifies catabolic process in skeletal muscle.

This occurs in part through activation of the JAK/STAT3 pathway, where phosphorylated STAT3 up regulates catabolic pathways such as atrogin-1, and MuRF1, thereby accelerating the ubiquitin-proteasome system and autophagy while diminishing protein synthesis (24,31,101,107). Furthermore, TNF-α signals through TNF-R1 to generate reactive oxygen species and activate NF-κB, which likewise increases UPS component expression and suppresses mTORC1-mediated anabolism (24,105–107,112). These cytokine-driven catabolic cues are compounded by chemotherapy-related oxidative stress that further impairs mitochondrial function and promotes proteolysis. Continuous activation of IL-6-STAT3 and TNF-α-NF-κB signaling contributes to the progressive cachexia seen in many patients undergoing chemotherapy (25,27,29,106,124,129,130).

2.2 Endothelial Cells and Their Role in Vascular and Skeletal muscle

2.2.1 Skeletal Muscle Microvasculature

Skeletal muscle contains a dense and intricately organized microvascular network that is essential for sustaining its high metabolic demands (131). This network is composed primarily of capillaries, small-diameter vessels formed by a single layer of endothelial cells surrounded by a basement membrane and pericytes (131,132). These capillaries are closely aligned with individual muscle fibers, enabling efficient exchange of oxygen, glucose, amino acids, and other metabolites between blood and muscle tissue (83,85).

The capillary-to-fiber ratio varies across muscle types, with oxidative (type I) fibers exhibiting higher capillary density than glycolytic (type II) fibers, reflecting their differential reliance on aerobic metabolism (133,134). At rest, only a portion of these capillaries are

perfused, but during exercise or stress, perfusion increases dramatically through the opening of previously non-flowing capillaries and increased red blood cell velocity. Although capillaries themselves cannot vasodilate, they respond dynamically to changes in flow and metabolic cues via endothelial signaling (86,135,136). The functional integrity of the capillary network plays a crucial role in skeletal muscle performance, as capillarization significantly impacts oxygen and nutrient delivery to muscle fibers, supports mitochondrial density, and enhances the muscle's oxidative capacity (87,131,133,134,137).

In addition to nutrient and oxygen delivery, capillaries play an active role in immune surveillance and inflammatory regulation. Endothelial cells within the capillary wall sense inflammatory cytokines such as TNF-α and IL-6, which trigger signaling cascades that modulate vascular tone and permeability (27,29,138–141). This increased permeability facilitates the extravasation of immune cells from the circulation into the muscle interstitium during injury or infection (28–30,138–141). Moreover, endothelial cells express adhesion molecules (e.g., ICAM-1, VCAM-1) in response to inflammatory stimuli, promoting leukocyte adhesion and transmigration. Through these mechanisms, the capillary network serves not only as a pathway for nutrient exchange but also as a key regulator of immune cell trafficking and local inflammatory responses in skeletal muscle (27,29,138–141).

2.2.2 Endothelial Cells in Microvascular Regulation

Angio-adaptation refers to the dynamic and coordinated remodeling of the skeletal muscle microvasculature in response to physiological stimuli (137,142,143). This process is regulated by two key cellular players: skeletal muscle fibers, which release angiogenic factors (angiokines), and skeletal muscle endothelial cells (SMECs), which respond to these cues and

serve as the principal structural and functional components of capillaries. This bidirectional communication ensures that vascular remodeling is closely aligned with the metabolic and functional demands of the muscle (96,137,142–144). Beyond nutrient regulation, endothelial cells serve as paracrine signaling, secreting growth factors and cytokines that influence nearby myofibers and immune cells. Through crosstalk with muscle tissue, endothelial cells contribute to fiber maintenance, muscle tone, and basal trophic support. These microvascular regulatory functions underpin the muscle's capacity to adapt to both physiological and pathological stimuli, establishing endothelial cells as key guardians of skeletal muscle homeostasis (131,133,135,137,145–147).

2.2.3 Endothelial Response to Mechanical Stimuli and Muscle Health

Endothelial cells are highly responsive to mechanical stimuli, such as shear stress from blood flow and mechanical loading during exercise. These forces stimulate the production of vasodilators like NO, which improve blood flow, and growth factors like VEGF, which promote angiogenesis, the formation of new capillaries. Angiogenesis is essential for maintaining vascular networks in skeletal muscle, particularly during hypertrophy or repair following exercise or injury (90,93,148–152) .

Endothelial cells also interact directly with skeletal muscle fibers, supporting muscle growth and repair by ensuring adequate nutrient and oxygen supply. This interaction is mediated through signaling pathways, such as VEGF-driven angiogenesis and NO pathways, which enhance vascular and metabolic support for muscle tissues (131,137,148,149,153). Importantly, the Akt pathway plays a central role in these processes. Akt activation in skeletal muscle promotes VEGF-A expression (154). while in endothelial cells, Akt signaling facilitates NO

synthesis through phosphorylation of endothelial nitric oxide synthase (eNOS) and supports endothelial survival, migration, and lumen formation (155,156). Through its downstream effectors, including mTOR, Akt integrates angiogenic and anabolic signals, linking vascular remodeling with muscle protein synthesis and growth (154,156,157)

Additionally, endothelial cells rely on autocrine VEGF-A signaling to maintain survival, regulate metabolism, and promote angiogenic behavior under stress conditions (156,158–160). This autocrine loop ensures sustained endothelial function and vascular stability during periods of high metabolic demand, further supporting skeletal muscle homeostasis (156–160).

2.2.4 Endothelial Mediated Signaling Pathways in Skeletal Muscle Health

VEGF plays a central role in endothelial-mediated support for skeletal muscle health. Produced by endothelial cells in response to physical activity and low oxygen levels, VEGF stimulates angiogenesis, ensuring that growing or repairing muscle tissue has sufficient vascular supply to meet metabolic demands. This process is particularly important during muscle hypertrophy and recovery (82).

Among angiogenic regulators, VEGF-A functions as a potent pro-angiogenic signal, whereas Thrombospondin-1 (THBS-1) exerts angiostatic effects. Experimental deletion of VEGF-A in skeletal muscle reduces capillary density and impairs endurance performance, underscoring its critical role in vascular remodeling. In contrast, THBS-1 deletion has been associated with increased capillarization, reinforcing its function as a negative regulator of skeletal muscle angio-adaptation (143,144,161).

Disruptions in these signaling pathways, whether through inflammation, oxidative stress, or therapeutic interventions such as chemotherapy, can compromise endothelial function and

contribute to skeletal muscle dysfunction. These maladaptive changes are explored further in the following sections.

2.3 Endothelial Dysfunction and Muscle Atrophy

2.3.1 Chemotherapy-Induced Endothelial Dysfunction

Chemotherapy-induced stress in endothelial cells often activates the p53 pathway, a key regulator of cellular responses to DNA damage. Upon activation, p53 upregulates p21, a cyclin-dependent kinase inhibitor that induces cell cycle arrest or apoptosis. This response compromises endothelial integrity, contributing to capillary rarefaction and impaired muscle perfusion (162).

Chemotherapy has been shown to damage vascular endothelial cells, leading to impaired blood vessel function and reduced nitric oxide (NO) availability, and triggers vascular inflammation, all of which negatively impact skeletal muscle health (14,149,163). These changes disrupt the balance of vascular homeostasis and reduce delivery of oxygen and nutrient to skeletal muscle. As a result, endothelial apoptosis, inflammation, and impaired blood vessel function exacerbate the loss of skeletal muscle mass during cancer treatment (14,164).

2.3.1.1 Endothelial Apoptosis and Vascular Complications (14,149,163)

Chemotherapy induces oxidative stress in endothelial cells, generating excessive reactive oxygen species (ROS) that damage cellular components, including mitochondrial membranes, nuclear DNA, and cytoskeletal proteins (14,163,165). This oxidative burden promotes endothelial apoptosis, compromising vascular integrity and reducing capillary density. As a result, reduced blood flow makes it harder for muscles to get enough oxygen and nutrients, which leads to further muscle loss (14,163).

Furthermore, endothelial apoptosis disrupts angiogenic signaling pathways, such as those mediated by vascular endothelial growth factor (VEGF), thereby reducing the muscle's capacity to adapt to physiological stress or injury. VEGF plays a critical role in endothelial survival through autocrine signalling mechanisms that regulates metabolism and autophagy (147,149,166). Nitric oxide (NO), another key signaling molecule, also supports endothelial cell function by promoting vasodilation and cellular resilience. Chemotherapy-induced depletion of NO impairs vasodilation and contributes to inadequate nutrient delivery, creating a hypoxic and nutrient-deficient environment that accelerates atrophy (149,166).

2.3.1.2 Increased Inflammation and Cytokine Release

Endothelial cells subjected to chemotherapy increase their production of pro-inflammatory cytokines such as interleukin-6 (IL-6), tumor necrosis factor-alpha (TNF-α), and interleukin-1 beta (IL-1β) (14,23,25,138,139,141,167). These cytokines perpetuate vascular inflammation, further compromising endothelial function. The release of inflammatory mediators also activates systemic catabolic pathways, such as the ubiquitin-proteasome system (UPS) and autophagy-lysosome pathways, which drive muscle protein degradation (23,138,141,168).

Increased cytokine release from dysfunctional endothelial cells contributes to the recruitment and activation of immune cells, amplifying the inflammatory environment. This inflammation suppresses anabolic signaling in skeletal muscle by inhibiting the Akt/mTOR pathway while promoting the activation of FOXO transcription factors and muscle-specific E3 ligases, such as MuRF1 and Atrogin-1 (14,23,25,138,139,141,167). The combined effects of vascular inflammation and cytokine release create a feedback loop that exacerbates both endothelial dysfunction and muscle atrophy.

2.3.2 Endothelial-Myotube Crosstalk and Chemotherapy-Induced Muscle Atrophy

The interaction between endothelial cells and skeletal muscle fibers is crucial for coordinating muscle maintenance. Thos intercellular crosstalk involves the steady exchange of growth factors, cytokines, and nutrients, endothelial cells help to regulate muscle protein synthesis, angiogenesis, and metabolic demand (151). This cooperative signaling network allows endothelial cells to actively support muscle health through the secretion of anabolic mediators such as IGF-1 and VEGF (169–171).

Chemotherapy disrupts this communication by impairing endothelial function, reducing availability of these signals, and weakening nutrient support to myofibers (169–171). Even in the absence of direct myofiber damage, this breakdown in vascular muscle signaling compromises anabolic pathways and contributes to the progression of muscle atrophy (123,169).

2.3.2.1 Chemotherapy-Induced Disruption of Protein Synthesis

Endothelial dysfunction induced by chemotherapy interferes with the delivery of key nutrients and signaling molecules required for muscle protein synthesis. Endothelial cells produce growth factors, such as insulin-like growth factor-1 (IGF-1), which activate anabolic signaling pathways in skeletal muscle, including the AKT/mTOR axis (123,148,168,172). Chemotherapy reduces the secretion of these factors, suppressing muscle protein synthesis and contributing to muscle atrophy (14,122,173).

Moreover, vascular dysfunction impairs the transport of amino acids, glucose, and oxygen to muscle fibers, which are essential substrates for protein synthesis and energy production (53,72,122,174). Reduced capillary perfusion and nutrient transport hinder the ability of skeletal muscle to repair and grow, particularly during periods of metabolic stress or following

exercise. The diminished supply of nutrients exacerbates the muscle's catabolic state, accelerating the loss of muscle mass and function (53,72,122,174).

2.3.2.2 Endothelial-Mediated Catabolic Pathways

Endothelial dysfunction promotes catabolic signaling pathways in skeletal muscle through the release of inflammatory cytokines and ROS. Studies have shown that exposure of endothelial cells to TNF-α and IL-1β leads to elevated ROS levels and FOXO1 activation, which upregulates the expression of muscle specific E3 Ligases such as MuRF1 and Atrogin-1 in neighboring muscle cells (23,101,105,175). Additionally, ROS generated in endothelial cells under stress can impair nitric oxide signaling and activate FOXO-dependent pathways that promote proteolysis in muscle tissue. This leads to the induction of the ubiquitin-proteasome system and enhanced autophagy, contributing to the degradation of cellular proteins and organelles (61,114,121,138).

In addition to these catabolic signaling cascades, the BCKD (branched-chain α-ketoacid dehydrogenase) complex controls BCAA oxidation and is regulated by phosphorylation through BCKD kinase (BDK). Changes in BCKD activity or phosphorylation status within endothelial cells may alter BCAA flux, energy production, and nutrient signaling, potentially affecting muscle metabolism during stress conditions such as chemotherapy (82).

In parallel, dysfunctional endothelial cells impair angiogenesis by disrupting VEGF signalling (143,150,177). Chemotherapy suppresses VEGF signaling, limiting the ability of muscle tissue to adapt to increased metabolic demands (92,176,178).For instance, studies have shown that treatment with agents such as doxorubicin or 5-flurouracil significantly reduces VGEF-A expression in endothelial cells, leading to impaired angiogenesis and reduced capillary density in muscle tissue (169,179). This downregulation is mediated through increased oxidative

stress and suppression of HIF-1α, a key transcription factor that drives VEGF-A expression under hypoxic conditions (169,179). The resulting impairment of vascular remodeling restricts nutrient and oxygen supply to growing or regenerating myofibers, further worsening muscle atrophy.

Chapter 3 Rationale, Objective and Hypotheses

3.1 Rationale

The overarching goal of this thesis is to investigate how a combination of chemotherapy drugs (CPT-11, 5-FU, and leucovorin) and pro-inflammatory cytokines (IL-6 and TNF-α) affect skeletal muscle cells and skeletal muscle-derived endothelial cells, examining their impact on anabolic signaling, amino acid metabolism, and cellular stress responses under different conditions. IL-6 and TNF-α were included to mimic the inflammatory environment present in cancer and during chemotherapy, where elevated circulating cytokines activate STAT3- and NF-κB-mediated catabolic pathways in skeletal muscle. Incorporating these cytokines allowed the in-vitro model to better represent the combined cytotoxic and inflammatory stress that contributes to muscle wasting in vivo. Treatments were applied at two concentrations, full dose (equivalent to concentration used in C2C12 models) and half of this concentration, across two time points (24 h and 48 h) to capture both immediate and progressive effects. A post-treatment recovery phase was also included to determine whether cellular function, assessed using the same markers, could partially rebound after drug withdrawal. While the interaction between these cell populations is of growing interest, this thesis examines them independently to establish foundational knowledge that can inform future studies on their potential crosstalk.

Previous work in our laboratory has shown that chemotherapy disrupts anabolic signaling, amino acid transport, and myotube morphology in L6 myotubes. Building on these findings, the present study investigates similar outcomes in C2C12 myotubes while expanding the model to include primary skeletal muscle derived endothelial cells, inflammatory cytokines, and a defined recovery phase. These additions allow the study to explore chemotherapy related

muscle loss within a broader biological context, incorporating both muscle cells and the microvascular environment.

3.2 Objectives

This research focused on two primary experimental models: C2C12 myotubes and skeletal muscle endothelial cells. For C2C12 myotubes, the objective was to evaluate the impact of chemotherapy and cytokines on myotube morphology, anabolic signaling pathways, BCAA metabolism, and amino acid transporter expression across treatment durations, and to assess how these markers behaved after treatment withdrawal during the recovery phase. For endothelial cells, the objective was to determine the response of stress-related signaling markers (p53, p21) to chemotherapy and cytokine treatment at both full and half doses, as well as to examine whether these markers returned toward baseline following drug removal. Together, these objectives aimed to capture both immediate and recovery-phase adaptations in two distinct but interrelated cell types, providing insight into cell-specific responses to chemotherapeutic and inflammatory stressors.

3.3 Hypothesis

1. This study hypothesizes that exposure to a chemotherapy drug cocktail combined with inflammatory cytokines will impair cellular homeostasis in both skeletal muscle myotubes and endothelial cells through disruptions in protein turnover and stress-response pathways.
2. In C2C12 myotubes, treatment will reduce myofibrillar protein abundance, disrupt anabolic signaling, and alter amino acid metabolism.

3. During the recovery phase, markers of anabolic signaling and amino acid metabolism in C2C12 myotubes are expected to show partial reversal toward baseline, with incomplete recovery after full-dose treatments compared to half-dose treatments.
4. In endothelial cells, treatment will activate stress-related pathways, reflected by increased expression of p53 and p21
5. Full-dose treatments in endothelial cells are anticipated to induce a more pronounced stress response and exhibit less recovery compared to half-dose treatments, demonstrating a dose- and time-dependent effect, with greater impairments expected at 48 hours than at 24 hours.
6. During the recovery phase, stress marker expression (p53, p21) in endothelial cells is expected to decline toward baseline, with more complete recovery after half-dose treatments compared to full-dose treatments.

Chapter 4

CATABOLIC EFFECTS OF CHEMOTHERAPY DRUGS-INFLAMMATORY CYTOKINES COMBINATION ON C2C12 MYOTUBES AND SKELETAL MUSCLE MICROVASCULAR ENDOTHELIAL CELLS

Armita Helforoush[1] , Olasunkanmi A.J. Adegoke[1]

Muscle Health Research Centre, School of Kinesiology and Health Science, York University, Toronto, ON, M3J 1P3

Corresponding Author: Dr. Olasunkanmi A.J. Adegoke

Muscle Health Research Centre, School of Kinesiology and Health Science, York University, Toronto, ON, Canada. Tel: 416-7362100 Ext 20887. Fax: 416-736- 5774. Email: oadegoke@yorku.ca

Keywords: Cachexia, Chemotherapy, Inflammatory Cytokines, BCAA Metabolism,

Figures: 8

4.1 Materials and Methods

4.1.1-Reagents

For C2C12 cells, Dulbecco's Modified Eagle's Medium (DMEM) was purchased from Sigma Aldrich (#D5796-500). Growth media (GM) was made by supplementing DMEM with 10% fetal bovine serum (FBS 12483-020,) and 1% Antibiotic and Antimycotic reagent (#15240-062) purchased from Gibco. Differentiation media (DM) was made by supplementing 1% Antibiotic-Antimycotic and 2% horse serum (#26050088) purchased from Gibco. Phosphate buffered saline (PBS #311-010-CL) and trypsin (25200-056) were purchased from Gibco. Protease inhibitor cocktail (#P8340), Phosphate (#P5726) inhibitor cocktail, interleukin-6 (IL6, #19646), irinotecan hydrochloride (CPT-11, #I1406), 5-Flurouracil (5-FU, #F6627), folinic acid calcium salt hydrate (Leucovorin, #F7878) and dimethyl sulfoxide (DMSO, #D5879) were purchased from Sigma Aldrich. TNF-Alpha was purchased from R&D systems (#80-235). Radioactive valine (^{14}C -valine, #ARC0678) was purchased from American radiolabelled chemicals.

For the primary skeletal muscle microvascular Endothelial cells, the medium was prepared using Endothelial Cell Medium with Supplement Kit (Cell Biologics, Cat. No. M1168). The supplement kit included: Endothelial Cell Growth Supplement (0.5 mL), heparin (0.5 mL), fetal bovine serum (FBS, 25 mL), antibiotic-antimycotic solution (5 mL), vascular endothelial growth factor (VEGF, 0.5 mL), Epidermal Growth Factor (EGF, 0.5 mL), and Hydrocortisone (0.5 mL). In addition, 5ml of GlutaMAX (Gibco, Cat. No. 35050-061) was added to the 500 ml of media. Trypsin, included in the kit, was used for subculturing the endothelial cells. Gelatin Type A (BioShop, Cat. No. 771.500) was used to coat culture flasks. PBS, trypsin, protease and

phosphatase inhibitor cocktails, IL-6, TNF-α, CPT-11, 5-FU, Leucovorin, and DMSO were the same as described above for C2C12 cells.

4.1.2-Cell Culture Procedure for C2C12 Myotubes and Endothelial Cells

C2C12 mouse myoblasts were obtained from ATCC (CRL-1772). These myoblasts were cultured in growth medium (GM) and incubated at 37°C with 5% CO_2. When cells reached 70-80% confluency, they were subcultured, typically every other day. Two days before the experiment began (day -2), cells were plated in 6-well plates (with a surface area of 9.5 cm^2) at a density of 200,000 cells per well, corresponding to approximately 31,000 cells/cm^2 for western blot and BCKD assay. For immunofluorescence studies, cells were seeded 12-well plates (with a surface area of 3.8 cm^2) at a density of 100,000 cells per well, which also corresponds to approximately 31,000 cells/cm^2. Once confluency was achieved (day 0), the medium was switched to differentiation medium (DM). The horse serum in DM, which has less proliferative factors compared to that of FBS, slows down the proliferation of myoblasts, providing the ability for myotubes to differentiate rather than proliferate. This medium was replaced every 48 hours until day 5, by which time myotubes were fully formed and prepared. schematic summarizing this procedure is shown in figure 4.1.

Primary skeletal muscle microvascular endothelial cells derived from C57BL/6 mouse skeletal muscle (Cell Biologics, Cat. No. C57-6220) were received cryopreserved at passage 3. Cells were thawed in a 37°C water bath and transferred into T75 flasks pre-coated with 1.5% Gelatin Type A (BioShop, Cat. No. GEL771.500). For details on the coating procedure, refer to Appendix F. Cells were cultured in growth media prepared using the Endothelial Cell Medium

with Supplement Kit and were expanded up to passage 6 for experiments and seeded at a density of 9,500 cells/cm², corresponding to approximately 57,000 cells per well in 6-well plates and ~712,500 cells per T75 flask.

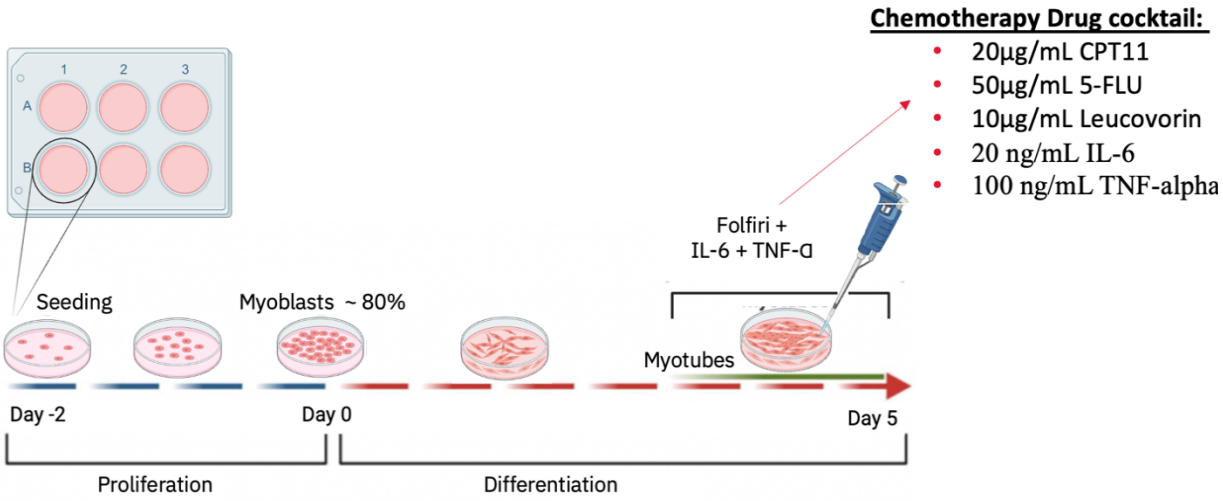

Figure 4.1. Summary of C2C12 myotube culture and treatment protocol. C2C12 myoblasts were seeded in 6-well plates at day –2 and maintained in growth medium until ~80% confluency (day 0), after which differentiation medium was introduced to promote myotube formation. Differentiation continued until day 5, when fully formed myotubes were treated with a chemotherapy drug cocktail (FOLFIRI) and inflammatory cytokines. Created with BioRender.

4.1.2.1 Chemotherapy and Cytokine Treatments

This study used FOLFIRI chemotherapy regimen, consisting of CPT-11, 5-fluorouracil (5-FU), and leucovorin. Stock solutions were prepared by dissolving 50 mg of CPT-11 and 50 mg of 5-FU each in 1 mL of DMSO, while 20 mg of leucovorin was dissolved in 1 mL of double-distilled water (ddH_2O). For cytokines, 5,000 ng of interleukin-6 (IL-6) and 25,000 ng of

tumor necrosis factor-alpha (TNF-α) were each dissolved in 1 mL of ddH_2O. The concentrations used for chemotherapy drugs and cytokines in this study were selected based on previous in vitro work modeling clinically relevant plasma levels observed in patients receiving FOLFIRI treatment, which have been shown to induce metabolic and catabolic responses in skeletal muscle and endothelial cells (4,22,27,28,31–39). The cytokine concentrations (20 ng/mL IL-6 and 100 ng/mL TNF-α) were chosen based on commonly used ranges reported in multiple studies that model inflammatory conditions in skeletal muscle and endothelial cell cultures ((24,28,33,38)).

On day 5 of differentiation, C2C12 myotubes were treated in 6-well plates with 2 mL per well of a differentiation medium containing the chemotherapy-cytokine cocktail. The final concentrations used were 20 µg/mL CPT-11, 50 µg/mL 5-FU, 10 µg/mL leucovorin, 20 ng/mL IL-6, and 100 ng/mL TNF-α (24,33,35–38,107). Treatments were applied for either 24 hours (DC-24) or 48 hours (DC-48). A recovery condition (DC+Rec) involved 24 hours of treatment followed by PBS wash and a 24-hour incubation in fresh, drug and cytokine-free differentiation media to assess the potential for recovery. The experimental design for C2C12 cells is illustrated in **figure 4.2**

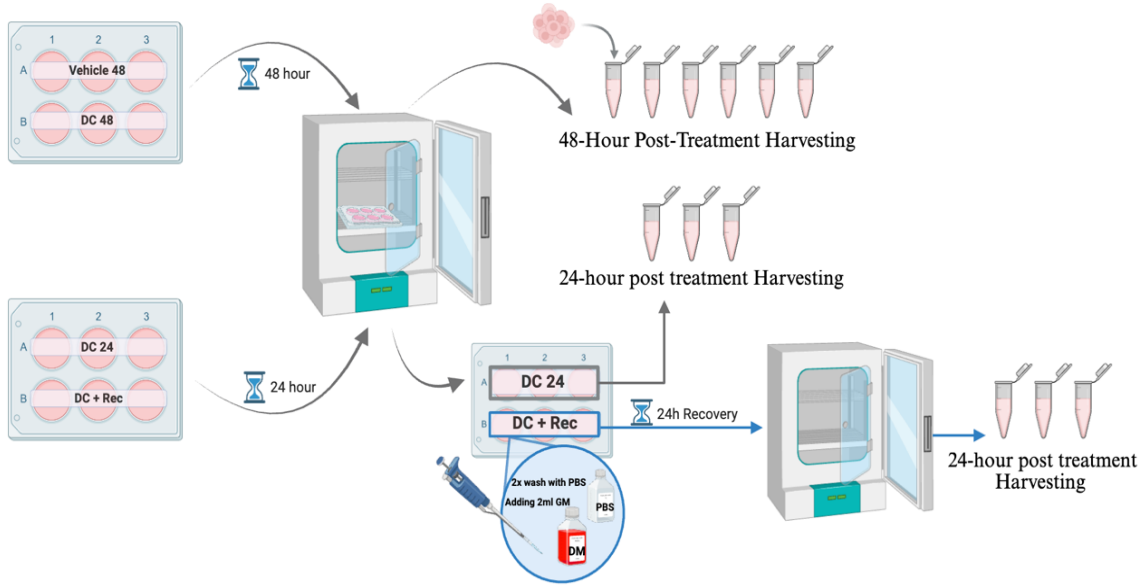

Figure 4.2 Experimental design for C2C12 myotube treatments and harvesting timeline. On day 5 of differentiation, C2C12 myotubes were treated in 6-well plates with 2 mL per well of differentiation medium containing a chemotherapy-cytokine cocktail (CPT-11: 20 µg/mL, 5-FU: 50 µg/mL, leucovorin: 10 µg/mL, IL-6: 20 ng/mL, and TNF-α: 100 ng/mL). Treatments were administered for either 24 hours (DC-24) or 48 hours (DC-48). A recovery condition (DC+Rec) consisted of 24 hours of drug exposure followed by two PBS washes and a 24-hour incubation in drug- and cytokine-free differentiation medium to assess recovery potential. Following the designated incubation periods, myotubes were harvested for analysis at 24 hours, 48 hours, or 24 hours post-recovery. Created with BioRender.

Endothelial cells were treated with the same chemotherapy and cytokine combination at either full dose (100%) or half dose (50%). The 100% dose matched the concentrations used for C2C12 myotubes, while the 50% cocktail contained 10 µg/mL CPT-11, 25 µg/mL 5-FU, 5 µg/mL leucovorin, 10 ng/mL IL-6, and 50 ng/mL TNF-α. Each well contained 2 mL of endothelial growth medium with the appropriate drug combination. Stock volumes were calculated and added directly to the medium as described in Appendix A.

Endothelial cell treatments were organized into the following conditions: vehicle control (V), half-dose treatment (DC-Half) or full-dose treatment (DC-Full) for 24 or 48 hours, and recovery conditions following each treatment. In recovery conditions, cells were washed twice with PBS after treatment and incubated in normal endothelial growth medium for 24 hours. As a result, the total duration was 48 hours for 24-hour treatment followed by recovery and 72 hours for 48-hour treatment followed by recovery. The experimental design for endothelial cell treatments is illustrated in figure 4.3.

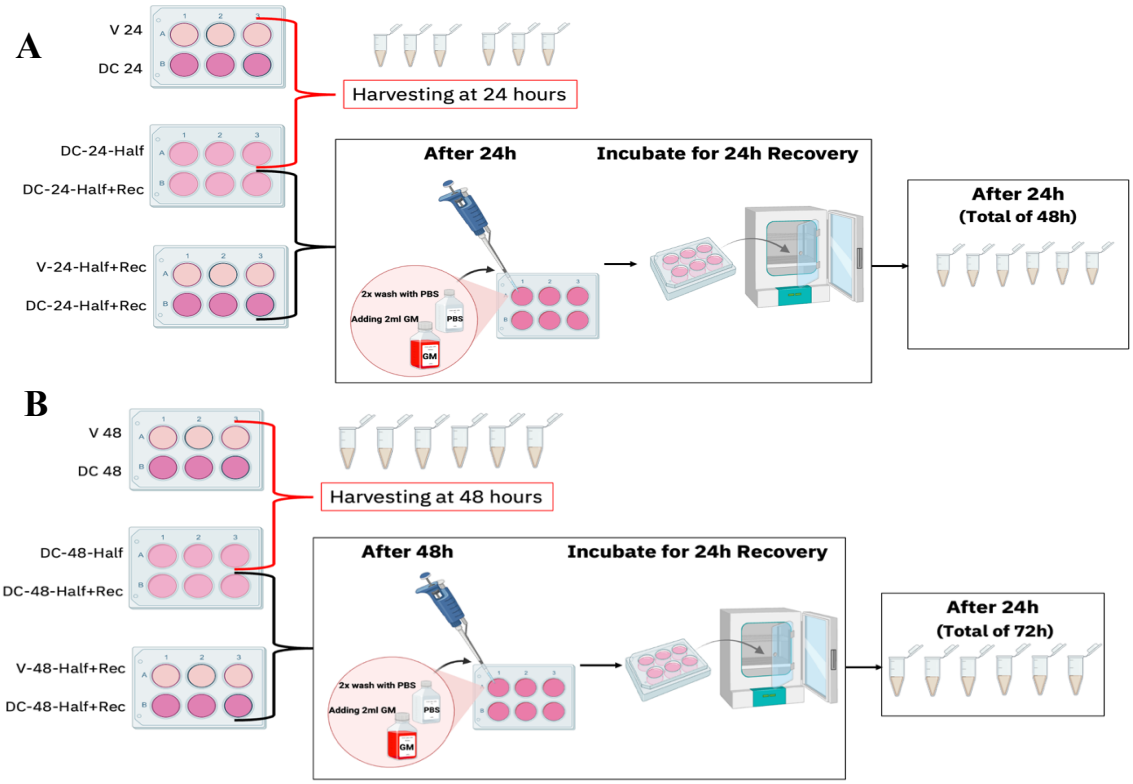

Figure 4.3 Schematic representation of the endothelial cell experimental design. figure **A** shows the 24-hour treatment groups, and figure **B** shows the 48-hour treatment groups. Endothelial cells were exposed to chemotherapy drugs (CPT-11, 5-FU, leucovorin) and inflammatory cytokines (TNF-α, IL-6) at two different concentrations: 50% (DC-Half) and 100% (DC-Full), corresponding to half and full doses, respectively. In recovery conditions (DC+Rec), cells were first treated for 24 or 48 hours, then washed twice with PBS and incubated with normal drug- and cytokine-free endothelial growth media for an additional 24 hours. This resulted in a total treatment period of 48 hours for 24h + recovery groups and 72 hours for 48h + recovery groups.

4.2 Harvesting Cells and Western Blotting

Myotubes in each treatment were washed in 1mL PBS and 100µL lysed (lysis buffer containing 1mM EDTA, 2% SDS, 25 mM Tris-HCL pH 7.5, 10µL/mL protease inhibitor cocktail, 10µL/mL phosphatase inhibitor cocktail, and 1mM DTT). A scraper was utilized to gather the cells and Cell lysates were repeatedly passed through a 1mL syringe, prior to being stored at -20 until analysis. Protein concentration of each sample was determined by using the Pierce BCA Protein Assay Kit (Thermo fisher, cat#23225). Samples (~25ug) were loaded onto 10 or 15% SDS-PAGE gels, with the chosen percentage based on the molecular weights of the proteins being studied. Following the gel electrophoresis, proteins were transferred onto PVDF membranes. The effectiveness of the transfer was determined via Ponceau S staining.

Molecular weight markers (in kDa) were annotated on each Ponceau-stained membrane to verify transfer efficiency and confirm band migration prior to blocking. The same membrane was reused only when the target proteins had different molecular weights, ensuring that previously detected bands did not overlap with the new targets. In such cases, membranes were washed several times with TBST before incubation with a new primary antibody. When additional proteins of similar molecular weights were required, new membranes were run using the same set of samples and replicates to maintain consistency in data comparison. This approach ensured accurate detection across all proteins while preserving membrane integrity and reproducibility of results.

All membranes were blocked in a solution of 5% milk powder in TBST at room temperature for 1h. The membranes were then washed in TBST (3x5 minutes), followed by an overnight incubation at 4°C with primary antibodies of interest seen below:

Primary Antibody	Dilution	Purchased from	Secondary Antibody
Gamma-Tubulin	1:1000	Sigma Aldrich #T6557	Anti-Mouse
MHC	1:500	DSHB #MF-20	Anti-Mouse
Troponin	1:400	DSHB (JLT-12)	Anti-Mouse
Tropomyosin	1:400	DSHB (CH1)	Anti-Mouse
Ph-S6K1 (Thr389)	1:1000	Cell Signaling (#9234)	Anti-Rabbit
Ph-S6 (Ser235/6)	1:2000	Cell Signaling #4858	Anti-Mouse
Ph-Akt (Ser473)	1:2000	Cell Signaling #4060	Anti-Rabbit
BCAT2	1:1000	ProteinTech #16417-1-AP	Anti-Rabbit
BCKD	1:1000	Sigma Aldrich #90198	Anti-Rabbit
Ph-BCKD (Ser293)	1:1000	Sigma Aldrich #40368	Anti-Rabbit
BDK	1:1000	Thermo Fisher #PA5-31455	Anti-Rabbit
Akt	1:1000	Cell Signaling #4691	Anti-Rabbit
S6K1	1:1000	Cell Signaling #9202	Anti-Rabbit
SNAT-1	1:1000	Cell Signaling #36057	Anti-Rabbit
LAT-1	1:500	Invitrogen #PA5-50485	Anti-Rabbit
P53	1:1000	Cell Signaling #32532	Anti-Rabbit
P21	1:1000	Cell Signaling #64016	Anti-Rabbit

The following day, membranes were washed (3x5 minutes in TBST) and then incubated in anti-rabbit (CST #7074) or anti-mouse (CST #7076) secondary antibodies conjugated to HRP at 1:10000 dilution in a solution of TBST mixed with 5% milk powder. The incubation lasted for 3 hours. After the incubation period, the membranes were washed again, and an HRP chemical

luminescent substrate (BioRad, #1705060S) were applied to each membrane prior to signal detection using the BioRad ChemiDoc XRS+ system. Image Lab software was used to quantify images.

4.3 Immunofluorescence Microscopy: Measuring Myotube Diameter

In this study, C2C12 myoblasts were cultured on glass coverslips situated in 12-well plates (Fisher Scientific #092815-9). These cells grow until they achieve a confluence level of 90-100% (Day 0), at which point the growth media (GM) is replaced with differentiation medium (DM) to initiate myotube formation. On Day 5, myotubes were treated with 2 mL/well of either 1.4uL/mL of DMSO (Vehicle 24 or vehicle 48) or chemotherapy (20µg/mL CPT-11, 50µg/mL 5-Fluorouracil, 10µg/mL Leucovorin) and cytokines (20 ng/mL IL-6 and 100 ng/mL TNF-alpha) for 24 (DC-24) and 48 hours (DC-48). In a separate group, myotubes were treated for 24h with chemotherapy and cytokines, but then washed in PBS and treated with DM for an additional 24h (DCW).

Following treatment, the medium was discarded, and each well was rinsed twice with 1 mL of PBS under sterile conditions. Subsequently, cell fixation was carried out by adding 1 mL of 4% paraformaldehyde (PFA) in phosphate-buffered saline (PBS) to each well, ensuring full coverage of the coverslips, and letting it sit for 10 minutes at room temperature with a gentle rocking motion. After fixation, the cells were permeabilized by treating them with 1 mL of 0.03% Triton X-100 in PBS per well, also at room temperature, for 10 minutes. Following permeabilization, a PBS wash was administered to each well. The samples were then blocked with 400µL per well of 10% horse serum in PBS, at room temperature, for one hour to prevent non-specific binding.

Post-blocking, the coverslips are incubated overnight with a primary antibody solution directed against myosin heavy chain (MHC), prepared at a concentration of 2.5µg/ml in a solution containing 1% bovine serum albumin (BSA) in PBS at room temperature. Following this incubation period, the coverslips are treated with 500µL per well of Texas Red-conjugated anti-mouse IgG secondary antibody, preceding the application of DAPI staining to visualize nuclei. Finally, the prepared samples are mounted onto glass slides for microscopic examination. Imaging of the slides is conducted using the EVOS FL Auto microscope (from Life Technologies), using integrated EVOS FL Auto software for capturing images.

4.4 BCKD Activity Assay

Following 24 or 48 hours of chemotherapy and cytokine treatment, myotubes were washed twice with PBS (Wisent, #311-010-CL) and replaced with 200 µL of fresh differentiation media (DM). The BCKD activity assay was then initiated by adding 856 µL of Krebs Ringer Buffer (KRB) supplemented with 1 mg of thiamine hydrochloride and 61 µL of radioactive reaction mix to each well. Filter paper wicks (1.3 cm × 2 cm), pre-soaked with 60 µL of 2M NaOH, were suspended over each well using clear Scotch tape (3M), to trap the released $14CO_2$. Plates were sealed tightly and incubated at 37°C for 1 hour. After incubation, the filter wicks were carefully removed and transferred to scintillation vials (Perkin-Elmer, #6008118) containing 3.5 mL of scintillation fluid (Ecoscint A, National Diagnostics, #LS-273) for radioactivity measurement. Additionally, 100 µL of media from each well was collected and transferred into separate scintillation vials with 3.5 mL of Ecoscint A for analysis of total released CO_2. Remaining contents in the wells were aspirated, rinsed twice with cold PBS, and lysed in 100 µL of lysis buffer for protein assay to quantify protein levels in each condition. For more information on the process, refer to Appendix C.

This procedure employed 14C-L-valine as the radiolabeled substrate to trace BCKD activity. The resulting CO_2, generated through BCKD-mediated decarboxylation, was captured on NaOH-soaked filter paper wicks. Valine was specifically chosen because its corresponding keto acid, KIV (α-ketoisovalerate), serves as the preferred substrate for the BCKD complex (76). The radiolabeled bicarbonate trapped on the wicks was measured by scintillation counting and expressed as counts per minute (CPM), which was subsequently converted to mol CO_2 per μg of protein based on protein assay results. For more information on the conversion process, refer to Appendix D.

4.5 Graphical Representation of Western Blots and Statistics

Statistical analysis was conducted using GraphPad Prism 10 software. Each data set represents biological replicates (n=3 or 5 independent experiments) which technical triplicates of each condition within experiments. Data distributions are variance homogeneity were assessed using Brown-Forsythe and Bartlett's test, which confirmed equal variances across groups. One way ANOVA was performed using Tukey's multiple comparisons to test differences among means between vehicle and chemotherapy-cytokines treated groups. Tukey's post-hoc tests was used to determine statistically significant differences among means. Data were presented as mean ± SEM. Significance was determined as $p < 0.05$.

4.6 Additional information on protein measurements and isoforms:

The monoclonal antibody MF-20 recognizes a conserved epitope common to all skeletal muscle myosin heavy chain (MHC) isoforms, allowing quantification of total MHC content regardless of fiber type. Myosin heavy chain 1 (MHC1), encoded by the MYH1 gene, is a major structural and contractile protein that binds actin and drives muscle contraction through ATP

hydrolysis (180,181). The JLT-12 antibody (DSHB) selectively detects fast skeletal muscle troponin T isoforms and does not cross-react with slow isoforms. Troponin T (TnT) anchors the troponin complex to tropomyosin, while Troponin I (TnI) acts as the inhibitory subunit that blocks actomyosin ATPase activity in the absence of calcium, and Troponin C (TnC) binds calcium ions to trigger contraction. Each of these subunits exists in distinct isoforms (fast, slow, and cardiac), which differ in calcium sensitivity and contraction kinetics (182,183).

Collectively, these antibodies provided a comprehensive measure of myofibrillar protein composition, capturing both total MHC content and fast-type contractile protein expression in response to chemotherapy and cytokine treatments.

Results

Chemotherapy Drugs and Cytokines Induce Myotube Atrophy and Reduce Myofibrillar Protein Abundance

Immunofluorescence staining for myosin heavy chain (MHC-1) revealed that chemotherapy and cytokine treatment significantly reduced myotube diameter by 26% and 29% in the DC-24h (drug and cytokine treatment for 24 hours) and DC-48h (drug and cytokine treatment for 48 hours) groups, respectively, compared to vehicle (figure 4.4 A–C). Although the DC+Rec group showed a slight increase in myotube diameter, this change was not statistically significant, and the number of nuclei remained unchanged across all treatment groups (figure 4.4 A-C). Western blot analysis of myofibrillar proteins showed differential reductions across treatment conditions (figure 4.4 D-F). MHC-1 levels decreased notably in both DC-24h and DC-48h compared to vehicle, while DC+Rec showed a slight reduction (figure 4.1D). Troponin-T levels were most reduced in DC-48h, with a partial restoration observed in DC+Rec, though still lower than vehicle (figure 4.4 E). Tropomyosin was significantly lower in DC-24h and DC-48h compared to vehicle, and also remained reduced in DC+Rec (figure 4.4 E). All protein levels were normalized to Ponceau S (figure 4.4 D–F). The MHC-1 antibody used to measure total myosin heavy chain across all isoforms, while Troponin specifically recognizes fast skeletal troponin T. Therefore, the observed reductions indicate loss of overall myofibrillar proteins, with a greater effect on fast-type contractile components, consistent with chemotherapy-associated muscle atrophy.

Relative to the vehicle group, there was a reduction in myofibrillar protein abundance in myotubes that were treated with the drug-cytokine combination for 48 hours (DC-48h). Downward trend was observed in MHC-1, with levels decreasing by approximately 35% in DC-

24h, 36% in DC-48h compared to vehicle (figure 4.4 D). Although there was no significant difference among the DC+Rec group in MHC-1 levels, there was a reduction by 27% compared to vehicle (figure 4.4 D). Troponin levels were significantly reduced, showing a 76% decrease in DC-48h and 65% in DC+Rec compared to vehicle ($p < 0.05$), suggesting partial recovery of troponin expression (figure 4.4 E). Tropomyosin expression significantly decreased by 65% in the DC-24h group and 67% in the DC-48h group ($p < 0.05$) compared to vehicle, with a 51% reduction in DC+Rec that did not reach statistical significance but showed a trend ($p \leq 0.1$) (figure 4.4 F).

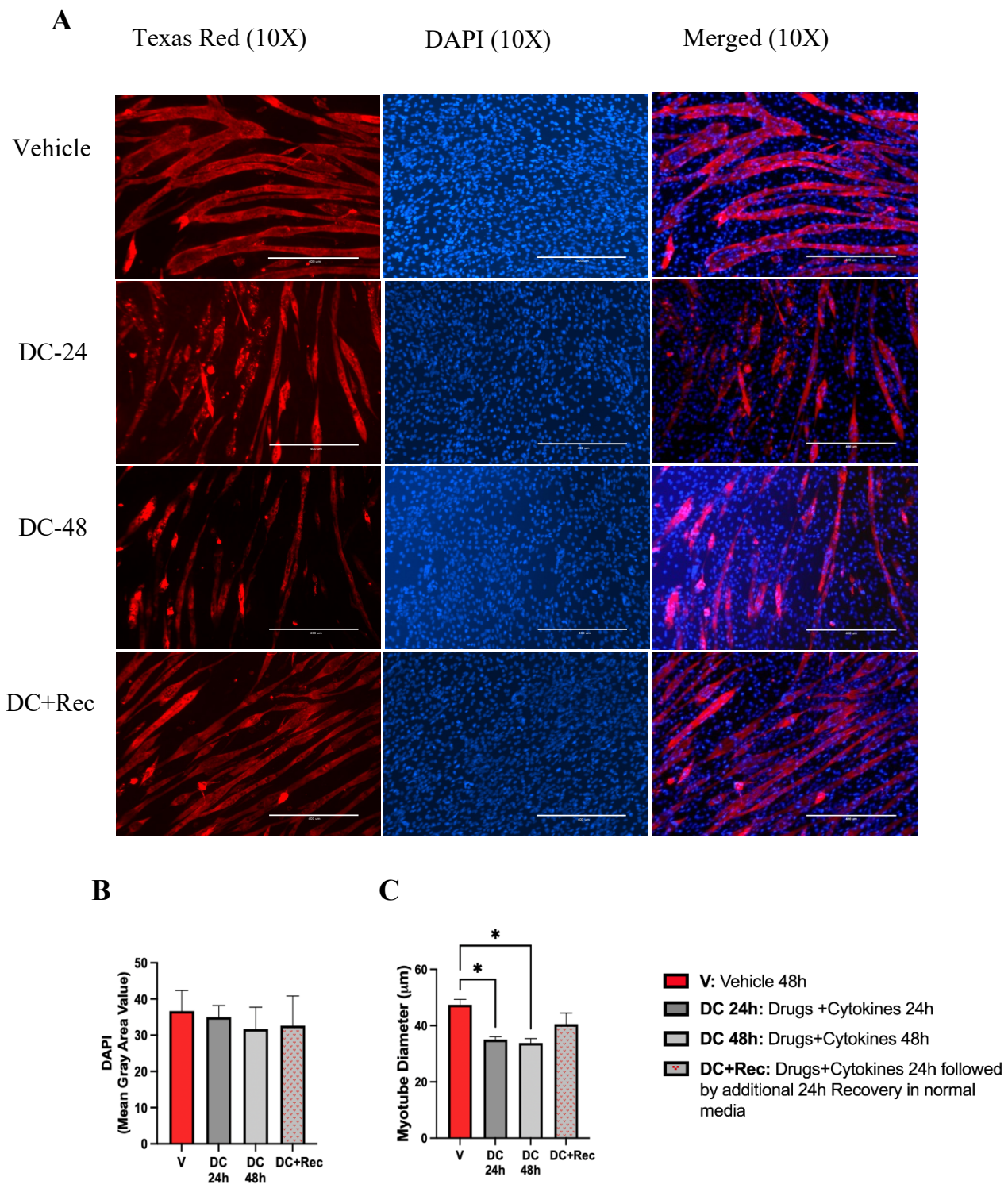
A
Texas Red (10X)
DAPI (10X)
Merged (10X)
Vehicle
DC-24
DC-48
DC+Rec
B
DAPI (Mean Gray Area Value)
50
40
30
20
10
0
V
DC 24h
DC 48h
DC+Rec
C
Myotube Diameter (μm)
60
40
20
0
*
*
V
DC 24h
DC 48h
DC+Rec
V: Vehicle 48h
DC 24h: Drugs +Cytokines 24h
DC 48h: Drugs+Cytokines 48h
DC+Rec: Drugs+Cytokines 24h followed by additional 24h Recovery in normal media

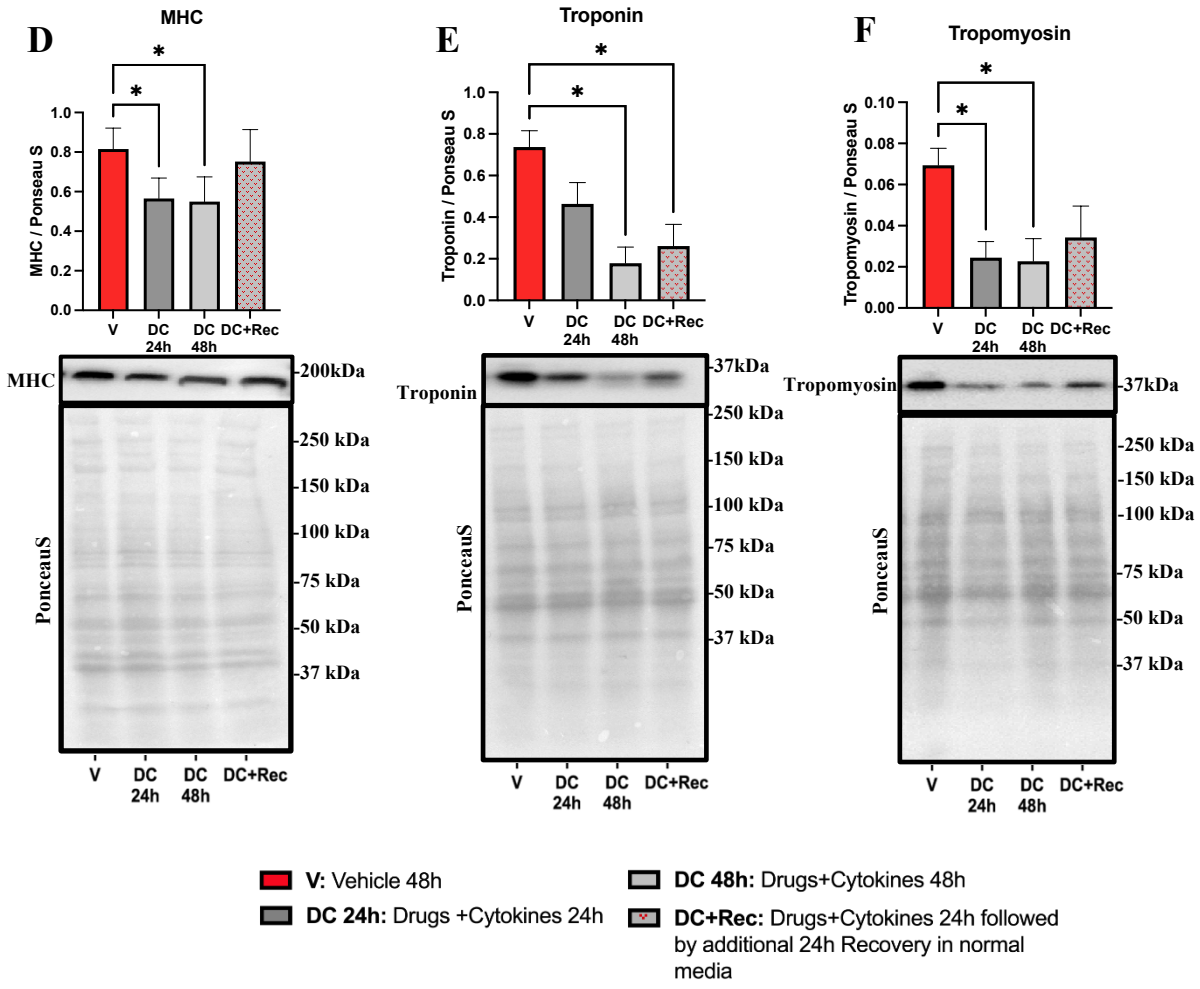

Figure 4.4 Chemotherapy and cytokine treatment reduces myotube diameter and myofibrillar protein expression. Myotubes were treated with a combination of chemotherapy drugs (20 µg/mL CPT-11, 50 µg/mL 5-Fluorouracil, 10 µg/mL Leucovorin) and inflammatory cytokines (20 ng/mL IL-6, 100 ng/mL TNF-α) or vehicle (DMSO, referred as V) for 24 h (DC 24h), 48 h (DC 48h), or treated for 24 h followed by 24 h recovery in differentiation media (DC+Rec). **(A)** Immunofluorescence staining for myosin heavy chain-1 (MHC-1), which is stained with Texas Red, and DAPI-labeled nuclei (Bar, 400 µM). Quantification of myotube diameter **(B)** and number of nuclei per myotube **(C).** Western blot analysis **(D–F)** and quantification of MHC-1 **(D)**, troponin-T **(E),** and tropomyosin **(F)**, normalized to Ponceau S. Troponin-T and tropomyosin levels were significantly decreased in DC 48h groups compared to vehicle, with partial recovery in DC+Rec. Data are presented as mean ± SEM from n = 4 independent experiments with at least three technical replicates per condition. *p < 0.05 vs. vehicle. MHC-1, myosin heavy chain-1; DAPI, 4′,6-diamidino-2-phenylindole; V, vehicle; DC, drug + cytokine; Rec, recovery; h, hours; DMSO, dimethyl sulfoxide.

Chemotherapy drugs and inflammatory cytokines suppress anabolic signaling with partial recovery after treatment removal

Combined treatment with chemotherapy drugs (FOLFIRI) and pro-inflammatory cytokines (IL-6 and TNF-α) suppressed key anabolic signaling pathways in C2C12 myotubes, including upstream (Akt) and downstream (S6K1 and S6) targets of mTORC1.

Phosphorylated S6K1 (ph-S6K1) levels, shown in figure 4.5A, did not differ significantly between treatment groups. However, total S6K1 protein levels (figure 4.5B) were significantly reduced at 48 hours (–48% vs. vehicle; $p < 0.05$), and remained similarly suppressed in the DC+Rec group (–44% vs. vehicle). Consequently, the ratio of ph-S6K1 to total S6K1 (figure 4.5C) progressively increased with treatment duration: +33% at 24h, +88% at 48h, and +149% in the recovery group, although this increase was not statistically significant ($p > 0.05$; figure 4.5C), this might indicating a potential relative enhancement of phosphorylation efficiency despite total protein loss.

We examined another anabolic signaling protein, Akt, which acts upstream of mTORC1. Although changes in Akt phosphorylation were not statistically significant, there was an interesting trend across the treatment groups. Phosphorylated Akt (ph-Akt, Ser473) levels (figure 4.5D) showed a decreasing trend at 24h (–60%) and 48h (–35%) relative to the vehicle, suggesting possible inhibition of upstream signaling. Total Akt protein levels (figure 4.5E) remained stable. The ph-Akt/total Akt ratio (figure 4.5 F) exhibited a modest increase in the DC+Rec group (+7.2%) compared to vehicle, indicating a trend toward recovery following treatment removal.

Phosphorylated ribosomal protein S6 (ph-S6, Ser235/236; figure 4.5G), a downstream target of mTORC1, showed no statistically significant differences between each condition ($p > 0.05$). However, there was a clear trend of decreased phosphorylation: –28% at 24h and –65% at 48h compared to vehicle. In the recovery group (DC+Rec), ph-S6 levels remained suppressed (–50%), suggesting that chemotherapy and cytokine treatment may impair mTORC1 signaling, with only partial recovery observed following treatment removal.

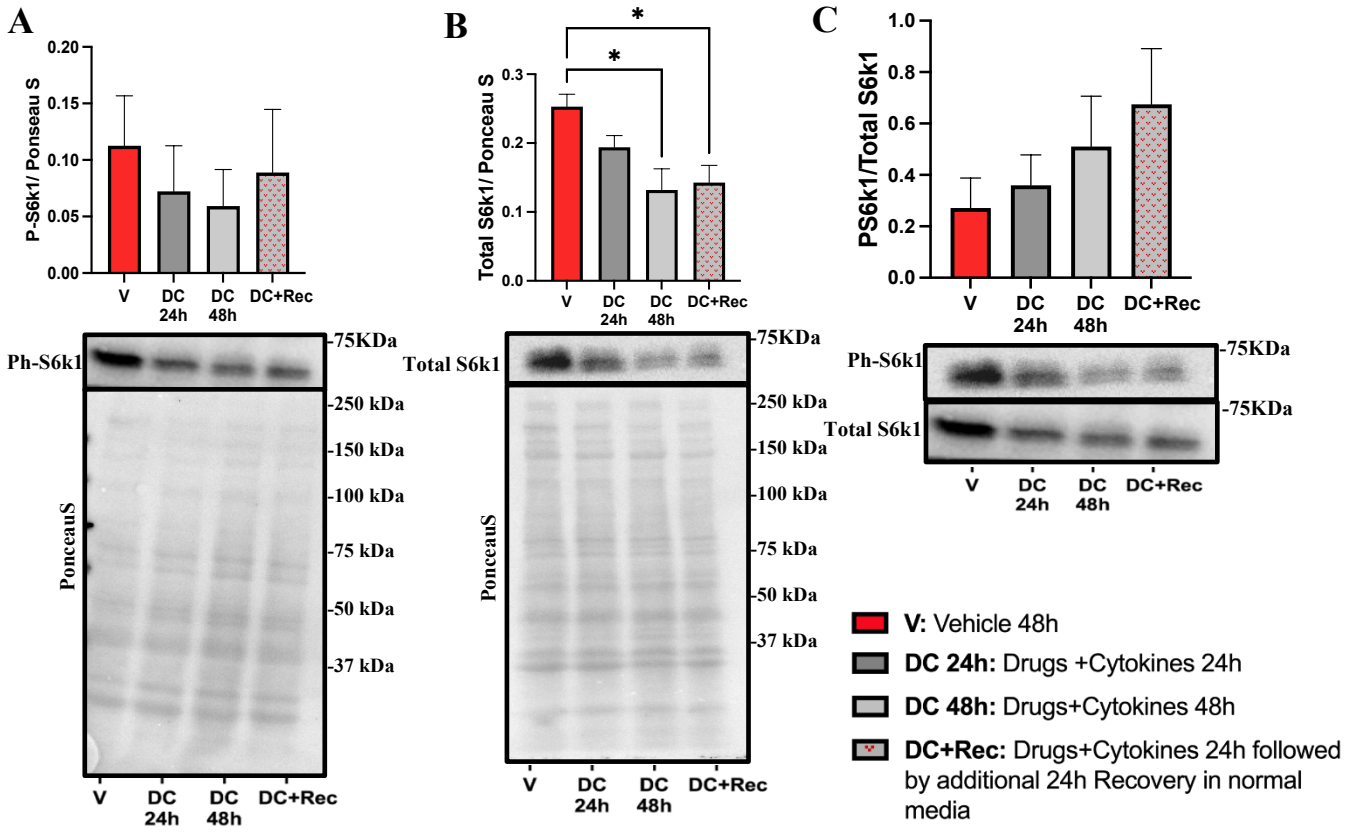

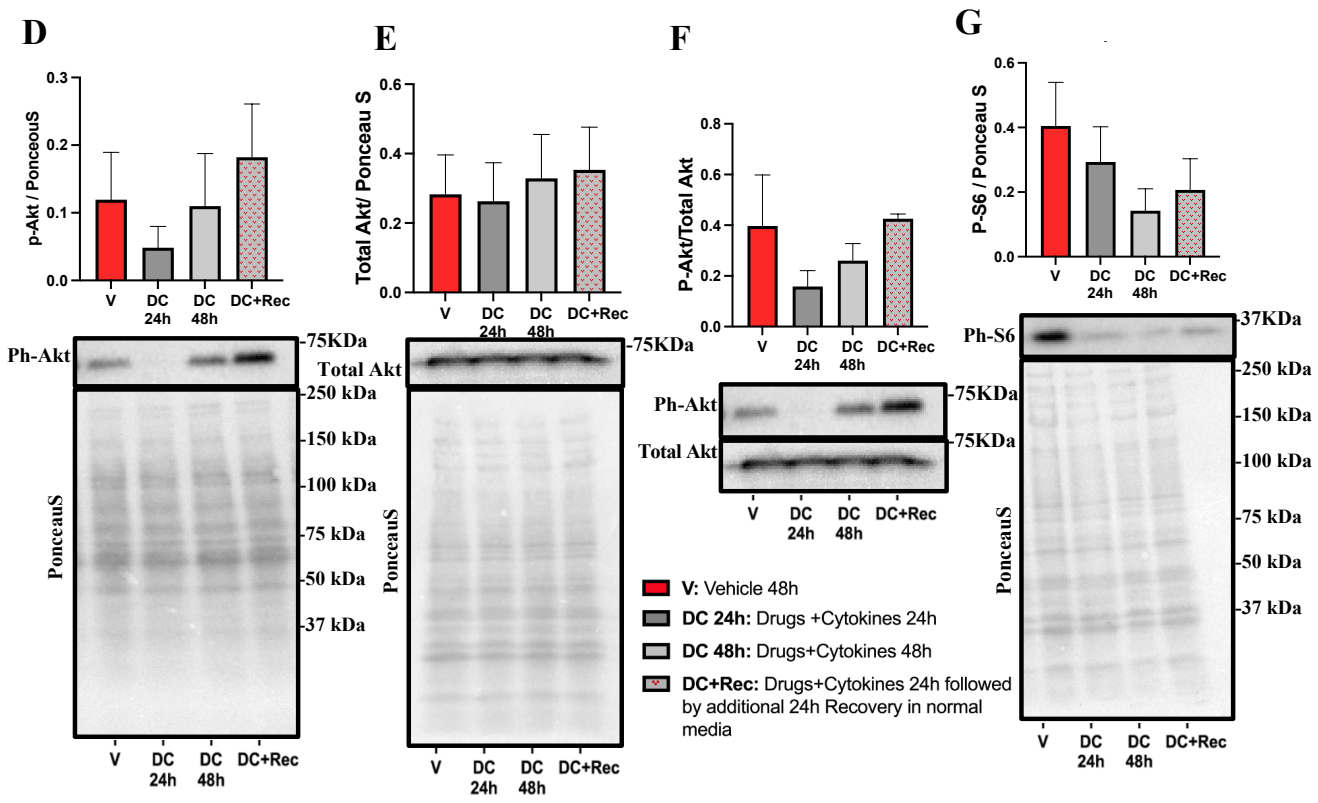

Figure 4.5 Chemotherapy and cytokine treatment suppress anabolic signaling in C2C12 myotubes. C2C12 myotubes were treated with chemotherapy and inflammatory cytokines for 24h (DC-24), 48h (DC-48), or for 24h followed by a 24h recovery period in normal differentiation media (DC+Rec). (**A–C**) Phosphorylated S6K1 (ph-S6K1; **A**) levels remained unchanged across all treatment groups. In contrast, total S6K1 protein levels (**B**) were significantly reduced at 48h and in the recovery group compared to vehicle ($p = 0.0274$ and $p = 0.0453$, respectively). As a result, the ph-S6K1 to total S6K1 ratio (**C**) increased across all conditions, although this trend was not statistically significant ($p > 0.05$). (**D–F**) Phosphorylated Akt (ph-Akt; **D**) showed a decreasing trend at 24h and 48h, while total Akt protein (**E**) remained stable. The ratio of ph-Akt to total Akt (**F**) showed a non-significant increase in the DC+Rec group ($p > 0.05$). (**G**) Phosphorylation of ribosomal protein S6 (ph-S6) was reduced at 24h and 48h and remained suppressed during recovery, though these changes were not statistically significant ($p > 0.05$). Representative Western blot images and Ponceau S loading controls illustrate band expression for each target protein. Data are shown as mean ± SEM (n = 3). *$p < 0.05$ vs. vehicle.

Chemotherapy and Inflammatory Cytokines Enhances BCAA Catabolism

Decreases in amino acid levels, particularly BCAA, intrigued us to explore BCAA catabolism in C2C12 myotubes. Protein expression of BCAT2 showed a moderate increase at 48h (+21%) that was not statistically significant, while a decrease (–21%) was observed in the drug recovery (DC+Rec) group (figure 4.6A). BDK expression, which inhibits BCKD through phosphorylation, showed similar trend as BCAT2 for DC48 and DC+Rec, where it was elevated by 57% at 48 hours and declined by 21% in the DC+Rec group compared to vehicle, though these changes were not significant (figure 4.6B). Likewise, phosphorylation of BCKD normalized to Ponceau staining showed no significant differences (figure 4.6C). However, when normalized to total BCKD, phosphorylation at Ser293, which suppresses enzymatic activity, was reduced at 48 hours by 55% ($p = 0.0682$) and remained suppressed in the DC+Rec group (figure4.6E). Interestingly, BCKD activity, measured by the release of $^{14}CO_2$ from ^{14}C-labeled valine, significantly increased in the DC+Rec group compared to vehicle (figure 4.6F).

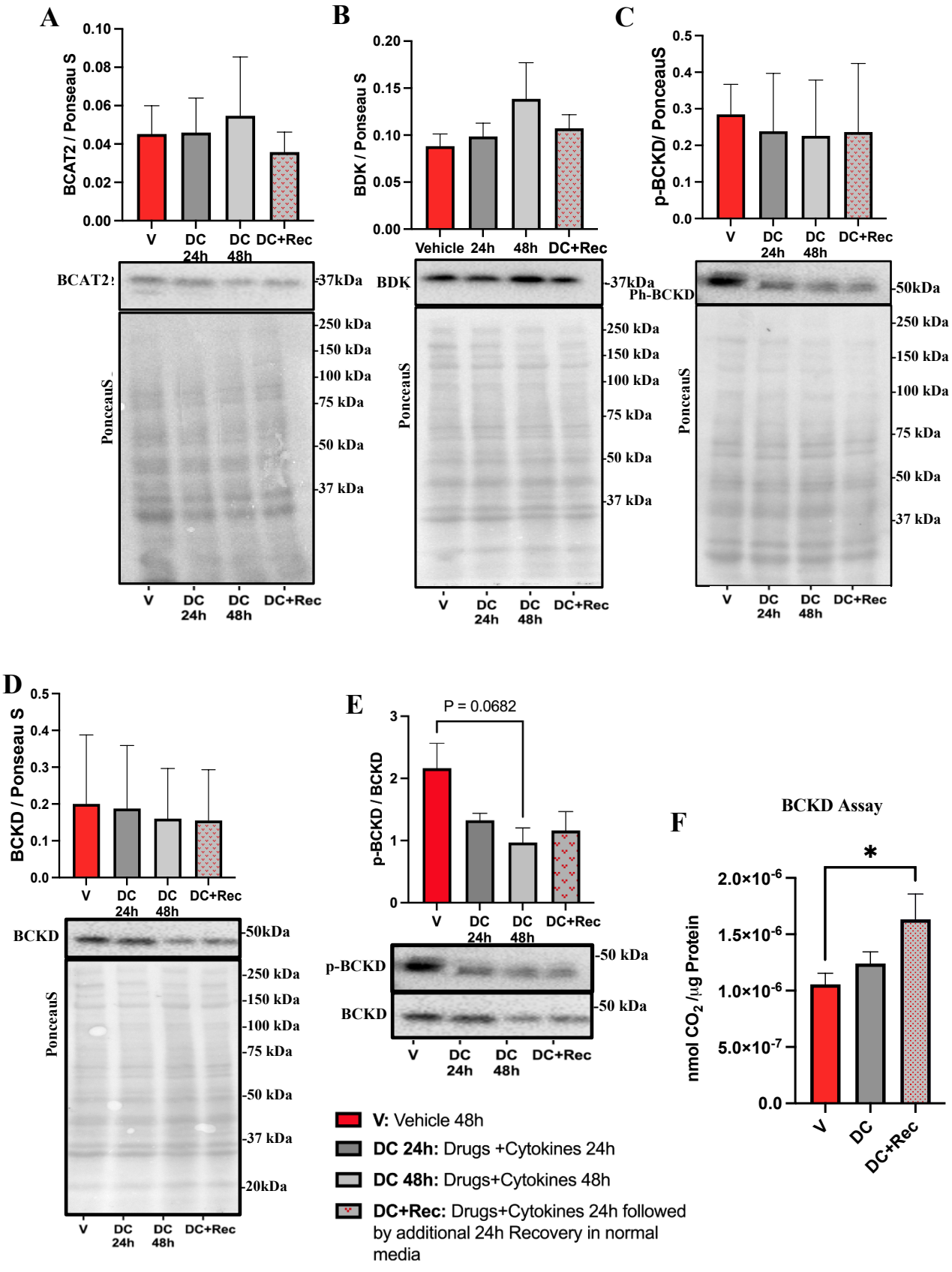
A
BCAT2 / Ponseau S
0.10
0.08
0.06
0.04
0.02
0.00
V
DC 24h
DC 48h
DC+Rec
BCAT2
37kDa
PonceauS
250 kDa
150 kDa
100 kDa
75 kDa
50 kDa
37 kDa
B
BDK / Ponseau S
0.20
0.15
0.10
0.05
0.00
Vehicle 24h
48h
DC+Rec
BDK
37kDa
PonceauS
250 kDa
150 kDa
100 kDa
75 kDa
50 kDa
37 kDa
C
p-BCKD/ PonceauS
0.5
0.4
0.3
0.2
0.1
0.0
V
DC 24h
DC 48h
DC+Rec
Ph-BCKD
50kDa
PonceauS
250 kDa
150 kDa
100 kDa
75 kDa
50 kDa
37 kDa
D
BCKD / Ponseau S
0.5
0.4
0.3
0.2
0.1
0.0
V
DC 24h
DC 48h
DC+Rec
BCKD
50kDa
PonceauS
250 kDa
150 kDa
100 kDa
75 kDa
50 kDa
37 kDa
20kDa
E
P = 0.0682
p-BCKD / BCKD
3
2
1
0
V
DC 24h
DC 48h
DC+Rec
p-BCKD
50 kDa
BCKD
50 kDa
F
BCKD Assay
*
nmol CO2 /µg Protein
2.0×10-6
1.5×10-6
1.0×10-6
5.0×10-7
0.0
V
DC
DC+Rec
V: Vehicle 48h
DC 24h: Drugs +Cytokines 24h
DC 48h: Drugs+Cytokines 48h
DC+Rec: Drugs+Cytokines 24h followed by additional 24h Recovery in normal media

Figure 4.6 Chemotherapy and Inflammatory Cytokines Enhance BCAA Catabolism. C2C12 myotubes were treated with chemotherapy and inflammatory cytokines for 24h (DC-24), 48h (DC-48), or for 24h followed by a 24h recovery period in normal differentiation media (DC+Rec). Samples were harvested and immunoblots (**A–E**), along with quantified data for BCAT2 (**A**), BDK (**B**), and phosphorylated BCKD normalized to Ponceau (**C**), total BCKD normalized to Ponceau (**D**), and the ratio of ph-BCKDSer293 to total BCKD (**E**), which showed a decrease in the DC+Rec group compared to vehicle ($p = 0.0682$). BCKD activity, measured by the release of $^{14}CO_2$ from ^{14}C-labeled valine (**F**), significantly increased in the DC+Rec group compared to vehicle. Data are presented as mean ± SEM from $n = 4$ independent experiments, each with at least three technical replicates. $p < 0.05$. V, Vehicle; DC, Drug + Cytokines; DC+Rec, Drug + Cytokines followed by Washout and Recovery; h, hours.

Increased SNAT-1 and LAT-1 Expression following Chemotherapy and inflammatory Cytokines treatment

Chemotherapy and inflammatory cytokines significantly increased the expression of amino acid transporters SNAT1 and LAT1 in C2C12 myotubes. SNAT1 protein levels were significantly elevated at DC 48h compared to vehicle (+78%, $p < 0.05$) and also compared to DC 24h (+48%, $p < 0.05$; figure 4.7 A). In the DC+Rec group, SNAT1 expression declined slightly (–29% vs. 48h), but remained higher than vehicle (+49%), although this difference was not statistically significant ($p > 0.05$), indicating only partial reversal following drug removal. LAT1 expression remained unchanged at 24h and 48h but was significantly increased in the DC+Rec group (+127% vs. vehicle, $p < 0.05$; figure 4.7B). These findings indicate that chemotherapy and cytokines enhance amino acid transporter expression, potentially reflecting increased demand for amino acid uptake under stress conditions.

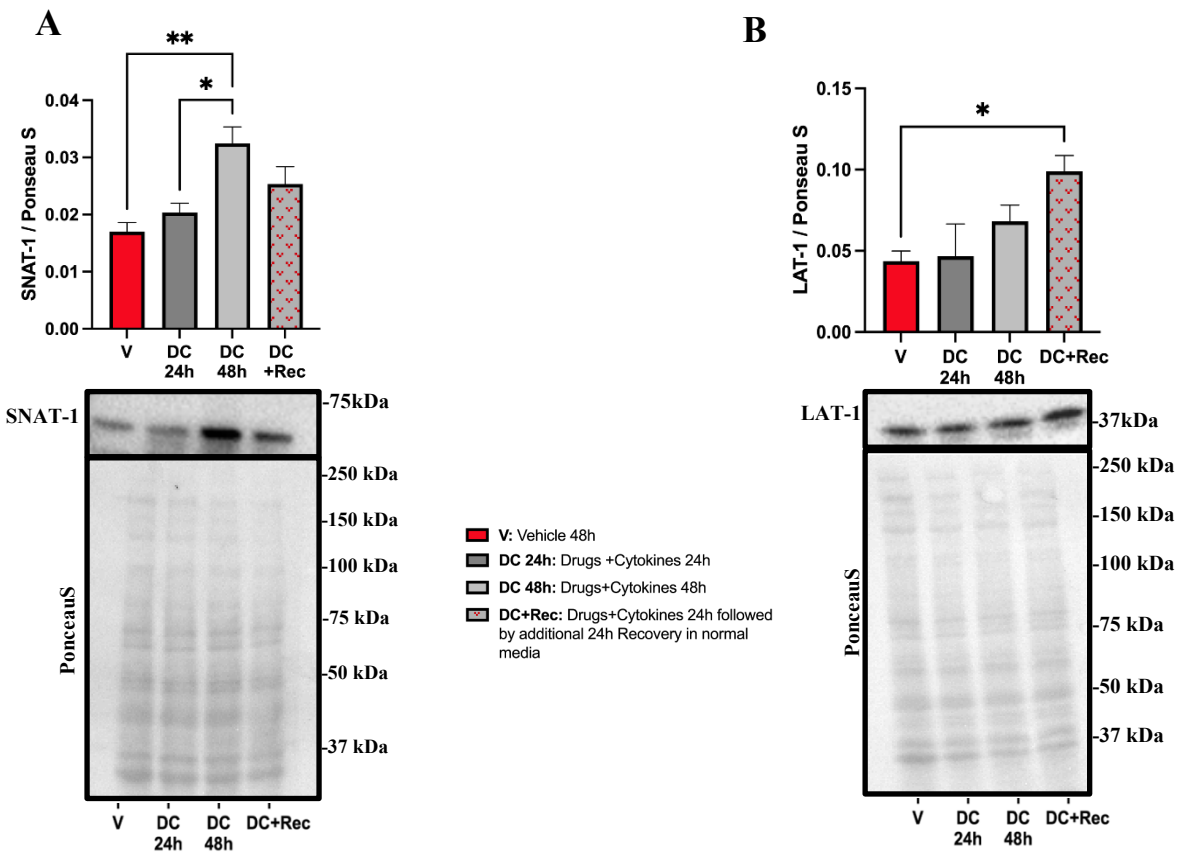

Figure 4.7 Chemotherapy and Inflammatory Cytokines Increase Amino Acid Transporter Expression. C2C12 myotubes were treated with chemotherapy and inflammatory cytokines for 24h (DC-24), 48h (DC-48), or for 24h followed by a 24h recovery period in normal differentiation media (DC+Rec). Samples were harvested and immunoblots were performed. Western blot analysis showing SNAT1 (**A**) and LAT1 (**B**) expression levels in C2C12 myotubes. SNAT1 expression was significantly increased in the DC 48h group compared to vehicle and DC 24h ($p < 0.05$). LAT1 levels remained unchanged at 24h and 48h but were significantly elevated in DC+Rec relative to vehicle ($p < 0.05$). Protein levels were normalized to Ponceau S. Data are presented as mean ± SEM (n = 3). $p < 0.05$ vs. vehicle. Representative Western blot images are shown below each bar graph.

Upregulation of Stress-Responsive Markers in Skeletal Muscle Microvascular Endothelial Cells Following Chemotherapy and Pro-Inflammatory Cytokine Treatment

Chemotherapy and inflammatory cytokines significantly increased the expression of the cancer-associated stress markers p53 and p21 in mouse skeletal muscle microvascular endothelial cells. The cells were treated with chemotherapeutic agent FOLFIRI and Pro-inflammatory cytokines at two different dosages, followed by a 24-hour recovery period (DC+Rec), assessed at two different tumpepoints:24 and 48 hours, as described in the methods section (figure 4.3). After 24 hours of treatment, p53 levels rose by +917% in the DC-Half group and +504% in the DC-Full group compared to vehicle ($p < 0.01$; figure 4.8 A). Interestingly, the expression was lower in DC-Full compared to DC-Half (–40.6%, $p < 0.05$) at 24 hours. Following 24-hour recovery, p53 levels declined in both recovery groups (–71.6% in DC-Half + Rec and –56.4% in DC-Full + Rec), but remained above vehicle, indicating that the stress response had not fully recovered after drug removal. At 48 hours, p53 expression remained elevated (+497% in DC-Half and +369% in DC-Full vs. vehicle; $p < 0.01$) (figure 4.8B), with a slight reduction in the full-dose group (–21.5%, $p < 0.05$). Recovery groups showed a decrease in p53 (–77.8% in DC-Half + Rec, –55.1% in DC-Full + Rec), but expression levels did not fully recover, supporting residual activation of the stress response pathway (figure 4.8B).

p21 expression (figure 4.8C) showed a similar pattern. At 24h, p21 increased by +561% in DC-Half and +466% in DC-Full compared to vehicle ($p < 0.01$), with slightly lower expression in the full-dose condition (–14.4% vs. DC-Half, $p < 0.05$, figure 4.8C). Moreover, at 48h, p21 levels remained high (+468% in DC-Half and +491% in DC-Full vs. vehicle, figure 4.8D), with a small but significant increase in the full-dose group (+3.9%, $p < 0.05$). In the

recovery groups, p21 declined (–62.6% in DC-Half + Rec and –23.4% in DC-Full + Rec), but remained elevated, particularly in DC-Full + Rec (+353% vs. vehicle; $p < 0.05$; figure 4.8D).

Total Akt expression remained relatively unchanged across all timepoints and treatment conditions. Neither the 24-hour nor 48-hour treatments resulted in statistically significant changes in Akt levels. Similarly, no significant differences were observed following the recovery periods, indicating that Akt protein abundance was largely unaffected by the chemotherapy and cytokine treatments (figure 4.8E).

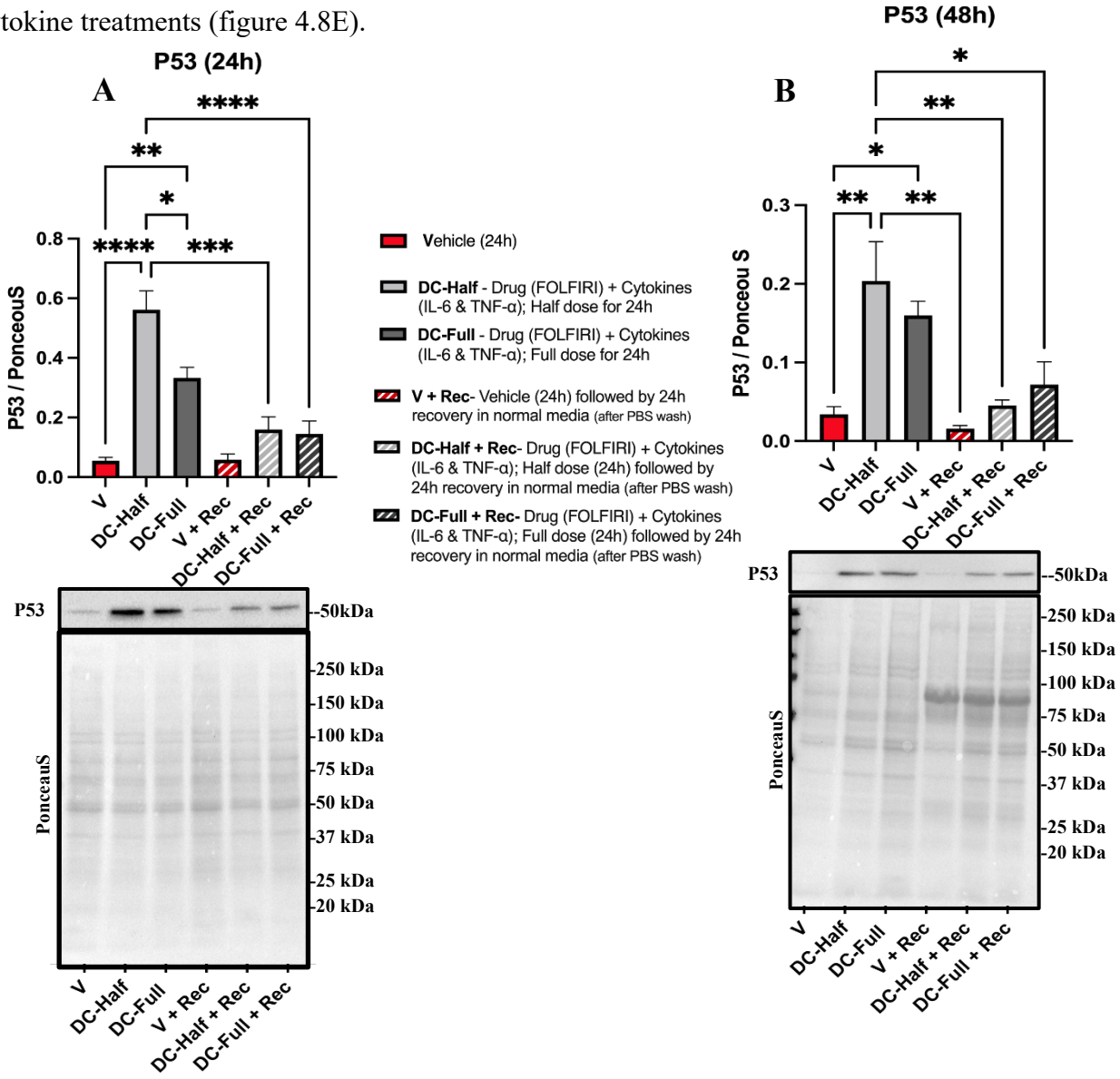

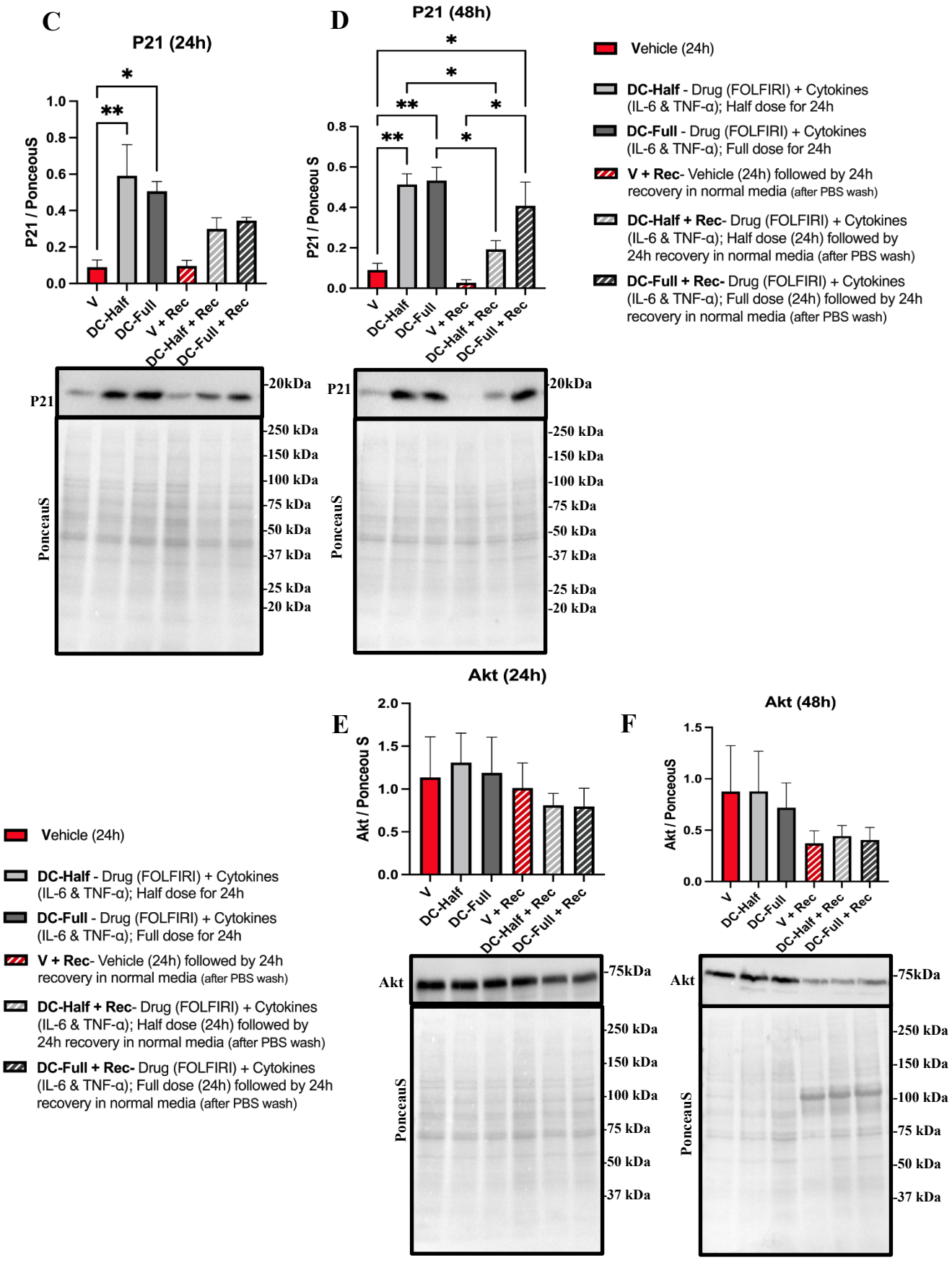
C
P21 (24h)
P21 / PonceouS
1.0
0.8
0.6
0.4
0.2
0.0
*
**
V
DC-Half
DC-Full
V + Rec
DC-Half + Rec
DC-Full + Rec
D
P21 (48h)
P21 / Ponceou S
0.8
0.6
0.4
0.2
0.0
*
**
*
*
V
DC-Half
DC-Full
V + Rec
DC-Half + Rec
DC-Full + Rec
Vehicle (24h)
DC-Half - Drug (FOLFIRI) + Cytokines (IL-6 & TNF-α); Half dose for 24h
DC-Full - Drug (FOLFIRI) + Cytokines (IL-6 & TNF-α); Full dose for 24h
V + Rec- Vehicle (24h) followed by 24h recovery in normal media (after PBS wash)
DC-Half + Rec- Drug (FOLFIRI) + Cytokines (IL-6 & TNF-α); Half dose (24h) followed by 24h recovery in normal media (after PBS wash)
DC-Full + Rec- Drug (FOLFIRI) + Cytokines (IL-6 & TNF-α); Full dose (24h) followed by 24h recovery in normal media (after PBS wash)
P21
20kDa
PonceauS
250 kDa
150 kDa
100 kDa
75 kDa
50 kDa
37 kDa
25 kDa
20 kDa
P21
20kDa
PonceauS
250 kDa
150 kDa
100 kDa
75 kDa
50 kDa
37 kDa
25 kDa
20 kDa
Akt (24h)
E
Akt / Ponceou S
2.0
1.5
1.0
0.5
0.0
V
DC-Half
DC-Full
V + Rec
DC-Half + Rec
DC-Full + Rec
F
Akt (48h)
Akt / PonceouS
1.5
1.0
0.5
0.0
V
DC-Half
DC-Full
V + Rec
DC-Half + Rec
DC-Full + Rec
Vehicle (24h)
DC-Half - Drug (FOLFIRI) + Cytokines (IL-6 & TNF-α); Half dose for 24h
DC-Full - Drug (FOLFIRI) + Cytokines (IL-6 & TNF-α); Full dose for 24h
V + Rec- Vehicle (24h) followed by 24h recovery in normal media (after PBS wash)
DC-Half + Rec- Drug (FOLFIRI) + Cytokines (IL-6 & TNF-α); Half dose (24h) followed by 24h recovery in normal media (after PBS wash)
DC-Full + Rec- Drug (FOLFIRI) + Cytokines (IL-6 & TNF-α); Full dose (24h) followed by 24h recovery in normal media (after PBS wash)
Akt
75kDa
PonceauS
250 kDa
150 kDa
100 kDa
75 kDa
50 kDa
37 kDa
Akt
75kDa
PonceauS
250 kDa
150 kDa
100 kDa
75 kDa
50 kDa
37 kDa

Figure 4.8 Chemotherapy and cytokine treatment increases p53 and p21 expression in endothelial cells, with only partial return to baseline after recovery, and reduced total Akt levels. Mouse skeletal muscle microvascular endothelial cells were treated with chemotherapy (FOLFIRI) and inflammatory cytokines (IL-6 and TNF-α) for 24 or 48 hours at half (DC-Half) or full (DC-Full) doses. Additional groups were allowed to recover in normal endothelial growth media for 24 hours following treatment and PBS wash (DC-Half + Rec, DC-Full + Rec). Figure (**A–B**) p53 protein levels were significantly increased at both 24h (**A**) and 48h (**B**), especially in DC-Half groups. Expression decreased in recovery groups but remained above vehicle levels. Figure (**C–D**) p21 expression followed a similar pattern, with strong increases at 24h (**C**) and continued elevation at 48h (**D**). Recovery groups showed lower expression than treatment groups but did not return completely to vehicle levels. Figure (**E–F**) Total Akt levels remained steady during treatment (24h, **E**; 48h, **F)** but dropped noticeably in all recovery groups at both timepoints. Representative western blots and Ponceau S loading controls are shown below each graph. Data are presented as mean ± SEM (n = 3). *p < 0.05, **p < 0.01, ***p < 0.001, ****p < 0.0001 vs. indicated comparisons.

Discussion

This study investigated the impact of FOLFIRI chemotherapy in combination with pro-inflammatory cytokines (IL-6 and TNF-α) on skeletal muscle and endothelial cells to better understand mechanisms contributing to cancer-associated cachexia. Using C2C12 myotubes, we measured changes in anabolic signaling and BCAA metabolism, while in primary skeletal muscle microvascular endothelial cells we focused on stress-responsive pathways. The goal was to determine how these treatments disrupt cellular homeostasis and whether short-term recovery could reverse these effects. The findings indicate that chemotherapy and inflammation impair both muscle integrity and vascular function through complementary but distinct mechanisms, ultimately converging on pathways that limit anabolic capacity and metabolic resilience.

One of the most notable observations in this study was the impaired anabolic signaling pathway. Total S6K1 protein levels were significantly reduced following 48 hours of treatment, indicating suppression of mTORC1 activity. Although the ratio of ph-S6K1 to total S6K1 increased, this likely reflects a compensatory adjustment to the drop in total S6K1, rather than an actual boost in anabolic signaling. Since the phosphorylated form did not increase and total S6K1 was reduced, mTORC1's ability to support protein synthesis may still be impaired. These findings are consistent with prior reports (98,123,184) that emphasize how a higher ph/total ratio can sometimes reflect stoichiometric shifts rather than enhanced activity. Phosphorylated Akt levels remained unchanged across treatment groups, suggesting that the upstream IGF/PI3K/Akt pathway may not be the primary site of disruption under these conditions. Although it was not statistically significant ($p > 0.05$) but the downward trend in Akt phosphorylation after treatment and its partial rebound during recovery suggest an early impairment in Akt activation rather than

its degradation, since total Akt levels were preserved. These findings, in conjunction with reductions in downstream effectors like S6K1 and S6, indicate that anabolic signaling may be disrupted at multiple levels along the IGF-Akt-mTORC1 cascade. The lack of correspondence between stable Akt phosphorylation and suppressed downstream mTORC1 targets supports prior reports (98,184), which propose that nutrient sensing signals and cellular stress, rather than growth factor input alone, may dominate mTORC1 regulation under stressed skeletal muscle conditions.

The observed anabolic deficits were accompanied by alterations in BCAA catabolic regulation. While expression levels of BCAT2 and BDK remained stable, phosphorylated BCKD at ser293, normalized to total BCKD, showed a decreasing trend, indicating potential activation of BCKD through dephosphorylation. This aligns with the significant increase in BCKD enzyme activity observed in the recovery group, suggesting that post-treatment, myotubes may engage in elevated BCAA oxidation as part of a metabolic recovery process. This adaptation likely reflects a metabolic strategy to generate energy when anabolic signalling is supressed, and nutrient stress intensifies. By enhancing BCKD activity, cells can funnel BCAA derived carbon skeletons into the TCA cycle as acetyl-CoA and succinyl-CoA, supporting ATP production under conditions where glucose or lipid oxidation may be limited. This shift could serve as an adaptive mechanism to fuel mitochondrial energy production during recovery or reflect a delayed response to upstream catabolic stress (98,112,123).

The analysis of amino acid transporter expression further supports this hypothesis. SNAT1 expression significantly increased at 48 hours and remained elevated in the recovery condition, indicating enhanced uptake of small neutral amino acids during and after treatment.

LAT1 expression, which facilitates large neutral amino acid uptake including BCAAs, was increased only during the recovery phase. This pattern may suggest that the cellular machinery upregulates transporter systems post-treatment to replenish intracellular amino acid pools depleted during chemotherapy-induced stress, potentially restoring the building blocks for protein synthesis and repair.

While our previous lab study by Dr. Stephen Mora presented a reduction in SNAT1 and LAT1 expression using L6 myotubes treated with FOLFIRI (185), our findings in C2C12 cells showed the opposite trend. These contrasting outcomes likely stem from differences in cell line characteristics and experimental design. C2C12 myotubes, derived from mouse tibialis anterior muscle, are insulin-sensitive and express the GLUT4 glucose transporter, which may enhance anabolic responses and nutrient uptake compared to L6 myotubes, which lack GLUT4. Additionally, our experimental model incorporated both chemotherapy and inflammatory cytokines (IL-6 and TNF-α), whereas Mora's study investigated chemotherapy alone. The inclusion of cytokines may have intensified cellular stress and triggered adaptive responses, such as upregulation of amino acid transporters (24–27). These combined factors likely contributed to the observed differences in SNAT1 and LAT1 expression between the two studies.

In summary, our study indicates how chemotherapy and inflammation impair skeletal muscle homeostasis. While some compensatory mechanisms, such as transporter upregulation and increased BCKD activity, may offer limited recovery capacity, the persistent disruption of anabolic signaling and structural protein integrity underscores the challenge of restoring muscle function in cachexia.

The parallel experiments in primary endothelial cells revealed a distinct yet complementary pattern of disruption centered on stress-responsive signalling rather than direct suppression of anabolic pathways. Exposure to chemotherapy and cytokines significantly elevated P53 and P21 expression. The upregulation of p53 observed in both the DC-Half and DC-Full groups at 24 and 48 hours highlights its central role as a molecular sensor of genotoxic and inflammatory stress. While recovery led to partial downregulation of p53, levels did not return to vehicle baseline, suggesting sustained transcriptional activity even after drug withdrawal. This prolonged p53 activation is consistent with its known role in promoting senescence, cell cycle arrest, or apoptosis pathways that could all potentially impair endothelial cell function (186–188).

Interestingly, p53 and p21 expression were consistently higher in the DC-Half group compared to the DC-Full condition, despite the latter involving a higher intensity of chemotherapy and cytokine exposure. This pattern indicates a dose-dependent but non-linear response, where increasing stress does not necessarily result in a proportional increase in stress marker expression. One possible explanation is that moderate levels of stress, such as those in DC-Half, activate protective pathways like the p53–p21 signaling pathway to promote DNA repair, cell cycle arrest, and cellular adaptation (186,187,189,190). However, under more intense treatment conditions, as seen in DC-Full, this response may become impaired.

At higher doses, the stress burden may exceed a critical threshold, leading to partial loss of function or damage in endothelial cells. This could reduce the number of cells capable of mounting a full stress response. Previous studies have shown that high levels of DNA damage or oxidative stress can reduce the expression of p53 target genes through mechanisms such as

chromatin remodeling, protein degradation, or the activation of other forms of cell death (189–191). This supports a threshold-based model, where lower levels of stress engage adaptive signaling, while higher doses overwhelm the system and result in reduced transcriptional activity. This concept is also reflected in other studies showing that high-dose chemotherapy can blunt p53 activity in endothelial cells due to mitochondrial dysfunction, ATP depletion, or epigenetic changes (14,90,141,187,188,190,192,193).

Importantly, studies by Dr. Roudier have demonstrated the role of p53 in capillary rarefaction during muscle unloading. Their work reported that p53 (TP53) expression is upregulated in the soleus muscle during atrophy, alongside upregulation of the anti-angiogenic factor thrombospondin-1 (THBS1) (194,195). These findings, indicate that persistent p53 activation can impair angiogenic potential by promoting anti-angiogenic signalling (194,195). In skeletal muscle, such a response compromises capillary maintenance and remodeling, reducing perfusion and potentially exacerbating muscle wasting (196). Our observation of sustained p53 activation in endothelial cells suggests that chemotherapy-induced stress may trigger a similar anti-angiogenic environment, contributing to vascular dysfunction in cachexia.

Additionally, Akt signaling, a major regulator of anabolic pathways, negatively controls p53 stability through its interaction with MDM2, the primary ubiquitin ligase targeting p53 for degradation (70,155,188,197,198). Akt-mediated phosphorylation of MDM2 promotes its nuclear localization, where it binds to and targets p53 for ubiquitination and proteasomal degradation. This regulatory relationship suggests that a reduction in Akt activity, as observed under chemotherapy and pro-inflammatory cytokine conditions, may contribute to sustained p53 activation and reinforcing anti-angiogenic signaling and endothelial stress responses

(71,155,156,188,197,198) Notably, our C2C12 data showed a downward trend in Akt phosphorylation after treatment, suggesting that similar upstream impairments may occur in both cell types. This shared disruption of Akt signaling may represent a unifying mechanism linking impaired muscle anabolism to endothelial dysfunction during cachexia.

Although our study did not directly distinguish between apoptosis, senescence, or cell cycle arrest in treated endothelial cells, the concurrent upregulation of p21 indicates a phenotype consistent with prolonged cell cycle arrest and possible senescence. This sustained growth arrest, even after the recovery period, may impair the proliferative capacity and barrier integrity of endothelial cells, increasing permeability or structural instability. Given the specialized continuous endothelium of skeletal muscle capillaries, such dysfunction could compromise nutrient and oxygen delivery to myofibers, further linking vascular impairment to muscle atrophy (151,177,193,196). Interestingly, total Akt expression remained relatively stable during active treatment, suggesting that acute Akt-mediated survival signaling may be preserved in the short term. Taken together, these findings suggest that chemotherapy and inflammatory stressors elicit a sustained activation of p53/p21 signaling in skeletal muscle endothelial cells, which may hinder angiogenic remodeling and contribute to vascular rarefaction. These molecular changes could represent a key mechanistic link between endothelial dysfunction and the progression of cancer-associated muscle wasting. Further studies evaluating markers of apoptosis, senescence, and endothelial permeability will be essential to delineate the specific outcomes of p53 activation in this context (163,165,187,193,196,199–201).

Overall, this study provides new insight into how chemotherapy and inflammatory cytokines disrupt skeletal muscle homeostasis through combined effects on myotubes and

endothelial cells. By examining both anabolic signaling and BCAA metabolism in C2C12 myotubes alongside stress-responsive pathways in endothelial cells, we identified Akt–p53 signaling as a potential mechanistic link between impaired muscle anabolism and vascular dysfunction. These findings emphasize that cachexia is not solely a myofiber-driven process but involves vascular adaptations that may exacerbate metabolic stress and limit recovery. From a translational perspective, targeting pathways that preserve endothelial integrity and muscle anabolic capacity may represent a promising strategy to mitigate chemotherapy-induced muscle wasting and improve patient outcomes. Future work incorporating co-culture models and in vivo validation will be critical for advancing these therapeutic concepts.

Limitations and Future Directions

This study highlights the catabolic effects of chemotherapy and cytokines on myotubes and stress responses in endothelial cells; however, several limitations should be noted.

The in vitro design, while useful for isolating cell-specific effects, lacks the physiological complexity of in vivo systems, and treatments were applied separately, leaving endothelial-myotube crosstalk unexplored.

Some recovery trends were non-significant, likely due to limited sample size, and only two fixed doses were tested. Notably, endothelial cells tolerated full-dose chemotherapy, suggesting future studies may prioritize this dose, while the stronger stress response at half dose warrants investigation into possible non-linear effects.

Future research should use co-culture or conditioned media models, extend recovery periods, and include metabolic and functional assays. Our findings also support exploring interventions such as anti-inflammatory agents or amino acid supplementation to preserve muscle and vascular integrity during chemotherapy.

Additionally, future work should evaluate molecular pathways that link endothelial stress responses to signaling dysregulation. Specifically, it would be valuable to measure phosphorylated Akt and phosphorylated MDM2 (pMDM2) in skeletal muscle endothelial cells to determine whether reduced Akt activity could limit MDM2 activation, leading to stabilization and upregulation of p53. This approach could provide insight into the mechanistic balance between pro-survival and pro-apoptotic pathways in endothelial cells exposed to chemotherapy and inflammatory stress.

References

1. DeRidder L, Rubinson DA, Langer R, Traverso G. The past, present, and future of chemotherapy with a focus on individualization of drug dosing. Journal of Controlled Release. 2022 Dec 1;352:840–60.
2. Daly LE, Ní Bhuachalla ÉB, Power DG, Cushen SJ, James K, Ryan AM. Loss of skeletal muscle during systemic chemotherapy is prognostic of poor survival in patients with foregut cancer. J Cachexia Sarcopenia Muscle [Internet]. 2018 Apr 1 [cited 2024 Jan 3];9(2):315–25. Available from: https://pubmed.ncbi.nlm.nih.gov/29318756/
3. Nunes EA, Stokes T, McKendry J, Currier BS, Phillips SM. Disuse-induced skeletal muscle atrophy in disease and non-disease states in humans: mechanisms, prevention, and recovery strategies. Am J Physiol Cell Physiol [Internet]. 2022 Jun 1 [cited 2024 Jan 4];322(6):C1068–84. Available from: https://journals.physiology.org/doi/10.1152/ajpcell.00425.2021
4. Hossain MB, Haldar Neer AH. Chemotherapy. Cancer Treat Res [Internet]. 2023 [cited 2024 Jan 3];185:49–58. Available from: https://link.springer.com/chapter/10.1007/978-3-031-27156-4_3
5. Coletti D. Chemotherapy-induced muscle wasting: an update. Eur J Transl Myol [Internet]. 2018 Apr 4 [cited 2024 Jan 3];28(2):153–7. Available from: /pmc/articles/PMC6036312/
6. Evans WJ, Morley JE, Argilés J, Bales C, Baracos V, Guttridge D, et al. Cachexia: A new definition. Clinical Nutrition. 2008 Dec;27(6):793–9.
7. Félétou M. The Endothelium. The Endothelium: Part 1: Multiple Functions of the Endothelial Cells—Focus on Endothelium-Derived Vasoactive Mediators [Internet]. 2011 [cited 2024 Jan 4];24(1):10–2. Available from: https://www.ncbi.nlm.nih.gov/books/NBK57149/
8. Verma M, Asakura Y, Murakonda BSR, Pengo T, Latroche C, Chazaud B, et al. Muscle Satellite Cell Cross-Talk with a Vascular Niche Maintains Quiescence via VEGF and Notch Signaling. Cell Stem Cell [Internet]. 2018 Oct 4 [cited 2025 Jul 30];23(4):530-543.e9. Available from: https://www-cell-com.ezproxy.library.yorku.ca/action/showFullText?pii=S1934590918304442
9. Bentzinger CF, Wang YX, Dumont NA, Rudnicki MA. Cellular dynamics in the muscle satellite cell niche. EMBO Rep [Internet]. 2013 Nov 15 [cited 2025 Jul 30];14(12):1062–72. Available from: https://www-embopress-org.ezproxy.library.yorku.ca/doi/10.1038/embor.2013.182
10. Terwoord JD, Beyer AM, Gutterman DD. Endothelial dysfunction as a complication of anti-cancer therapy. Pharmacol Ther [Internet]. 2022 Sep 1 [cited 2025 Oct 19];237:108116. Available from: https://pmc.ncbi.nlm.nih.gov/articles/PMC9294076/
11. Hsu PY, Mammadova A, Benkirane-Jessel N, Désaubry L, Nebigil CG. Updates on Anticancer Therapy-Mediated Vascular Toxicity and New Horizons in Therapeutic Strategies. Front Cardiovasc Med [Internet]. 2021 Jul 27 [cited 2025 Oct 19];8:694711. Available from: www.frontiersin.org
12. Cameron AC, Touyz RM, Lang NN. Vascular Complications of Cancer Chemotherapy. Can J Cardiol [Internet]. 2016 Jul 1 [cited 2025 Oct 19];32(7):852. Available from: https://pmc.ncbi.nlm.nih.gov/articles/PMC4989034/
13. Kim YM, Sanborn MA, Vijeth S, Gajwani P, Wang X, Jung D, et al. Skeletal muscle endothelial dysfunction through the activin A–PGC1α axis drives progression of cancer

cachexia. Nature Cancer 2025 6:8 [Internet]. 2025 May 26 [cited 2025 Oct 19];6(8):1350–69. Available from: https://www.nature.com/articles/s43018-025-00975-6
14. Terwoord JD, Beyer AM, Gutterman DD. Endothelial dysfunction as a complication of anti-cancer therapy. Pharmacol Ther. 2022 Sep 1;237:108116.
15. Tang K, Breen EC, Gerber HP, Ferrara NMA, Wagner PD. Capillary regression in vascular endothelial growth factor-deficient skeletal muscle. Physiol Genomics. 2004 Oct;18:63–9.
16. Longley DB, Harkin DP, Johnston PG. 5-Fluorouracil: mechanisms of action and clinical strategies. Nature Reviews Cancer 2003 3:5 [Internet]. 2003 May [cited 2025 Nov 9];3(5):330–8. Available from: https://www.nature.com/articles/nrc1074
17. Kubota T, Fujita S, Kodaira S, Yamamoto T, Josui K, Arisawa Y, et al. Antitumor Activity of Fluoropyrimidines and Thymidylate Synthetase Inhibition. Japanese Journal of Cancer Research. 1991;82(4):476–82.
18. Cao S, Frank C, Rustum YM. Role of fluoropyrimidine schedule and (6R,S)leucovorin dose in a preclinical animal model of colorectal carcinoma. J Natl Cancer Inst. 1996 Apr 3;88(7):430–6.
19. Tisdale MJ. Mechanisms of cancer cachexia. Physiol Rev [Internet]. 2009 Apr [cited 2025 Nov 9];89(2):381–410. Available from: https://journals.physiology.org/doi/10.1152/physrev.00016.2008
20. Clarke SJ, Yip S, Brown C, Van Hazel GA, Ransom DT, Goldstein D, et al. Single-agent irinotecan or FOLFIRI as second-line chemotherapy for advanced colorectal cancer; results of a randomised phase II study (DaVINCI) and meta-analysis [corrected]. Eur J Cancer [Internet]. 2011 [cited 2025 Jul 18];47(12):1826–36. Available from: https://pubmed.ncbi.nlm.nih.gov/21665462/
21. Zhang X, Duan R, Wang Y, Liu X, Zhang W, Zhu X, et al. FOLFIRI (folinic acid, fluorouracil, and irinotecan) increases not efficacy but toxicity compared with single-agent irinotecan as a second-line treatment in metastatic colorectal cancer patients: a randomized clinical trial. Ther Adv Med Oncol [Internet]. 2022 Jan 1 [cited 2025 Jul 18];14. Available from: https://pubmed.ncbi.nlm.nih.gov/35069808/
22. Picchi A, Gao X, Belmadani S, Potter BJ, Focardi M, Chilian WM, et al. Tumor necrosis factor-alpha induces endothelial dysfunction in the prediabetic metabolic syndrome. Circ Res [Internet]. 2006 Jul [cited 2025 Nov 9];99(1):69–77. Available from: https://pubmed.ncbi.nlm.nih.gov/16741160/
23. Kułdo JM, Westra J, Àsgeirsdóttir SA, Kok RJ, Oosterhuis K, Rots MG, et al. Differential effects of NF-κB and p38 MAPK inhibitors and combinations thereof on TNF-α- and IL-1β-induced proinflammatory status of endothelial cells in vitro. Am J Physiol Cell Physiol [Internet]. 2005 Nov [cited 2025 Jul 10];289(5 58-5):1229–39. Available from: https://journals.physiology.org/doi/10.1152/ajpcell.00620.2004
24. Powrózek T, Pigoń-Zajac D, Mazurek M, Otieno MO, Rahnama-Hezavah M, Małecka-Massalska T. TNF-α Induced Myotube Atrophy in C2C12 Cell Line Uncovers Putative Inflammatory-Related lncRNAs Mediating Muscle Wasting. Int J Mol Sci [Internet]. 2022 Apr 1 [cited 2024 Apr 10];23(7). Available from: /pmc/articles/PMC8998797/
25. Onesti JK, Guttridge DC. Inflammation based regulation of cancer cachexia. Biomed Res Int. 2014;2014.
26. Webster JM, Kempen LJAP, Hardy RS, Langen RCJ. Inflammation and Skeletal Muscle Wasting During Cachexia. Front Physiol. 2020 Nov 19;11:597675.

27. Malla J, Zahra A, Venugopal S, Selvamani TY, Shoukrie SI, Selvaraj R, et al. What Role Do Inflammatory Cytokines Play in Cancer Cachexia? Cureus [Internet]. 2022 Jul 12 [cited 2024 Jan 8];14(7). Available from: https://www.cureus.com/articles/91540-what-role-do-inflammatory-cytokines-play-in-cancer-cachexia
28. White JP, Puppa MJ, Gao S, Sato S, Welle SL, Carson JA. Muscle mTORC1 suppression by IL-6 during cancer cachexia: a role for AMPK. Am J Physiol Endocrinol Metab [Internet]. 2013 May 15 [cited 2025 Jul 14];304(10):E1042. Available from: https://pmc.ncbi.nlm.nih.gov/articles/PMC3651620/
29. Flint TR, Janowitz T, Connell CM, Roberts EW, Denton AE, Coll AP, et al. Tumor-Induced IL-6 Reprograms Host Metabolism to Suppress Anti-tumor Immunity. Cell Metab. 2016 Nov 8;24(5):672–84.
30. Freire PP, Cury SS, Lopes LO, Fernandez GJ, Liu J, de Moraes LN, et al. Decreased mir-497-5p suppresses il-6 induced atrophy in muscle cells. Cells. 2021 Dec 1;10(12).
31. Kartikasari AER, Huertas CS, Mitchell A, Plebanski M. Tumor-Induced Inflammatory Cytokines and the Emerging Diagnostic Devices for Cancer Detection and Prognosis. Front Oncol. 2021 Jul 7;11.
32. Mangano GD, Fouani M, D'amico D, Di Felice V, Barone R. Cancer-related cachexia: the vicious circle between inflammatory cytokines, skeletal muscle, lipid metabolism and the possible role of physical training. Int J Mol Sci. 2022 Mar 1;23(6):3004.
33. Bussu F, Graziani C, Gallus R, Cittadini A, Galli J, De Corso E, et al. IFN-γ and other serum cytokines in head and neck squamous cell carcinomas. Acta Otorhinolaryngologica Italica [Internet]. 2018 Apr 1 [cited 2025 Nov 9];38(2):94. Available from: https://pmc.ncbi.nlm.nih.gov/articles/PMC6028810/
34. Lin WW, Karin M. A cytokine-mediated link between innate immunity, inflammation, and cancer. Journal of Clinical Investigation. 2007 May 1;117(5):1175–83.
35. White JP, Puppa MJ, Gao S, Sato S, Welle SL, Carson JA. Muscle mTORC1 suppression by IL-6 during cancer cachexia: a role for AMPK. Am J Physiol Endocrinol Metab [Internet]. 2013 May 15 [cited 2025 Nov 9];304(10). Available from: https://pubmed.ncbi.nlm.nih.gov/23531613/
36. Kaplanski G, Marin V, Montero-Julian F, Mantovani A, Farnarier C. IL-6: A regulator of the transition from neutrophil to monocyte recruitment during inflammation. Trends Immunol. 2003 Jan 1;24(1):25–9.
37. Grivennikov SI, Greten FR, Karin M. Immunity, Inflammation, and Cancer. Cell. 2010 Mar;140(6):883–99.
38. Lippitz BE, Harris RA. Cytokine patterns in cancer patients: A review of the correlation between interleukin 6 and prognosis. Oncoimmunology [Internet]. 2016 May 3 [cited 2025 Nov 9];5(5):e1093722. Available from: https://pmc.ncbi.nlm.nih.gov/articles/PMC4910721/
39. Webster JM, Kempen LJAP, Hardy RS, Langen RCJ. Inflammation and Skeletal Muscle Wasting During Cachexia. Front Physiol. 2020 Nov 19;11.
40. Frontera WR, Ochala J. Skeletal muscle: a brief review of structure and function. Calcif Tissue Int [Internet]. 2015 Mar 4 [cited 2024 Jan 4];96(3):183–95. Available from: https://pubmed.ncbi.nlm.nih.gov/25294644/
41. Wolfe RR. The underappreciated role of muscle in health and disease. Am J Clin Nutr. 2006 Dec 1;84(3):475–82.

42. Cadot B, Gomes ER. Skeletal Muscle. Encyclopedia of Cell Biology: Volume 1-6, Second Edition. 2023 Jan 1;3:189–96.
43. Janssen I, Heymsfield SB, Ross R. Low relative skeletal muscle mass (sarcopenia) in older persons is associated with functional impairment and physical disability. J Am Geriatr Soc. 2002;50:889–96.
44. Baracos VE, Martin L, Korc M, Guttridge DC, Fearon KCH. Cancer-associated cachexia. Nat Rev Dis Primers. 2018 Jan 18;4.
45. Argilés JM, Busquets S, Stemmler B, López-Soriano FJ. Cancer cachexia: Understanding the molecular basis. Vol. 14, Nature Reviews Cancer. Nature Publishing Group; 2014. p. 754–62.
46. Cruz-Jentoft AJ, Sayer AA. Sarcopenia. Vol. 393, The Lancet. Lancet Publishing Group; 2019. p. 2636–46.
47. Dent E, Morley JE, Cruz-Jentoft AJ, Arai H, Kritchevsky SB, Guralnik J, et al. International Clinical Practice Guidelines for Sarcopenia (ICFSR): Screening, Diagnosis and Management. Journal of Nutrition, Health and Aging. 2018 Dec;22:1148–61.
48. Tipton KD, Wolfe RR. Exercise, protein metabolism, and muscle growth. In: International Journal of Sport Nutrition. Human Kinetics Publishers Inc.; 2001. p. 109–32.
49. Phillips SM, Glover EI, Rennie MJ. Alterations of protein turnover underlying disuse atrophy in human skeletal muscle. Vol. 107, Journal of Applied Physiology. 2009. p. 645–54.
50. Atherton PJ, Smith K. Muscle protein synthesis in response to nutrition and exercise. Vol. 590, Journal of Physiology. 2012. p. 1049–57.
51. Phillips SM. A brief review of critical processes in exercise-induced muscular hypertrophy. Sports Medicine. 2014;44.
52. Schoenfeld BJ. The mechanisms of muscle hypertrophy and their application to resistance training. Vol. 24, Journal of Strength and Conditioning Research. 2010. p. 2857–72.
53. Glass DJ. Skeletal muscle hypertrophy and atrophy signaling pathways. Vol. 37, International Journal of Biochemistry and Cell Biology. Elsevier Ltd; 2005. p. 1974–84.
54. Biolo G, Williams BD, Fleming RYD, Wolfe RR. Insulin action on muscle protein kinetics and amino acid transport during recovery after resistance exercise. Diabetes. 1999;48:949–57.
55. Velloso CP. Regulation of muscle mass by growth hormone and IGF-I. Vol. 154, British Journal of Pharmacology. 2008. p. 557–68.
56. Adams GR, McCue SA. Localized infusion of IGF-I results in skeletal muscle hypertrophy in rats. J Appl Physiol. 1998;84:1716–22.
57. Schiaffino S, Mammucari C. Regulation of skeletal muscle growth by the IGF1-Akt/PKB pathway: insights from genetic models. Skelet Muscle. 2011 Jan;1:4.
58. Vingren JL, Kraemer WJ, Ratamess NA, Anderson JM, Volek JS, Maresh CM. Testosterone physiology in resistance exercise and training: The up-stream regulatory elements. Vol. 40, Sports Medicine. 2010. p. 1037–53.
59. Bhasin S, Woodhouse L, Storer TW. Proof of the effect of testosterone on skeletal muscle. Journal of Endocrinology. 2001;170:27–38.
60. West DWD, Phillips SM. Anabolic processes in human skeletal muscle: Restoring the identities of growth hormone and testosterone. Vol. 38, Physician and Sportsmedicine. 2010. p. 97–104.

61. Fryburg DA, Jahn LA, Hill SA, Oliveras DM, Barrett EJ. Insulin and insulin-like growth factor-I enhance human skeletal muscle protein anabolism during hyperaminoacidemia by different mechanisms. Journal of Clinical Investigation. 1995;96:1722–9.
62. Velloso CP. Regulation of muscle mass by growth hormone and IGF-I. Vol. 154, British Journal of Pharmacology. 2008. p. 557–68.
63. Bhasin S, Woodhouse L, Storer TW. Proof of the effect of testosterone on skeletal muscle. Journal of Endocrinology. 2001;170:27–38.
64. Laplante M, Sabatini DM. MTOR signaling in growth control and disease. Vol. 149, Cell. Elsevier B.V.; 2012. p. 274–93.
65. Glass DJ. Skeletal muscle hypertrophy and atrophy signaling pathways. Vol. 37, International Journal of Biochemistry and Cell Biology. Elsevier Ltd; 2005. p. 1974–84.
66. Schiaffino S, Mammucari C. Regulation of skeletal muscle growth by the IGF1-Akt/PKB pathway: Insights from genetic models. Vol. 1, Skeletal Muscle. 2011.
67. Schiaffino S, Mammucari C. Regulation of skeletal muscle growth by the IGF1-Akt/PKB pathway: Insights from genetic models. Vol. 1, Skeletal Muscle. 2011.
68. Schiaffino S, Mammucari C. Regulation of skeletal muscle growth by the IGF1-Akt/PKB pathway: Insights from genetic models. Vol. 1, Skeletal Muscle. 2011.
69. Rommel C, Bodine SC, Clarke BA, Rossman R, Nunez L, Stitt TN, et al. Mediation of IGF-1-induced skeletal myotube hypertrophy by Pl(3)K/Alt/mTOR and Pl(3)K/Akt/GSK3 pathways. Nat Cell Biol. 2001;3:1009–13.
70. Hers I, Vincent EE, Tavaré JM. Akt signalling in health and disease. Vol. 23, Cellular Signalling. 2011. p. 1515–27.
71. Manning BD, Cantley LC. AKT/PKB Signaling: Navigating Downstream. Vol. 129, Cell. 2007. p. 1261–74.
72. Sandri M. Signaling in muscle atrophy and hypertrophy. Physiology [Internet]. 2008 Jun [cited 2025 Jul 3];23(3):160–70. Available from: https://journals.physiology.org/doi/10.1152/physiol.00041.2007
73. Saxton RA, Sabatini DM. mTOR Signaling in Growth, Metabolism, and Disease. Cell [Internet]. 2017 Mar 9 [cited 2025 Jul 3];168(6):960–76. Available from: https://www.cell.com/action/showFullText?pii=S0092867417301824
74. Laplante M, Sabatini DM. MTOR signaling in growth control and disease. Cell [Internet]. 2012 Apr 13 [cited 2025 Jul 3];149(2):274–93. Available from: https://www.cell.com/action/showFullText?pii=S0092867412003510
75. Tee AR, Manning BD, Roux PP, Cantley LC, Blenis J. Tuberous Sclerosis Complex gene products, Tuberin and Hamartin, control mTOR signaling by acting as a GTPase-activating protein complex toward Rheb. Current Biology [Internet]. 2003 Aug 5 [cited 2025 Jul 3];13(15):1259–68. Available from: https://www.cell.com/action/showFullText?pii=S0960982203005062
76. Branched-chain Amino Acids: Catabolism in Skeletal Muscle and Implications for Muscle and Whole-body Metabolism. 2025;
77. Ma XM, Blenis J. Molecular mechanisms of mTOR-mediated translational control. Nature Reviews Molecular Cell Biology 2009 10:5 [Internet]. 2009 Apr 2 [cited 2025 Jul 3];10(5):307–18. Available from: https://www.nature.com/articles/nrm2672
78. Ruvinsky I, Meyuhas O. Ribosomal protein S6 phosphorylation: from protein synthesis to cell size. Trends Biochem Sci [Internet]. 2006 Jun 1 [cited 2025 Jul 3];31(6):342–8. Available from: https://www.cell.com/action/showFullText?pii=S0968000406001137

79. Magnuson B, Ekim B, Fingar DC. Regulation and function of ribosomal protein S6 kinase (S6K) within mTOR signalling networks. Biochemical Journal [Internet]. 2012 Jan 1 [cited 2025 Jul 3];441(1):1–21. Available from: /biochemj/article/441/1/1/47374/Regulation-and-function-of-ribosomal-protein-S6
80. Laplante M, Sabatini DM. MTOR signaling in growth control and disease. Cell [Internet]. 2012 Apr 13 [cited 2025 Jul 3];149(2):274–93. Available from: https://www.cell.com/action/showFullText?pii=S0092867412003510
81. Gingras AC, Raught B, Sonenberg N. Regulation of translation initiation by FRAP/mTOR. Genes Dev [Internet]. 2001 Apr 1 [cited 2025 Jul 3];15(7):807–26. Available from: http://genesdev.cshlp.org/content/15/7/807.full
82. Mann G, Mora S, Madu G, Adegoke OAJ. Branched-chain Amino Acids: Catabolism in Skeletal Muscle and Implications for Muscle and Whole-body Metabolism. Front Physiol [Internet]. 2021 Jul 20 [cited 2025 Jul 12];12:702826. Available from: https://pmc.ncbi.nlm.nih.gov/articles/PMC8329528/
83. Poole DC, Kano Y, Koga S, Musch TI. August Krogh: Muscle capillary function and oxygen delivery. Comp Biochem Physiol A Mol Integr Physiol [Internet]. 2020 Mar 1 [cited 2025 Jul 5];253:110852. Available from: https://pmc.ncbi.nlm.nih.gov/articles/PMC7867635/
84. Kusters YHAM, Barrett EJ. Muscle microvasculature's structural and functional specializations facilitate muscle metabolism. Am J Physiol Endocrinol Metab [Internet]. 2015 [cited 2025 Jul 5];310(6):E379. Available from: https://pmc.ncbi.nlm.nih.gov/articles/PMC4888529/
85. Beer G, Yonce LR. Blood flow, oxygen uptake, and capillary filtration in resting skeletal muscle. https://doi.org/101152/ajplegacy19722233492 [Internet]. 1972 [cited 2025 Jul 5];223(3):492–8. Available from: https://journals.physiology.org/doi/10.1152/ajplegacy.1972.223.3.492
86. Kissane RWP, Al-Shammari AA, Egginton S. The importance of capillary distribution in supporting muscle function, building on Krogh's seminal ideas. Comp Biochem Physiol A Mol Integr Physiol. 2021 Apr 1;254:110889.
87. Howlett RA, Gonzalez NC, Wagner HE, Fu Z, Britton SL, Koch LG, et al. Selected contribution: skeletal muscle capillarity and enzyme activity in rats selectively bred for running endurance. J Appl Physiol (1985) [Internet]. 2003 Apr 1 [cited 2025 Jul 5];94(4):1682–8. Available from: https://pubmed.ncbi.nlm.nih.gov/12482771/
88. Timmerman KL, Lee JL, Dreyer HC, Dhanani S, Glynn EL, Fry CS, et al. Insulin Stimulates Human Skeletal Muscle Protein Synthesis via an Indirect Mechanism Involving Endothelial-Dependent Vasodilation and Mammalian Target of Rapamycin Complex 1 Signaling. J Clin Endocrinol Metab [Internet]. 2010 [cited 2025 Jul 5];95(8):3848. Available from: https://pmc.ncbi.nlm.nih.gov/articles/PMC2913031/
89. Betz MW, Fuchs CJ, Chedd F, Monsegue AP, Hendriks FK, van Kranenburg JMX, et al. Post-Exercise Cooling Lowers Skeletal Muscle Microvascular Perfusion and Blunts Amino Acid Incorporation into Muscle Tissue in Active Young Adults. Med Sci Sports Exerc [Internet]. 2025 [cited 2025 Jul 5]; Available from: https://pubmed.ncbi.nlm.nih.gov/40249909/
90. Pi X, Xie L, Patterson C. Emerging roles of vascular endothelium in metabolic homeostasis. Circ Res [Internet]. 2018 [cited 2025 Jul 5];123(4):477. Available from: https://pmc.ncbi.nlm.nih.gov/articles/PMC6205216/

91. Ramanlal R, Gupta V. Physiology, Vasodilation. StatPearls [Internet]. 2023 Jan 23 [cited 2025 Jul 5]; Available from: https://www.ncbi.nlm.nih.gov/books/NBK557562/
92. Mueller BJ, Roberts MD, Mobley CB, Judd RL, Kavazis AN. Nitric oxide in exercise physiology: past and present perspectives. Front Physiol. 2024 Jan 9;15:1504978.
93. Green DJ, Maiorana A, O'Driscoll G, Taylor R. Effect of exercise training on endothelium-derived nitric oxide function in humans. J Physiol [Internet]. 2004 Nov 15 [cited 2025 Jul 5];561(Pt 1):1. Available from: https://pmc.ncbi.nlm.nih.gov/articles/PMC1665322/
94. McCall GE, Byrnes WC, Dickinson A, Pattany PM, Fleck SJ. Muscle fiber hypertrophy, hyperplasia, and capillary density in college men after resistance training. J Appl Physiol (1985) [Internet]. 1996 [cited 2025 Jul 5];81(5):2004–12. Available from: https://pubmed.ncbi.nlm.nih.gov/8941522/
95. Pugh CF, Paton CD, Ferguson RA, Driller MW, Martyn Beaven C. Acute physiological responses of blood flow restriction between high-intensity interval repetitions in trained cyclists. Eur J Sport Sci [Internet]. 2024 Jun 1 [cited 2025 Jul 5];24(6):777–87. Available from: https://pubmed.ncbi.nlm.nih.gov/38874956/
96. Ross M, Kargl CK, Ferguson R, Gavin TP, Hellsten Y. Exercise-induced skeletal muscle angiogenesis: impact of age, sex, angiocrines and cellular mediators. Eur J Appl Physiol [Internet]. 2023 Jul 1 [cited 2025 Jul 5];123(7):1415–32. Available from: https://pubmed.ncbi.nlm.nih.gov/36715739/
97. Xia Q, Huang X, Huang J, Zheng Y, March ME, Li J, et al. The Role of Autophagy in Skeletal Muscle Diseases. Front Physiol [Internet]. 2021 Mar 25 [cited 2025 Jul 5];12:638983. Available from: www.frontiersin.org
98. Pang XS, Zhang P, Chen XP, Liu WM. Ubiquitin-proteasome pathway in skeletal muscle atrophy. Front Physiol [Internet]. 2023 [cited 2025 Jul 5];14:1289537. Available from: https://pmc.ncbi.nlm.nih.gov/articles/PMC10690626/
99. Damanti S, Senini E, De Lorenzo R, Merolla A, Santoro S, Festorazzi C, et al. Molecular constraints of sarcopenia in the ageing muscle. Frontiers in Aging [Internet]. 2025 Jul 3 [cited 2025 Jul 5];6:1588014. Available from: https://www.frontiersin.org/articles/10.3389/fragi.2025.1588014/full
100. Vazeille E, Codran A, Claustre A, Averous J, Listrat A, Béchet D, et al. The ubiquitin-proteasome and the mitochondria-associated apoptotic pathways are sequentially downregulated during recovery after immobilization-induced muscle atrophy. Am J Physiol Endocrinol Metab [Internet]. 2008 Nov [cited 2025 Jul 5];295(5). Available from: https://pubmed.ncbi.nlm.nih.gov/18812460/
101. Bodine SC, Baehr LM. Skeletal muscle atrophy and the E3 ubiquitin ligases MuRF1 and MAFbx/atrogin-1. Am J Physiol Endocrinol Metab. 2014 Sep 15;307(6):E469–84.
102. Larsson L, Degens H, Li M, Salviati L, Lee Y Il, Thompson W, et al. Sarcopenia: Aging-Related Loss of Muscle Mass and Function. Physiol Rev [Internet]. 2018 Jan 1 [cited 2025 Jul 5];99(1):427. Available from: https://pmc.ncbi.nlm.nih.gov/articles/PMC6442923/
103. Cruz-Jentoft AJ, Bahat G, Bauer J, Boirie Y, Bruyère O, Cederholm T, et al. Sarcopenia: revised European consensus on definition and diagnosis. Age Ageing [Internet]. 2019 Jan 1 [cited 2025 Jul 5];48(1):16–31. Available from: https://pubmed.ncbi.nlm.nih.gov/30312372/

104. Sandri M. Signaling in muscle atrophy and hypertrophy. Physiology (Bethesda) [Internet]. 2008 Jun [cited 2025 Jul 5];23(3):160–70. Available from: https://pubmed.ncbi.nlm.nih.gov/18556469/
105. Sandri M, Sandri C, Gilbert A, Skurk C, Calabria E, Picard A, et al. Foxo transcription factors induce the atrophy-related ubiquitin ligase atrogin-1 and cause skeletal muscle atrophy. Cell [Internet]. 2004 Apr 30 [cited 2025 Jul 5];117(3):399–412. Available from: https://pubmed.ncbi.nlm.nih.gov/15109499/
106. Patel HJ, Patel BM. TNF-α and cancer cachexia: Molecular insights and clinical implications. Life Sci. 2017 Feb 1;170:56–63.
107. Carotenuto F, Coletti D, Di Nardo P, Teodori L. αα-linolenic acid reduces TNF-induced apoptosis in C2C12 myoblasts by regulating expression of apoptotic proteins. Eur J Transl Myol. 2016 Nov 17;26(4).
108. Brooks NE, Myburgh KH. Skeletal muscle wasting with disuse atrophy is multi-dimensional: The response and interaction of myonuclei, satellite cells and signaling pathways. Front Physiol [Internet]. 2014 Mar 17 [cited 2025 Jul 5];5 MAR:75861. Available from: www.frontiersin.org
109. Wall BT, Dirks ML, Van Loon LJC. Skeletal muscle atrophy during short-term disuse: implications for age-related sarcopenia. Ageing Res Rev [Internet]. 2013 Sep [cited 2025 Jul 5];12(4):898–906. Available from: https://pubmed.ncbi.nlm.nih.gov/23948422/
110. Zeng N, D'Souza RF, MacRae CL, Figueiredo VC, Pileggi CA, Markworth JF, et al. Daily protein supplementation attenuates immobilization-induced blunting of postabsorptive muscle mTORC1 activation in middle-aged men. Am J Physiol Cell Physiol [Internet]. 2021 Apr 1 [cited 2025 Jul 5];320(4):C591–601. Available from: https://pubmed.ncbi.nlm.nih.gov/33471625/
111. Trendelenburg AU, Meyer A, Rohner D, Boyle J, Hatakeyama S, Glass DJ. Myostatin reduces Akt/TORC1/p70S6K signaling, inhibiting myoblast differentiation and myotube size. Am J Physiol Cell Physiol [Internet]. 2009 Jun [cited 2025 Jul 5];296(6). Available from: https://pubmed.ncbi.nlm.nih.gov/19357233/
112. Singh A, Phogat J, Yadav A, Dabur R. The dependency of autophagy and ubiquitin proteasome system during skeletal muscle atrophy. Biophys Rev [Internet]. 2021 Apr 1 [cited 2025 Jul 5];13(2):203–19. Available from: http://www.ncbi.nlm.nih.gov/pubmed/33927785
113. Ma K, Mallidis C, Bhasin S, Mahabadi V, Artaza J, Gonzalez-Cadavid N, et al. Glucocorticoid-induced skeletal muscle atrophy is associated with upregulation of myostatin gene expression. Am J Physiol Endocrinol Metab. 2003 Aug 1;285(2 48-2).
114. WEHLING M, CAI B, TIDBALL JG. Modulation of myostatin expression during modified muscle use. FASEB J [Internet]. 2000 Jan [cited 2025 Jul 5];14(1):103–10. Available from: https://pubmed.ncbi.nlm.nih.gov/10627285/
115. Kawakami Y, Akima H, Kubo K, Muraoka Y, Hasegawa H, Kouzaki M, et al. Changes in muscle size, architecture, and neural activation after 20 days of bed rest with and without resistance exercise. Eur J Appl Physiol. 2001;84(1–2):7–12.
116. Devries MC, Breen L, Von Allmen M, MacDonald MJ, Moore DR, Offord EA, et al. Low-load resistance training during step-reduction attenuates declines in muscle mass and strength and enhances anabolic sensitivity in older men. Physiol Rep [Internet]. 2015 [cited 2025 Jul 5];3(8):e12493. Available from: https://pmc.ncbi.nlm.nih.gov/articles/PMC4562579/

117. Atherton PJ, Greenhaff PL, Phillips SM, Bodine SC, Adams CM, Lang CH. Control of skeletal muscle atrophy in response to disuse: Clinical/preclinical contentions and fallacies of evidence. Am J Physiol Endocrinol Metab. 2016 Sep 1;311(3):E594–604.
118. Evans WJ. Skeletal muscle loss: Cachexia, sarcopenia, and inactivity. American Journal of Clinical Nutrition. 2010 Apr 1;91(4).
119. Drummond MJ, Dickinson JM, Fry CS, Walker DK, Gundermann DM, Reidy PT, et al. Bed rest impairs skeletal muscle amino acid transporter expression, mTORC1 signaling, and protein synthesis in response to essential amino acids in older adults. Am J Physiol Endocrinol Metab. 2012 May 1;302(9).
120. Bodine SC, Stitt TN, Gonzalez M, Kline WO, Stover GL, Bauerlein R, et al. Akt/mTOR pathway is a crucial regulator of skeletal muscle hypertrophy and can prevent muscle atrophy in vivo. Nat Cell Biol. 2001;3(11):1014–9.
121. Rudrappa SS, Wilkinson DJ, Greenhaff PL, Smith K, Idris I, Atherton PJ. Human skeletal muscle disuse atrophy: Effects on muscle protein synthesis, breakdown, and insulin resistance-A qualitative review. Front Physiol [Internet]. 2016 Aug 25 [cited 2025 Jul 5];7(AUG):211103. Available from: www.frontiersin.org
122. Bonaldo P, Sandri M. Cellular and molecular mechanisms of muscle atrophy. DMM Disease Models and Mechanisms. 2013 Jan;6(1):25–39.
123. Barreto R, Waning DL, Gao H, Liu Y, Zimmers TA, Bonetto A, et al. Chemotherapy-related cachexia is associated with mitochondrial depletion and the activation of ERK1/2 and p38 MAPKs. Oncotarget [Internet]. 2016 Jun 2 [cited 2025 Jul 9];7(28):43442–60. Available from: https://www.oncotarget.com/article/9779/text/
124. Rao VK, Das D, Taneja R. Cancer Cachexia: Signaling and Transcriptional Regulation of Muscle Catabolic Genes. Cancers 2022, Vol 14, Page 4258 [Internet]. 2022 Aug 31 [cited 2025 Jul 5];14(17):4258. Available from: https://www.mdpi.com/2072-6694/14/17/4258/htm
125. Bowen TS, Schuler G, Adams V. Skeletal muscle wasting in cachexia and sarcopenia: molecular pathophysiology and impact of exercise training. J Cachexia Sarcopenia Muscle. 2015 Sep 1;6(3):197–207.
126. Dalise S, Tropea P, Galli L, Sbrana A, Chisari C. Muscle function impairment in cancer patients in pre-cachexia stage. Eur J Transl Myol [Internet]. 2020 [cited 2025 Jul 9];30(2):258–67. Available from: https://pubmed.ncbi.nlm.nih.gov/32782760/
127. Olson B, Diba P, Korzun T, Marks DL. Neural mechanisms of cancer cachexia. Vol. 13, Cancers. MDPI; 2021.
128. von Haehling S, Anker SD. Cachexia as a major underestimated and unmet medical need: facts and numbers. J Cachexia Sarcopenia Muscle [Internet]. 2010 [cited 2024 Jan 3];1(1):1–5. Available from: https://pubmed.ncbi.nlm.nih.gov/21475699/
129. Tisdale MJ. Mechanisms of cancer cachexia. Physiol Rev. 2009 Apr;89(2):381–410.
130. Setiawan T, Sari IN, Wijaya YT, Julianto NM, Muhammad JA, Lee H, et al. Cancer cachexia: molecular mechanisms and treatment strategies. Journal of Hematology & Oncology 2023 16:1 [Internet]. 2023 May 22 [cited 2024 Jan 8];16(1):1–26. Available from: https://jhoonline.biomedcentral.com/articles/10.1186/s13045-023-01454-0
131. Kusters YHAM, Barrett EJ. Muscle microvasculature's structural and functional specializations facilitate muscle metabolism. Am J Physiol Endocrinol Metab [Internet]. 2016 [cited 2025 Jul 16];310(6):E379–87. Available from: https://journals.physiology.org/doi/10.1152/ajpendo.00443.2015

132. Pepe GJ;, Albrecht ED, Baum O, Pepe GJ, Albrecht ED. Microvascular Skeletal-Muscle Crosstalk in Health and Disease. International Journal of Molecular Sciences 2023, Vol 24, Page 10425 [Internet]. 2023 Jun 21 [cited 2024 Jan 6];24(13):10425. Available from: https://www.mdpi.com/1422-0067/24/13/10425/htm
133. Wüst RCI, Gibbings SL, Degens H. Fiber Capillary Supply Related To Fiber Size And Oxidative Capacity In Human And Rat Skeletal Muscle. Adv Exp Med Biol [Internet]. 2009 [cited 2025 Jul 16];645:75–80. Available from: https://link.springer.com/chapter/10.1007/978-0-387-85998-9_12
134. Dong H, Tsai SY. Mitochondrial Properties in Skeletal Muscle Fiber. Cells [Internet]. 2023 Sep 1 [cited 2025 Jul 16];12(17):2183. Available from: https://pmc.ncbi.nlm.nih.gov/articles/PMC10486962/
135. Hoppeler H. Vascular growth in hypoxic skeletal muscle. Adv Exp Med Biol. 2000;474:277–86.
136. Prior BM, Yang HT, Terjung RL. What makes vessels grow with exercise training? J Appl Physiol (1985) [Internet]. 2004 Sep [cited 2025 Jul 6];97(3):1119–28. Available from: https://pubmed.ncbi.nlm.nih.gov/15333630/
137. Lemieux P, Birot O. Altitude, Exercise, and Skeletal Muscle Angio-Adaptive Responses to Hypoxia: A Complex Story. Front Physiol [Internet]. 2021 Sep 6 [cited 2025 Jul 17];12:735557. Available from: www.frontiersin.org
138. Human endothelial cells produce IL-6. Lack of responses to exogenous IL-6 - PubMed [Internet]. [cited 2025 Jul 10]. Available from: https://pubmed.ncbi.nlm.nih.gov/2660697/
139. Ramos RB, Martino N, Chuy D, Lu S, Adam AP, Affiliations *. Regulation of endothelial DNA methylation by the sustained response to IL-6. [cited 2024 Apr 4]; Available from: https://doi.org/10.1101/2022.08.01.502384
140. Dinu M, Ruzzolini J, Higashi Y. Roles of Oxidative Stress and Inflammation in Vascular Endothelial Dysfunction-Related Disease. Antioxidants 2022, Vol 11, Page 1958 [Internet]. 2022 Sep 30 [cited 2025 Jul 10];11(10):1958. Available from: https://www.mdpi.com/2076-3921/11/10/1958/htm
141. Pate M, Damarla V, Chi DS, Negi S, Krishnaswamy G. Endothelial Cell Biology: Role in the Inflammatory Response. Adv Clin Chem. 2010 Jan 1;52(C):109–30.
142. Roudier E, Gineste C, Wazna A, Dehghan K, Desplanches D, Birot O. Angio-adaptation in unloaded skeletal muscle: new insights into an early and muscle type-specific dynamic process. J Physiol [Internet]. 2010 Nov [cited 2025 Jul 10];588(Pt 22):4579. Available from: https://pmc-ncbi-nlm-nih-gov.ezproxy.library.yorku.ca/articles/PMC3008859/
143. Lemieux P, Roudier E, Birot O. Angiostatic freeze or angiogenic move? Acute cold stress prevents angiokine secretion from murine myotubes but primes primary endothelial cells for greater migratory capacity. Front Physiol. 2022 Oct 17;13.
144. Olfert IM, Birot O. Importance of Anti-angiogenic Factors in the Regulation of Skeletal Muscle Angiogenesis. Microcirculation. 2011 May;18(4):316–30.
145. Bellamy LM, Johnston APW, De Lisio M, Parise G. Skeletal muscle-endothelial cell cross talk through angiotensin II. Am J Physiol Cell Physiol [Internet]. 2010 Dec [cited 2025 Jul 16];299(6):1402–8. Available from: https://journals.physiology.org/doi/10.1152/ajpcell.00306.2010
146. Lemieux P, Roudier E, Birot O. Angiostatic freeze or angiogenic move? Acute cold stress prevents angiokine secretion from murine myotubes but primes primary endothelial cells

for greater migratory capacity. Front Physiol [Internet]. 2022 Oct 17 [cited 2025 Jul 6];13:975652. Available from: https://pmc.ncbi.nlm.nih.gov/articles/PMC9618727/
147. Egginton S. Physiological factors influencing capillary growth. Acta Physiol (Oxf). 2011;202(3):225–39.
148. Trimm E, Red-Horse K. Vascular endothelial cell development and diversity. Nature Reviews Cardiology 2022 20:3 [Internet]. 2022 Oct 5 [cited 2025 Jul 10];20(3):197–210. Available from: https://www.nature.com/articles/s41569-022-00770-1
149. Dimmeler S, Zeiher AM. Nitric oxide ± an endothelial cell survival factor. [cited 2025 Jul 10]; Available from: http://www.stockton-press.co.uk/cdd
150. Ferrara N. Role of vascular endothelial growth factor in the regulation of angiogenesis. Kidney Int. 1999;56(3):794–814.
151. Méndez-barbero N, Gutiérrez-muñoz C, Blanco-Colio LM. Cellular Crosstalk between Endothelial and Smooth Muscle Cells in Vascular Wall Remodeling. International Journal of Molecular Sciences 2021, Vol 22, Page 7284 [Internet]. 2021 Jul 6 [cited 2025 Jul 6];22(14):7284. Available from: https://www.mdpi.com/1422-0067/22/14/7284/htm
152. dela Paz NG, Walshe TE, Leach LL, Saint-Geniez M, D'Amore PA. Role of shear-stress-induced VEGF expression in endothelial cell survival. J Cell Sci. 2012 Feb 15;125(4):831–43.
153. Nör JE, Christensen J, Mooney DJ, Polverini PJ. Vascular endothelial growth factor (VEGF)-mediated angiogenesis is associated with enhanced endothelial cell survival and induction of Bcl-2 expression. American Journal of Pathology. 1999;154(2):375–84.
154. Chen C, Xu Y, Song Y. IGF-1 gene-modified muscle-derived stem cells are resistant to oxidative stress via enhanced activation of IGF-1R/PI3K/AKT signaling and secretion of VEGF. Mol Cell Biochem [Internet]. 2014 Jan [cited 2025 Jul 30];386(1–2):167–75. Available from: https://pubmed-ncbi-nlm-nih-gov.ezproxy.library.yorku.ca/24126783/
155. Li F, Sawada J, Komatsu M. R-Ras-Akt axis induces endothelial lumenogenesis and regulates the patency of regenerating vasculature. Nat Commun [Internet]. 2017 Dec 1 [cited 2025 Jul 30];8(1):1720. Available from: https://pmc-ncbi-nlm-nih-gov.ezproxy.library.yorku.ca/articles/PMC5700916/
156. Dimmeler S, Fleming I, Fisslthaler B, Hermann C, Busse R, Zeiher AM. Activation of nitric oxide synthase in endothelial cells by Akt-dependent phosphorylation. Nature [Internet]. 1999 Jun 10 [cited 2025 Jul 30];399(6736):601–5. Available from: https://pubmed-ncbi-nlm-nih-gov.ezproxy.library.yorku.ca/10376603/
157. Domigan CK, Warren CM, Antanesian V, Happel K, Ziyad S, Lee S, et al. Autocrine VEGF maintains endothelial survival through regulation of metabolism and autophagy. J Cell Sci [Internet]. 2015 Jun 1 [cited 2025 Jul 30];128(12):2236–48. Available from: https://pubmed-ncbi-nlm-nih-gov.ezproxy.library.yorku.ca/25956888/
158. Yamamoto H, Rundqvist H, Branco C, Johnson RS. Autocrine VEGF Isoforms Differentially Regulate Endothelial Cell Behavior. Front Cell Dev Biol [Internet]. 2016 Sep 21 [cited 2025 Jul 30];4(SEP). Available from: https://pubmed-ncbi-nlm-nih-gov.ezproxy.library.yorku.ca/27709112/
159. Ju L, Zhou Z, Jiang B, Lou Y, Guo X. Autocrine VEGF and IL-8 Promote Migration via Src/Vav2/Rac1/PAK1 Signaling in Human Umbilical Vein Endothelial Cells. Cell Physiol Biochem [Internet]. 2017 May 1 [cited 2025 Jul 30];41(4):1346–59. Available from: https://pubmed-ncbi-nlm-nih-gov.ezproxy.library.yorku.ca/28278510/

160. Franco M, Roswall P, Cortez E, Hanahan D, Pietras K. Pericytes promote endothelial cell survival through induction of autocrine VEGF-A signaling and Bcl-w expression. Blood [Internet]. 2011 Sep 8 [cited 2025 Jul 30];118(10):2906–17. Available from: https://pubmed-ncbi-nlm-nih-gov.ezproxy.library.yorku.ca/21778339/
161. Aiken J, Roudier E, Ciccone J, Drouin G, Stromberg A, Vojnovic J, et al. Phosphorylation of murine double minute-2 on Ser166 is downstream of VEGF-A in exercised skeletal muscle and regulates primary endothelial cell migration and FoxO gene expression. FASEB Journal. 2016 Mar 1;30(3):1120–34.
162. Dameron KM, Volpert O V., Tainsky MA, Bouck N. Control of Angiogenesis in Fibroblasts by p53 Regulation of Thrombospondin-1. Science (1979). 1994 Sep 9;265(5178):1582–4.
163. Karsan A, Harlan JM. Modulation of endothelial cell apoptosis: mechanisms and pathophysiological roles. J Atheroscler Thromb. 1996;3(2):75–80.
164. Lee S, Chen TT, Barber CL, Jordan MC, Murdock J, Desai S, et al. Autocrine VEGF Signaling Is Required for Vascular Homeostasis. Cell. 2007 Aug 24;130(4):691–703.
165. O'connor DS, Schechner JS, Adida C, Mesri M, Rothermel AL, Li F, et al. Control of Apoptosis during Angiogenesis by Survivin Expression in Endothelial Cells. Am J Pathol. 2000 Feb 1;156(2):393–8.
166. Domigan CK, Warren CM, Antanesian V, Happel K, Ziyad S, Lee S, et al. Autocrine VEGF maintains endothelial survival through regulation of metabolism and autophagy. J Cell Sci [Internet]. 2015 Jun 1 [cited 2025 Jul 10];128(12):2236–48. Available from: https://dx.doi.org/10.1242/jcs.163774
167. Immanuel J, Yun S. Vascular Inflammatory Diseases and Endothelial Phenotypes. Cells 2023, Vol 12, Page 1640 [Internet]. 2023 Jun 15 [cited 2024 Jan 6];12(12):1640. Available from: https://www.mdpi.com/2073-4409/12/12/1640/htm
168. Abid MR, Guo S, Minami T, Spokes KC, Ueki K, Skurk C, et al. Vascular Endothelial Growth Factor Activates PI3K/Akt/Forkhead Signaling in Endothelial Cells. Arterioscler Thromb Vasc Biol. 2004 Feb;24(2):294–300.
169. Albertsson P, Lennernäs B, Norrby K. Dose effects of continuous vinblastine chemotherapy on mammalian angiogenesis mediated by VEGF-A. Acta Oncol (Madr). 2008;47(2):293–300.
170. Lennernäs B, Albertsson P, Lennernäs H, Norrby K. Chemotherapy and antiangiogenesis: Drug-specific, dose-related effects. Acta Oncol (Madr). 2003;42(4):294–303.
171. Cameron AC, Touyz RM, Lang NN. Vascular Complications of Cancer Chemotherapy. Can J Cardiol [Internet]. 2016 Jul 1 [cited 2025 Jul 10];32(7):852. Available from: https://pmc.ncbi.nlm.nih.gov/articles/PMC4989034/
172. Barreto R, Waning DL, Gao H, Liu Y, Zimmers TA, Bonetto A. Chemotherapy-related cachexia is associated with mitochondrial depletion and the activation of ERK1/2 and p38 MAPKs [Internet]. Vol. 7. 2016. Available from: www.impactjournals.com/oncotarget
173. YANG W, HUANG J, WU H, WANG Y, DU Z, LING Y, et al. Molecular mechanisms of cancer cachexiainduced muscle atrophy (Review). Mol Med Rep. 2020 Dec 1;22(6):4967–80.
174. Nicklin P, Bergman P, Zhang B, Triantafellow E, Wang H, Nyfeler B, et al. Bidirectional Transport of Amino Acids Regulates mTOR and Autophagy. Cell [Internet]. 2009 Feb 6 [cited 2025 Jul 4];136(3):521–34. Available from: https://www.cell.com/action/showFullText?pii=S0092867408015195

175. Milkiewicz M, Roudier E, Doyle JL, Trifonova A, Birot O, Haas TL. Identification of a mechanism underlying regulation of the anti-angiogenic forkhead transcription factor FoxO1 in cultured endothelial cells and ischemic muscle. American Journal of Pathology. 2011;178(2):935–44.
176. Förstermann U, Sessa WC. Nitric oxide synthases: regulation and function. Eur Heart J [Internet]. 2012 Apr [cited 2025 Jul 6];33(7). Available from: https://pubmed.ncbi.nlm.nih.gov/21890489/
177. Baum O, Da Silva-Azevedo L, Willerding G, Wöckel A, Planitzer G, Gossrau R, et al. Endothelial NOS is main mediator for shear stress-dependent angiogenesis in skeletal muscle after prazosin administration. Am J Physiol Heart Circ Physiol. 2004 Nov;287(5 56-5).
178. Andrew PJ, Mayer B. Enzymatic function of nitric oxide synthases. Cardiovasc Res. 1999 Aug 15;43(3):521–31.
179. Albertsson P, Lennerns B, Norrby K. Low-dose continuous 5-fluorouracil infusion stimulates VEGF-A-mediated angiogenesis. Acta Oncol [Internet]. 2009 [cited 2025 Jul 11];48(3):418–25. Available from: https://pubmed.ncbi.nlm.nih.gov/18932044/
180. Myh1 myosin, heavy polypeptide 1, skeletal muscle, adult [Mus musculus (house mouse)] - Gene - NCBI [Internet]. [cited 2025 Nov 13]. Available from: https://www.ncbi.nlm.nih.gov/gene/17879
181. MYH1E Antibody (MF 20) - DSHB [Internet]. [cited 2025 Nov 13]. Available from: https://dshb.biology.uiowa.edu/MF-20
182. TNNT3 Antibody (JLT12) - DSHB [Internet]. [cited 2025 Nov 13]. Available from: https://dshb.biology.uiowa.edu/JLT12
183. Han D, Lim Y, Lee S, Eyun S il. Troponin I – a comprehensive review of its function, structure, evolution, and role in muscle diseases. Anim Cells Syst (Seoul) [Internet]. 2025 [cited 2025 Nov 13];29(1):446. Available from: https://pmc.ncbi.nlm.nih.gov/articles/PMC12305882/
184. Ma X, Zhang S, He L, Rong Y, Wilz Brier L, Sun Q, et al. The Importance of mTORC1-Autophagy Axis for Skeletal Muscle Diseases. International Journal of Molecular Sciences 2023, Vol 24, Page 297 [Internet]. 2022 Dec 24 [cited 2025 Jul 14];24(1):297. Available from: https://www.mdpi.com/1422-0067/24/1/297/htm
185. Mora S, Adegoke OAJ. Maintenance of the branched-chain amino acid transporter LAT1 counteracts myotube atrophy following chemotherapy. Am J Physiol Cell Physiol [Internet]. 2024 Mar 1 [cited 2025 Jul 14];326(3):C866–79. Available from: https://journals.physiology.org/doi/10.1152/ajpcell.00537.2023
186. Ljungman M. Individual variation in p53 responsiveness. J Natl Cancer Inst [Internet]. 2001 Jan 17 [cited 2025 Jul 20];93(2):82–3. Available from: https://pubmed.ncbi.nlm.nih.gov/11208871/
187. Meek DW. Regulation of the p53 response and its relationship to cancer. Biochemical Journal [Internet]. 2015 Aug 1 [cited 2025 Jul 20];469(3):325–46. Available from: /biochemj/article/469/3/325/48587/Regulation-of-the-p53-response-and-its
188. Chibaya L, Karim B, Zhang H, Jones SN. Mdm2 phosphorylation by Akt regulates the p53 response to oxidative stress to promote cell proliferation and tumorigenesis. Proc Natl Acad Sci U S A. 2021 Jan 26;118(4).
189. Mirzayans R, Andrais B, Kumar P, Murray D. Significance of Wild-Type p53 Signaling in Suppressing Apoptosis in Response to Chemical Genotoxic Agents: Impact on

Chemotherapy Outcome. International Journal of Molecular Sciences 2017, Vol 18, Page 928 [Internet]. 2017 Apr 28 [cited 2025 Jul 20];18(5):928. Available from: https://www.mdpi.com/1422-0067/18/5/928/htm
190. Carlsen L, El-Deiry WS. Differential p53-Mediated Cellular Responses to DNA-Damaging Therapeutic Agents. International Journal of Molecular Sciences 2021, Vol 22, Page 11828 [Internet]. 2021 Oct 31 [cited 2025 Jul 20];22(21):11828. Available from: https://www.mdpi.com/1422-0067/22/21/11828/htm
191. Conklin KA. Chemotherapy-associated oxidative stress: impact on chemotherapeutic effectiveness. Integr Cancer Ther [Internet]. 2004 Dec [cited 2025 Jul 20];3(4):294–300. Available from: https://pubmed.ncbi.nlm.nih.gov/15523100/
192. Barreto R, Waning DL, Gao H, Liu Y, Zimmers TA, Bonetto A. Chemotherapy-related cachexia is associated with mitochondrial depletion and the activation of ERK1/2 and p38 MAPKs. Oncotarget [Internet]. 2016 [cited 2025 Jul 18];7(28):43442–60. Available from: https://pubmed.ncbi.nlm.nih.gov/27259276/
193. Wang B, Rasmussen-Ivey C, Little JB, Yuan ZM. The MDM2/MDMX/p53 axis in the adaptive stress response. Transl Cancer Res [Internet]. 2020 [cited 2025 Jul 20];9(3):1993–7. Available from: https://tcr.amegroups.org/article/view/36540/html
194. Dameron KM, Volpert O V., Tainsky MA, Bouck N. The p53 tumor suppressor gene inhibits angiogenesis by stimulating the production of thrombospondin. Cold Spring Harb Symp Quant Biol [Internet]. 1994 [cited 2025 Jul 18];59:483–9. Available from: https://pubmed-ncbi-nlm-nih-gov.ezproxy.library.yorku.ca/7587102/
195. Dameron KM, Volpert O V., Tainsky MA, Bouck N. Control of angiogenesis in fibroblasts by p53 regulation of thrombospondin-1. Science [Internet]. 1994 Sep 9 [cited 2025 Jul 18];265(5178):1582–4. Available from: https://pubmed-ncbi-nlm-nih-gov.ezproxy.library.yorku.ca/7521539/
196. Cui D, Qu R, Liu D, Xiong X, Liang T, Zhao Y. The Cross Talk Between p53 and mTOR Pathways in Response to Physiological and Genotoxic Stresses. Front Cell Dev Biol. 2021 Nov 18;9.
197. Ogawara Y, Kishishita S, Obata T, Isazawa Y, Suzuki T, Tanaka K, et al. Akt enhances Mdm2-mediated ubiquitination and degradation of p53. Journal of Biological Chemistry [Internet]. 2002 Jun 14 [cited 2025 Jul 30];277(24):21843–50. Available from: https://www.jbc.org/action/showFullText?pii=S0021925820704448
198. Dimmeler S, Fleming I, Fisslthaler B, Hermann C, Busse R, Zeiher AM. Activation of nitric oxide synthase in endothelial cells by Akt-dependent phosphorylation. Nature [Internet]. 1999 Jun 10 [cited 2025 Jul 19];399(6736):601–5. Available from: https://pubmed.ncbi.nlm.nih.gov/10376603/
199. Levkau B, Koyama H, Raines EW, Clurman BE, Herren B, Orth K, et al. Cleavage of p21Cip1/Waf1 and p27Kip1 mediates apoptosis in endothelial cells through activation of cdk2: Role of a caspase cascade. Mol Cell. 1998;1(4):553–63.
200. Ekshyyan O, Anandharaj A, Nathan CAO. Dual PI3K/mTOR inhibitors: Does p53 modulate response? Clinical Cancer Research. 2013 Jul 15;19(14):3719–21.
201. Ericksen RE, Lim SL, McDonnell E, Shuen WH, Vadiveloo M, White PJ, et al. Loss of BCAA catabolism during carcinogenesis enhances mTORCl activity and promotes tumor development and progression. Cell Metab [Internet]. 2019 May 7 [cited 2025 Jul 20];29(5):1151. Available from: https://pmc.ncbi.nlm.nih.gov/articles/PMC6506390/

Chapter 8 Appendix

Appendix A- In Vitro Drug and inflammatory cytokine Dosages

To prepare treatment media, each well was filled with 2 mL of chemotherapy-cytokine cocktail or vehicle control. With a total of 12 wells (two 6-well plates), 9 wells required treatment and 3 were assigned as vehicle controls. Therefore, 18 mL of cocktail was needed for the treatment group, and 6 mL for the vehicle group. To ensure sufficient volume for pipetting and to avoid shortages, an additional 2 mL was added to each group, resulting in a final volume of 20 mL for the drug cocktail and 8 mL for the vehicle control.

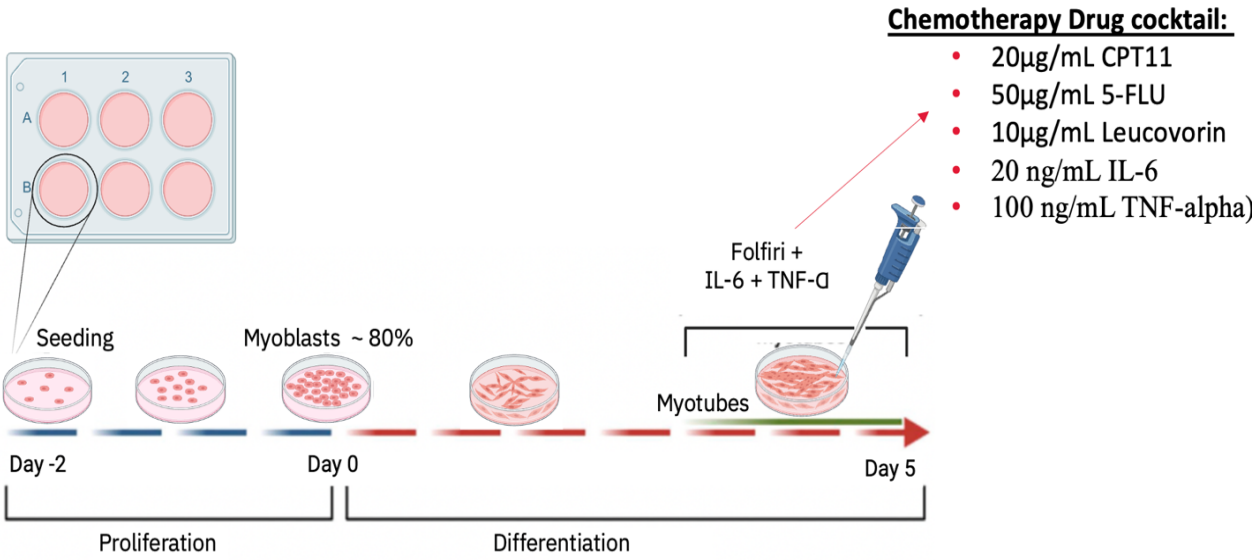

Figure A1. *Experimental timeline for myotube differentiation and chemotherapy-cytokine treatment.* Myoblasts were seeded and allowed to proliferate until ~80% confluence (Day 0), after which cells were switched to differentiation media to form myotubes (Day 0–Day 5). At Day 5, myotubes were treated with a chemotherapy drug cocktail (FOLFIRI: CPT-11 [20 µg/mL], 5-fluorouracil [50 µg/mL], and leucovorin [10 µg/mL]) combined with pro-inflammatory cytokines (IL-6 [20 ng/mL] and TNF-α [100 ng/mL]) for 24 or 48 hours. Created with BioRender.

Drug Stock Solutions:

CPT-11 (Sigma, #I1406): 50 mg dissolved in 1 mL DMSO (Sigma, #D5879)

- Weigh 50 mg of CPT-11 on thin filter paper
- Transfer into a 1.5 mL Eppendorf tube
- Add 1 mL of DMSO and vortex to dissolve
- Aliquot into 30µL amounts and store at −20°C

5-FU (Sigma, #F6627): 50 mg dissolved in 1 mL DMSO

- Weigh 50 mg of 5-FU on thin filter paper
- Transfer into a 1.5 mL Eppendorf tube
- Add 1 mL of DMSO and vortex to dissolve
- Aliquot into 30µL amounts and store at −20°C

Leucovorin (Sigma, #F7878): 20 mg dissolved in 1 mL ddH_2O

- Weigh 20 mg of leucovorin on thin filter paper
- Transfer into a 1.5 mL Eppendorf tube
- Add 1 mL of ddH_2O and vortex to dissolve
- Aliquot into 30µL amounts and store at −20°C

IL-6 (Sigma-Aldrich, #19646): 5,000 ng dissolved in 1 mL ddH_2O

- Reconstitute 5µg of IL-6 in 1 mL of ddH_2O
- Vortex gently to dissolve
- Aliquot into 50µL volumes and store at −20°C

TNF-α (R&D Systems, #80-235): 25,000 ng dissolved in 1 mL ddH_2O

- Reconstitute 25µg of TNF-α in 1 mL of ddH_2O
- Vortex gently to dissolve
- Aliquot into 50µL volumes and store at −20°C

Working Concentration Calculations (based on 20 mL total volume for 9 wells):

- CPT-11: 20 µg/mL → (20 µg/mL × 20 mL) ÷ 50,000 µg/mL = 8µL
- 5-FU: 50 µg/mL → (50 µg/mL × 20 mL) ÷ 50,000 µg/mL = 20µL
- Leucovorin: 10 µg/mL → (10 µg/mL × 20 mL) ÷ 20,000 µg/mL = 10µL
- IL-6: 20 ng/mL → (20 ng/mL × 20 mL) ÷ 5,000 ng/mL = 80µL
- TNF-α: 100 ng/mL → (100 ng/mL × 20 mL) ÷ 25,000 ng/mL = 80µL
- Vehicle Control (for 3 wells, 8 mL total):
  - Add 1.4 µL/mL of DMSO to differentiation media
  - 1.4µL × 8 mL = 11.2µL of DMSO to 8 mL of DM

Appendix B – Immunofluorescence Microscopy (*In-vitro)* Materials:

- 12-well plates (Petrie stores)
- Sterile autoclaved tweezers
- Cover Slips (Fisher Scientific, #12-54618CIR-2)
- PBS (Wisent, #311-010-CL)
- 4% Paraformaldehyde (Sigma, #6148)
- Triton X-100 (MP Biomedicals, LLC, #M2528)
- Bovine Serum Albumin (Biotech, #9048-46-9)
- Horse Serum (Gibco, #26050-088)
- MHC-1 primary antibody (Development Hybridoma, #MF 20 – s)
- Fluorochrome Secondary Antibody (Vector Labs, Vectashield, #TI-1000W0901)
- DAPI Mounting Medium (Vector Labs, Vectashield, #H-1200)

Protocol:

1. Sterilize cover slips by autoclaving them. Place a single cover slip into each well of a 12-well plate using sterile autoclaved tweezers.
2. Plate C2C12 myoblasts in the 12-well plate on top of cover slips. Grow myoblasts according to regular procedure.
3. When cells are confluent, change to differentiation medium.
4. Change medium every 24-48 hours until day 4 or 5 when myotubes are ready for treatment. On day 5, treat cells with the chemotherapy drug cocktail and inflammatory cytokines according to regular protocol.
5. Remove medium and rinse each well 2X with 1mL of PBS.
6. Fixing the cells: Inside the fume hood, add 1 mL of 4% paraformaldehyde (PFA in PBS) to each well to fix the cells. Gently rock the plate for 10 minutes at room temperature. Since the cells are light-sensitive, cover the plate with aluminum foil during this step. After 10 minutes, carefully aspirate the PFA and dispose of it in the designated waste container within the hood.
    - Sample Calculation for PFA
    - 4% PFA was already made in the lab, therefore, I did not have to make this. It is in 50 ml test tube at -20 C freezer.

- 11996.4ul of PBS
- 3.6uL of Triton

7. Do 3X quick rinse in PBS with 1mL/well.
8. PERMEABILIZATION: Permeabilize the cells by adding 1mL/well of 0.03% Triton X-100 in PBS. Incubate for 5 minutes.
    - Sample Calculation for Triton X-100 (To make 12mLs). Can make this in a 15mL test tube.
    - Triton is highly viscous at room temperature. To reduce its viscosity and make it easier to handle, transfer the required amount into a small beaker and microwave for approximately 30 seconds.
9. WASHING: Remove Triton solution and wash 5X, 1mL/wash, 5minutes/wash.
10. Blocking: Thaw a horse serum. Incubate with 400µL/well of blocking solution: 10% horse serum in PBS. Block at 37°C for 1hour with periodic swirl.
    - Sample Calculation for blocking solution (to make 5mLs)

        - 480uL of horse serum
        - 4320uL of PBS

11. Primary Antibody: Add sufficient amount of diluted antibody, ~500µL/well. (MHC-1 from DSHB #MF-20, 2.5µg/mL diluted in 1% BSA in PBS). Incubate overnight at 4°C with gentle rocking.

    - Sample calculation for primary antibody (to make 7mLs)
        - 5,425 uL of PBS
        - 700 uL of 1% BSA
        - 875 uL of MHC primary
            - For MHC, 2.5ug/mL (conc we want) x 7mLs (total volume) / 20 ug/mL (this value is conc on MHC tube) = 875 uL

12. Wash: Decant and save primary antibody. Do one quick rinse in PBS and then 3X wash in PBS, 5minutes/wash with gentle rocking.

13. Secondary Antibody: Dilute secondary antibody (Texas Red anti-mouse IgG, raised in horse). Dilute 1:100 with 1% BSA in PBS. After removing PBS from washing (step 12), add 500µL/well of the diluted secondary antibody and incubate for 2hour, room temperature on a rocker. Make sure to keep the wells covered and protected from light using aluminum foil. This is to ensure that no photo-damage takes place on the fluorochromes of the secondary antibody.
    - Sample calculation for secondary antibody (to make 5.5mLs)
        - 5445uL of PBS
        - 55uL of 1% BSA
        - 55uL of secondary (anti mouse, horse raised)
14. WASH: Remove secondary antibody and wash 5X, 10minutes/wash in PBS.
15. MOUNTING: Take appropriately labelled microscope slides. Put a drop of mounting medium on each slide. The mounting medium contains DAPI (to stain the nucleus) and antioxidants to prevent oxidation of the fluorochromes.
16. With a pair of tweezers, take the cover slip out and invert the slip on the mounting medium. Ensure the side on which the cells are face the DAPI mounting medium.
17. MICROSCOPY: Observe under the microscope.

Appendix C – In-vitro BCKD Activity Assay Materials and Protocol

Materials:

- Heat Pad
- PBS (Wisent, #311-010-CL)
- 1 mL Syringes (Petrie Stores)
- Cell Scraper
- Eppendorf Tubes (Petrie Stores)
- 6-Well Cell Culture Plates (Petrie Stores)
- Clear Scotch Tape
- Scintillation Vials (Perkin-Elmer, #6008118)
- Scintillation Fluid (Ecoscint A, National Diagnostics, #LS-273)
- Filter Paper Wicks (1.3 cm × 2 cm)
- 2M NaOH
- Heated Incubator (Non-shaking)
- Growth Media (GM), made by supplementing AMEM (Wisent Inc, #310-010-CL) with 10% FBS (Gibco, #12483-020) and 1% Antibiotic (Gibco, #15240-062)
- Krebs Ringer Buffer (KRB): 856 µL/well
- Thiamine Hydrochloride (Sigma, #T1270): 1 mg/856 µL of KRB
- Valine (Sigma, #V0513)
- Radioactive Valine (Perkin Elmer, #NEC291EU050UC)
- Lysis Buffer

Protocol:

1. C2C12 myotubes were seeded in 6-well plates at 200,000 cells/well and grown to day 0. Cells were differentiated and treated according to experimental conditions.
2. Prepare taping and filter paper wicks:
    - Four pieces of tape per 6-well plate: one for the long side with three wicks, three small pieces for the short side (one wick each)
3. Prepare KRB (856 µL/well) supplemented with thiamine hydrochloride (1 mg/856 µL)
4. Prepare 61 µL/well of reaction mix (radioactive; wear PPE and use radioactive bench)

5. In sterile conditions, aspirate the media from each well and replace with 200 µL of fresh DM
6. Move the plate to the radioactive bench
7. Add 856 µL/well of KRB + thiamine hydrochloride
8. Add 61 µL/well of reaction mix
9. Add two filter paper wicks with 60 µL of 2M NaOH in the center of designated control wells
10. Mount tape strips across the 6-well plate to suspend the filter paper wicks above each well; secure properly to avoid gaps
11. Place the lid on the plate and wrap it securely with clear tape to avoid contamination
12. Incubate at 37°C, 0 rpm for 1 hours
13. Meanwhile, label scintillation vials and fill with 3.5 mL scintillation fluid; also prepare lysis buffer and labeled Eppendorf tubes
14. After incubation, carefully remove the tape-wick assembly
15. Use forceps to transfer filter wicks into scintillation vials
16. Aspirate remaining media and rinse each well twice with ice-cold PBS
17. Add 100 µL of lysis buffer to each well
18. Harvest cells for protein content quantification

Appendix D – In-vitro BCKD Activity Assay Calculations

The activity of the BCKD enzyme was quantified by measuring the amount of radiolabeled carbon dioxide (^14CO_2) released during the decarboxylation of ^14C-valine. This ^14CO_2 was captured on NaOH-soaked filter paper wicks and quantified using a scintillation counter. The radioactivity was initially measured as **counts per minute (CPM)**, which reflects the number of decay events detected by the counter per minute. However, because scintillation counters do not detect every decay event, **CPM underestimates the actual radioactivity**. To obtain a more accurate measurement, **CPM was converted to disintegrations per minute (DPM)** by correcting for the instrument's counting efficiency, which was assumed to be **45%** in this experiment.

Step 1: CPM to DPM Conversion

DPM = CPM ÷ 0.45
Example: If CPM = 1350 → DPM = 1350 ÷ 0.45 = 3000

Step 2: DPM to Moles of CO_2

Using the known conversion:

- 1 μCi = 2.22×10^6 DPM
- Specific activity of ^14C-valine = 62 mCi/mmol

mol CO_2 = DPM ÷ $(2.22 \times 10^6 \times 62)$
Example: 3000 ÷ $(2.22 \times 10^6 \times 62) = 2.2 \times 10^{-8}$ mol CO_2

Step 3: Normalize to Protein

Protein content was measured using the BCA assay, and the final result was expressed as:

mol CO_2 per μg protein = mol CO_2 ÷ total protein in μg
Example: $2.2 \times 10^{-8} \div 20 = 1.1 \times 10^{-9}$ mol/μg

Appendix E - Preparation of 1.5% Gelatin Solution

Materials

- Gelatin Type A (BioShop, Cat. No. GEL771.500)
- Double-distilled water (ddH2O)
- Heat resistant glass container with lead
- Magnetic stirrer and stir bar
- Autoclave (liquid cycle)

Procedure

1. Weigh **1.5 g** of Gelatin Type A using a scale.
2. Add gelatin to a heat-resistant glass container and adjust the final volume to 100 mL with ddH_2O.
3. Place a sterile magnetic stir bar in the container and stir the solution on a magnetic stirrer.
4. Transfer the container to the autoclave room and autoclave on the liquids cycle until the gelatin is fully dissolved and sterilized. (gelatin will not dissolve and homogenize into the ddH20 if this step is not done).
5. After autoclaving, allow the solution to cool to room temperature before use.
6. Store the prepared gelatin solution at **4°C**.
   (notes: only open the bottle in the sterile fume hood)

Appendix F – Gelatin Coating Procedure

To coat plasticware with 1.5% Gelatin for Culturing Mouse Skeletal Muscle Microvascular Endothelial cells:

Coating Procedure:

1. In the sterile fume hood Add 1 mL of gelatin solution to each well of a 6-well plate, or 3 mL to a T75 flask.
2. Tilt to ensure entire surface is coated.
3. Incubate at room temperature for 5 minutes.
4. Aspirate and discard the gelatin solution.
5. Wash it once with 1× PBS.
6. Add complete Endothelial Cell Medium and equilibrate in the incubator before adding cells.